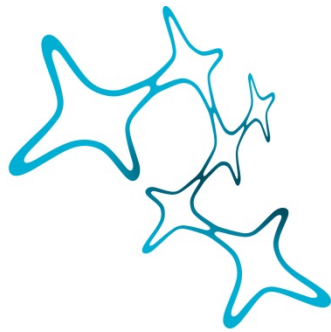


---

# THE ARYL HYDROCARBON RECEPTOR REGULATES FATE OF REACTIVE ASTROCYTES AFTER STAB WOUND INJURY

---

Sven Aschenbroich



Graduate School of  
Systemic Neurosciences  
LMU Munich



Dissertation der  
Graduate School of Systemic Neurosciences  
Ludwig-Maximilians-Universität München

May 23, 2022



Supervisor

Prof. Dr. Jovica Ninkovic

Biomedical Center (BMC)-Institute for Cell Biology and Anatomy

Faculty of Medicine

LMU Munich

Helmholtz Zentrum München

Institute of Stem Cell Research

First Reviewer: Prof. Dr. Jovica Ninkovic

Second Reviewer: Prof. Dr. Martin Kerschensteiner

External Reviewer: Dr. Ruth Beckervordersandforth-Bonk

Date of Submission: May 23, 2022

Date of Defense: September 26, 2022



“Truth has many dimensions, and the way  
you arrive at truth in complex situations  
is through many perspectives”

Eric Kandel

Spiegel International 2012



# List of Content

<b>Abstract</b> .....	<b>1</b>
<b>1 Introduction</b> .....	<b>3</b>
1.1 CNS response to traumatic brain injury .....	3
1.2 Astrocytes in health and disease.....	5
1.3 What can we learn from neural stem cells? .....	8
1.4 The aryl hydrocarbon receptor .....	13
1.5 Aims .....	17
<b>2 Results</b> .....	<b>19</b>
2.1 The aryl hydrocarbon receptor knock-out system.....	19
2.2 The role of AhR in acquiring stem cell potential .....	20
2.3 AhR signaling does not regulate astrocytes proliferation upon injury.....	23
2.4 Is leukocyte extravasation upon injury affected by the astrocytic AhR-deficiency?.....	27
2.5 Elucidating the role of AhR in astrocytes after injury using single-cell RNA sequencing.....	29
2.5.1 Quality control of sequenced cells .....	30
2.5.2 ACSA-2+ MACS sorting enriched for astrocytes and oligodendrocytes.....	31
2.5.3 Non-recombined astrocytes show heterogeneity in their expression profiles ...	34
2.5.4 AhR-deficient astrocytes maintain heterogeneous functions .....	38
2.5.5 Analysis of injured astrocytes reveals a subpopulation of astrocytes with stem cell characteristics .....	41
2.5.6 What are the AhR-dependent processes regulated in 5_5dpi astrocytes with stem cell characteristics?.....	49
2.5.7 Are dedifferentiated astrocytes derived from proliferating astroglia? .....	52
<b>3 Discussion</b> .....	<b>55</b>
3.1 The aryl hydrocarbon receptor is necessary for the dedifferentiation of astrocytes after injury .....	55
3.2 The astrocyte-specific AhR does not alter the proliferation of astrocytes and infiltration of leukocytes .....	57
3.3 Heterogeneity of astrocytes observed by scRNAseq .....	58
3.4 Downstream targets of AhR signaling involved in the acquisition of stem cell properties of reactive astrocytes .....	60
3.5 Concluding remarks .....	61
<b>4 Material and Methods</b> .....	<b>63</b>
4.1 Materials.....	63

4.1.1	Reagents and solutions .....	63
4.1.2	Laboratory equipment .....	67
4.1.3	Kits .....	69
4.1.4	Antibodies and dyes.....	69
4.1.5	Software.....	70
4.2	<i>Experimental animals</i> .....	71
4.3	<i>Genotyping</i> .....	71
4.3.1	DNA extraction from ear clips.....	71
4.3.2	Polymerase chain reaction.....	71
4.3.3	Gel electrophoresis .....	73
4.4	<i>Application of tamoxifen</i> .....	73
4.5	<i>Surgical procedure</i> .....	73
4.6	<i>BrdU and EdU labeling</i> .....	74
4.7	<i>Perfusion and brain sectioning</i> .....	74
4.8	<i>Immunohistochemistry and EdU detection</i> .....	75
4.9	<i>Confocal microscopy</i> .....	75
4.10	<i>Protein extraction and Western Blot</i> .....	75
4.11	<i>Neurosphere assay</i> .....	76
4.12	<i>Single cell RNA sequencing</i> .....	77
4.12.1	Sample preparation .....	77
4.12.2	Library preparation and sequencing.....	77
4.12.3	Analysis of sequenced data.....	78
4.12.4	Gene Ontology analysis.....	79
4.13	<i>Statistical analysis</i> .....	79
<b>5</b>	<b>Abbreviations</b> .....	<b>81</b>
<b>6</b>	<b>References</b> .....	<b>85</b>
<b>7</b>	<b>Acknowledgments</b> .....	<b>101</b>
<b>8</b>	<b>List of publications</b> .....	<b>103</b>
<b>9</b>	<b>List of contributions</b> .....	<b>105</b>

## List of Figures

Figure 1: Phases and time course of the multicellular response to acute focal injury in the CNS. ....	4
Figure 2: Neural stem cell niches in the adult mammalian brain. ....	9
Figure 3: Shared signals between reactive astrocytes after injury and neural stem cells in their niches. ....	10
Figure 4: Functional domains of AhR.....	13
Figure 5: AhR signaling pathway.....	14
Figure 6: AhR knock-out upon Cre-dependent recombination .....	19
Figure 7: AhR knock-out in astrocytes results in loss of neurosphere-forming capacity after injury.....	22
Figure 8: AhR knock-out does not alter proliferation of astrocytes at the injury site .....	25
Figure 9: AhR knock-out does not alter proliferation of heterogenous populations of astrocytes at the injury site.....	26
Figure 10: Leukocyte extravasation upon injury .....	28
Figure 11: Setup for scRNAseq experiment.....	30
Figure 12: Quality Control of scRNAseq experiment .....	31
Figure 13: Defining cell types identified in scRNAseq experiment .....	33
Figure 14: Characterization of subclustered non-recombined astrocytes .....	36
Figure 15: GO term-based characterization of NR subclustered astrocytes .....	37
Figure 16: Characterization of subclustered recombined AhR-KO astrocytes.....	40
Figure 17: GO term-based characterization of AhR-KO subclustered astrocytes.....	41
Figure 18: Characterization of subclustered astrocytes from injured brain.....	43
Figure 19: Comparison of NR and KO astrocytes of subclustered astrocytes from injured brain .....	44
Figure 20: Cluster 5_5dpi astrocytes show stem cell characteristics .....	45
Figure 21: KEGG Pathway of signaling pathways regulating pluripotency of stem cells .....	48
Figure 22: Transcription factor ranking of cluster 5_5dpi astrocytes.....	49
Figure 23: Differential gene expression analysis between NR and KO astrocytes in cluster 5_5dpi.....	51
Figure 24: Velocity analysis of injured astrocytes .....	53



## Abstract

Traumatic brain injury and degenerative diseases cause neuronal loss with detrimental outcomes in patients. The limited capacity of the adult mammalian central nervous system to replenish lost neurons harbors major challenges. Regenerative therapy aims to replace those lost neurons by using different strategies. Next to the transplantation of neural precursor cells, the direct reprogramming of brain-resident cells into neurons provides promising approaches for novel regenerative therapies. However, it is not clear which glial cells could be the prime target for direct conversion. Importantly, a subpopulation of astrocytes acquires stem cell properties after injury. Therefore, this subset is prone to be a great candidate for direct reprogramming into neurons. The mechanisms underlying astrocyte dedifferentiation and acquisition of stem cell properties are not fully understood. Recently, multiple studies have shown that the aryl hydrocarbon receptor (AhR) may potentially be involved in this process.

Hence, I used a conditional and inducible knock-out mouse model of AhR in astrocytes in combination with the neurosphere assay to investigate the stem cell potential of AhR-deficient astrocytes after stab wound injury. Notably, I could demonstrate that AhR is required for the neurosphere-forming capacity of astrocytes after brain injury. Furthermore, histological analysis revealed that the astrocyte-specific AhR knock-out did not alter astrocyte proliferation or leukocyte extravasation *in vivo*. Encouraged by these results, I used single-cell transcriptomics of magnetic-activated cell sorted non-recombined and AhR-deficient astrocytes to investigate the cell-autonomous regulation of astrocyte fate in an AhR specific manner. I could identify a group of astrocytes that reacts to injury in an AhR-dependent manner and upregulated characteristic genes of stem cell maintenance. Importantly, this population of astrocytes also upregulated Wnt signaling in response to injury, suggesting a potential role of the Wnt signaling cascade in AhR mediated acquisition of stem cell properties in a subpopulation of astrocytes. In addition, I used this data set of single-cell transcriptomics to investigate the heterogeneity of astrocytes. I could detect various subtypes of astrocytes based on their expression patterns in injured and intact conditions, such as reactive, homeostatic, pro-, and anti-inflammatory as well as proliferating astrocytes. Subtypes of homeostatic astrocytes could be linked to various functions such as neurovascular coupling, extracellular matrix organization, and neuronal support.

Taken together, I could demonstrate that AhR signaling is required for reactive astrocytes to dedifferentiate and subsequently acquire stem cell potential after injury. This process may be influenced by Wnt signaling in an AhR-specific manner. AhR is thus a potential target for novel therapeutic strategies in the context of regeneration after brain injuries.



# 1 Introduction

The brain is the central structure in our body that is responsible for processing our feelings, actions, learning, and memory. Together with the spinal cord, it forms the central nervous system (CNS) and regulates multiple functions in various organs that are essential to life. Damages to this highly complex and well-structured organ lead to irreversible loss of neurons, which is implicated in neural circuit malfunctions of the affected and connected CNS regions. The regenerative capacity in the adult mammalian CNS is vastly limited, and hence, therapies aiding the replacement of lost neurons are a major challenge in regenerative medicine.

## 1.1 CNS response to traumatic brain injury

Traumatic brain injury (TBI) is, next to ischemic stroke, a type of acute insult to the CNS and is also considered to be focal in form of a stab wound injury. TBI is a global health issue affecting up to 74 million people each year causing death and disability (Dewan et al., 2019; Haarbauer-Krupa et al., 2021). Despite its acute nature, TBI can also trigger additional chronic outcomes, such as seizures, psychiatric disorders, and dementia (Stocchetti & Zanier, 2016). These long-term effects impede the life of many TBI patients in multiple facets and it is thus imperative to better understand the cellular and molecular processes governing TBI.

The response of the CNS to TBI is characterized by a multicellular reaction that can be divided into three phases. In the primary phase of TBI, acute local cell death and neurite damage occur, followed by vascular breach resulting in an initial rapid response by platelet influx and subsequent coagulation, an important process of hemostasis (Figure 1) (Burda & Sofroniew, 2014; Moore et al., 2021). The vascular breach is associated with blood-brain barrier (BBB) leakage. In physiological conditions, the BBB is responsible for restricting large or hydrophilic molecules, pathogens, and hematopoietic cells circulating in the blood from entering the brain in a non-selective manner, a key feature to preserve brain homeostasis (Daneman & Prat, 2015). In addition, cellular damage causes the release of damage-associated molecular patterns (DAMP), which induce astrocytes and microglia to secrete a variety of chemokines and cytokines to instruct leukocytes to extravasate from the blood vessels to the brain parenchyma (Alam et al., 2020). The recruitment of infiltrating leukocytes is accelerated by the disruption of the BBB. These infiltrating leukocytes, especially neutrophils, but also CNS resident microglia promote cellular debris removal (Alam et al., 2020; Donat et al., 2017). In addition, astrocytes are implicated in phagocytosis upon insult and have the potential to compensate for dysfunctional microglia (Konishi et al., 2020; Morizawa et al., 2017). Noteworthy, a secondary injury like the

subacute neuronal loss is initiated soon after insult by glutamate overproduction at synapses that leads to Ca<sup>2+</sup>-mediated excitotoxicity via excessive glutamate receptor activation (P. Luo et al., 2019).

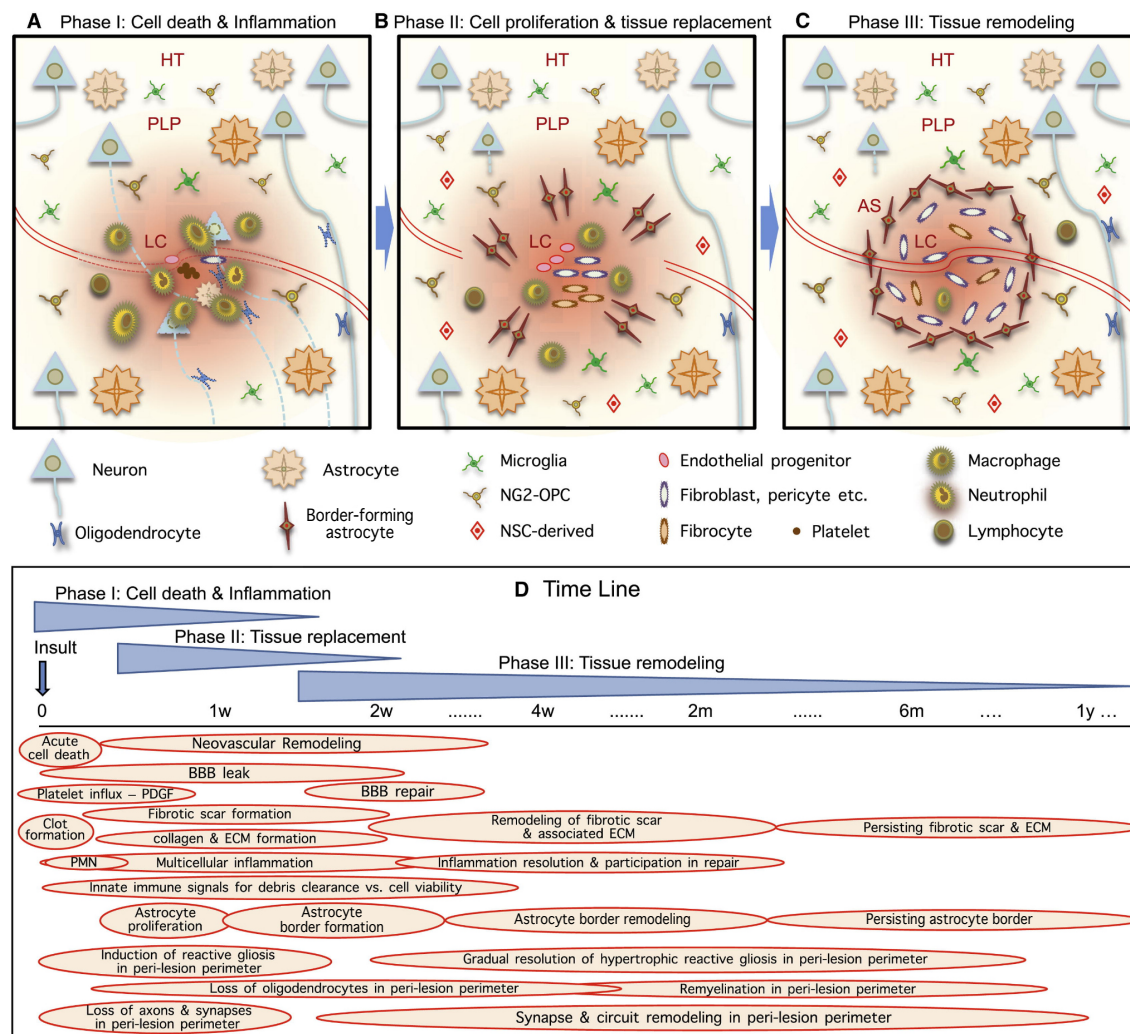


**Figure 1: Phases and time course of the multicellular response to acute focal injury in the CNS.**

(Adapted from Burda and Sofroniew 2014, <https://doi.org/10.1016/j.neuron.2013.12.034>, License Number: 5267231217506)

The response during the second phase of acute focal CNS injury, like stab wound injury or ischemia, is defined by the proliferation and migration of several cell types to assist in tissue replacement (Figure 1) (Burda & Sofroniew, 2014). Microglia and oligodendrocyte precursor cells (OPC) migrate towards the lesion site shortly after TBI and start to proliferate (Dimou & Götz, 2014; Donat et al., 2017; Hughes et al., 2013; Nimmerjahn et al., 2005). Some of the OPCs become hypertrophic and polarize towards the site of injury (von Streitberg et al., 2021). The accumulation of the proliferating OPCs at the injury site showed to be beneficial in brain repair (von Streitberg et al., 2021). Furthermore, non-neural cells like pericytes, fibrocytes, fibroblasts, and inflammatory cells migrate to the injury site and proliferate, ultimately resulting in a fibrotic scar tissue upon spinal cord insult (Dorrier et al., 2021; Göritz et al., 2011; Soderblom et al.,

2013). The proliferation of endothelial cells is linked to neovascularization (Casella et al., 2002). Astrocytes, however, do migrate towards the damaged area in the spinal cord but not in the brain (Bardehle et al., 2013; Okada et al., 2006). Upon TBI, astrocytes become hypertrophic and start to proliferate to form a border separating the highly inflammatory lesion core from the intact neural parenchyma (Anderson et al., 2016; Faulkner et al., 2004; Frik et al., 2018). To clarify, the border formed by astrocytes has been termed astroglial scar in the past decades. However, a recently published review strongly proposed to change the scar terminology into border formation due to the scar tissue definition in other well-studied organs (Sofroniew, 2020). Hence, I am going to use the term border-forming astrocytes throughout my thesis instead of scar-forming astrocytes.

The third phase of CNS response to TBI consists of tissue remodeling that includes BBB repair, fibrotic scar, and astrocyte border-tissue reorganization by changes in the extracellular matrix (ECM), as well as chronic neuroinflammation, which includes prolonged activation of microglia and astrocytes and the production of proinflammatory cytokines (Figure 1) (Burda & Sofroniew, 2014; Schimmel et al., 2017; Xiong et al., 2018). The long-lasting neuroinflammation upon TBI may lead to the development of neurodegenerative diseases such as Alzheimer's disease and chronic traumatic encephalopathy (Jassam et al., 2017). Release of ECM molecules and activation of proteases, mainly by microglia and astrocytes, results in long-term ECM remodeling of the injury site and peri-lesion region, which negatively impacts neuronal circuits (Burda & Sofroniew, 2014; George & Geller, 2018). In addition, a recent study conducted on zebrafish suggests that also OPCs may be involved in the remodeling process of the ECM upon injury (Sanchez-Gonzalez et al., 2022). A better understanding of chronic neuroinflammation and ECM remodeling processes upon TBI would allow the development of novel therapies for such detrimental injuries.

## 1.2 Astrocytes in health and disease

As described above, astrocytes play a crucial role in TBI response. Hence, I want to introduce this cell type in further detail. The central element of astrocytic function is to maintain homeostasis in the CNS. Water homeostasis is controlled by astrocytes via aquaporin 4 channels, localized at astrocyte endfeet, which are in close contact with blood vessels (Daneman & Prat, 2015; Min & van der Knaap, 2018). They are part of the BBB and allow neurovascular coupling, which is the effect of neural activity regulating the cerebral blood flow and is mediated by astrocytes via arachidonic acid metabolites and potassium ions (MacVicar & Newman, 2015). The regulation of the cerebral blood flow to the site of neural activation is important to compensate for the energy demands upon neural activity (MacVicar & Newman, 2015). In

addition, astrocytes provide neurons with various glycolytic metabolites and can store glucose in form of glycogen (Bélanger et al., 2011; Bonvento & Bolaños, 2021). Astrocytes do also maintain the homeostasis of important ions in synaptic signaling such as  $K^+$ ,  $Cl^-$  and  $Ca^{2+}$  (Verkhratsky & Nedergaard, 2018). Furthermore, astrocytes are noted for their critical contribution to neurotransmitter management through metabolic pathways and their supply to neurons with glutamine, a precursor for the excitatory and inhibitory neurotransmitters glutamate and  $\gamma$ -aminobutyric acid (GABA), respectively (Verkhratsky & Nedergaard, 2018). In addition to the close interactions of astrocytes and neuronal synapses, astrocytes are also involved in synaptogenesis in the healthy and injured adult CNS (Tsai et al., 2012). Moreover, astrocytes regulate neurogenesis in the adult brain (Asrican et al., 2020). Remarkably, astrocytes are also vital in maintaining systemic homeostasis like sleep and reproduction control (Verkhratsky & Nedergaard, 2018).

This functional diversity of astrocytes is linked to the morphological and molecular heterogeneity of this cell population across different brain regions (Sofroniew & Vinters, 2010; Verkhratsky & Nedergaard, 2018). Recent studies, however, also suggest astrocyte heterogeneity within the same brain region (Batiuk et al., 2020; Bayraktar et al., 2020; Lanjakornsiripan et al., 2018; Ohlig et al., 2021). A study observed morphological alterations of layer-specific astrocytes, and by utilizing fluorescent activated cell sorting of upper- and deep-layer astrocytes molecular differences in the somatosensory cortex have been identified (Lanjakornsiripan et al., 2018). This heterogeneity of astrocytes has been further corroborated by single-cell RNA sequencing (scRNAseq) experiments (Batiuk et al., 2020; Bayraktar et al., 2020; Ohlig et al., 2021). Furthermore,  $Ca^{2+}$  transient properties of astrocytes varied by the location in the cortex across the dorso-ventral axis, showing that the molecular heterogeneity results in functional differences (Batiuk et al., 2020). The field of astrocyte heterogeneity is particularly interesting due to the varying responses of reactive astrocytes to CNS damage, and thus, should be further investigated in health and disease.

Astrocyte reactivity describes the response of astrocytes to CNS injury and disease, and it is characterized by morphological changes like hypertrophy and polarization as well as upregulation of intermediate filaments such as glial acidic fibrillary protein (GFAP) and vimentin, which serve important functions in reactive astrocytes to limit CNS insult (Middeldorp & Hol, 2011; Pekny & Pekna, 2014). In addition, early studies investigating the transcriptome of reactive astrocytes resulted in altered gene expression compared to homeostatic astrocytes that were not exposed to injury (Sirko et al., 2015; Zamanian et al., 2012). This response of astrocytes is diverse across different CNS pathologies due to distinct signaling molecules derived from various sources (Sofroniew, 2020). A heterogeneous astrocyte reactivity can also be observed

within the same CNS pathology such as TBI. For example, reactive astrocytes primarily serve a pro-inflammatory purpose by guiding leukocytes from the blood periphery to the brain parenchyma via cytokines immediately after injury (Alam et al., 2020). However, another population of reactive astrocytes exhibits a mainly anti-inflammatory phenotype upon TBI, for example by repair of the BBB, thus restricting the spread of inflammatory cells after insult (Bush et al., 1999; Sofroniew, 2015). An important factor in limiting leukocyte extravasation is the signal transducer and activator of transcription 3 (STAT3) (Okada et al., 2006; Wanner et al., 2013). Experiments in the spinal cord demonstrated that STAT3 induces reactive astrocytes to surround fibrotic and inflammatory cells at the insulted area and is also associated with their proliferation upon injury (LeComte et al., 2015). The significance of STAT3 signaling in regulating the proliferation of reactive astrocytes in the brain was shown by Wanner and others using a stroke mouse model (Wanner et al., 2013). The proliferation of reactive astrocytes occurs mainly in invasive injuries with disrupted BBB, and they are crucial for BBB repair and astrocyte border formation (Frik et al., 2018; Sirko et al., 2013; Sofroniew, 2015, 2020). Additionally, it has been observed that the majority of proliferating astrocytes are located juxtavascular, adjacent to blood vessels (Bardehle et al., 2013; Frik et al., 2018; Heimann et al., 2017). The proliferation of astrocytes does not only have anti-inflammatory effects by limiting leukocyte infiltration but is also regulated by itself (Frik et al., 2018). This cross-talk of immune cells and astrocytes has long-term effects. Frik and colleagues have shown that the ablation of infiltrating leukocytes leads to increased astrocyte proliferation at the injury site, and reduced astrocyte border formation (Frik et al., 2018). This was accompanied by an increase of neurons at the injury site 4 weeks post-injury suggesting a neuroprotective outcome upon ablation of infiltrating leukocytes (Frik et al., 2018). The border formation of astrocytes separating the lesion core and intact neural tissue has been associated with limited regenerative potential by impeding axonal regeneration (Pekny & Pekna, 2014). However, a growing body of evidence suggests a beneficial role of reactive astrocyte borders upon CNS insult in neuroprotection, restricting neuroinflammation, and even in supporting axonal regrowth (Anderson et al., 2016; Bush et al., 1999; Faulkner et al., 2004; Sofroniew, 2015). A distinction between proliferative reactive astrocytes that contribute to the border formation and non-proliferative reactive astrocytes has been proposed, the latter ones being expected to interact with healthy tissue and support its physiological function (Sofroniew, 2020). Furthermore, some of the reactive astrocytes dedifferentiate upon TBI and acquire stem cell potential after injury *in vitro* (Buffo et al., 2008; Lang et al., 2004; Sirko et al., 2009, 2013). This is of particular interest in the field of regenerative medicine, which aims to replace lost neurons. It has thus been proposed to achieve this challenging task by transplanting neural progenitor cells or endogenous recruitment of aNSCs (Grade & Götz, 2017). The acquired plasticity of reactive astrocytes allows for potential new targets to replace neurons *in situ* in the

field of regenerative medicine (Grade & Götz, 2017). Indeed, it has been proven that reactive astrocytes can be reprogrammed into pyramidal neurons after TBI *in vivo* by overexpression of nuclear receptor related 1 protein (Nurr1) and Neurogenin 2 (Neurog2) (Mattugini et al., 2019). In addition, interneurons could be generated from cortical astrocytes by genetically blocking Notch signaling in astrocytes after injury, further supporting the potential use of reactive astrocytes for *in situ* regenerative approaches (Zamboni et al., 2020). However, the process of dedifferentiation, hence, the acquisition of stem cell potential in a subpopulation of reactive astrocytes is not fully understood.

In the year 2006 Takahashi and Yamanaka for the first time showed that somatic cells could be reprogrammed into so-called induced pluripotent stem cells (iPSC) and thus dedifferentiate by the use of the four transcription factors (Oct-3/4, Sox2, c-Myc, and Klf4) (Takahashi & Yamanaka, 2006). The idea behind this experiment was that embryonic stem cells were likely to express pluripotency-inducing factors that are important to maintain pluripotency (Takahashi & Yamanaka, 2006). Recently, the first clinical studies with iPSCs have been conducted in an attempt of treating Parkinson's Disease (Stoddard-Bennett & Reijo Pera, 2019). Dedifferentiation of somatic cells into stem cells thus has great potential in regenerative medicine. However, since the process of reactive astrocyte dedifferentiation is not fully understood and it is already known that reactive astrocytes share features with neural stem cells, it is important to understand the similarities of both cell populations and their respective environment.

### 1.3 What can we learn from neural stem cells?

To compare reactive astrocytes and neural stem cells, I first would like to explain the concept of stem cells and then assess the parallels between neural stem cells and reactive astrocytes. Stem cells are undifferentiated cells that are defined by self-renewal capacity and their potential to differentiate into specialized cell types (Do & Schöler, 2009). This definition is also referred to as stemness. The potency of a stem cell is organized hierarchically based on its developmental status, starting with the totipotent zygote and blastomeres that can differentiate into any cell type forming a whole organism. Pluripotent stem cells exist during early embryogenesis and are classified by the capability to differentiate into any cell type except those from the trophoblast lineage (Do & Schöler, 2009). Multipotency describes the ability of stem cells to give rise to multiple cell types within the same lineage. Neural stem cells (NSC) are defined as multipotent and can generate neurons and macroglia such as astrocytes, oligodendrocytes, and ependymal cells (Robel et al., 2011). Stem cells that can differentiate into only one cell type are considered unipotent (Do & Schöler, 2009). The stemness potential can

be investigated *in situ* for example by lineage tracing or live imaging (Barbosa et al., 2015; Bonaguidi et al., 2011; Calzolari et al., 2015; Pilz et al., 2018). In addition, it is also possible to test for self-renewal and multipotency of NSCs using the neurosphere assay *in vitro* (Reynolds & Weiss, 1992). Neurospheres are cellular aggregates derived from a single cell with self-renewal characteristics, which can be observed by the passage propagation of these neurospheres. The ability to give rise to neurons, astrocytes, and oligodendrocytes in differentiation conditions characterizes their multipotency (Robel et al., 2011).

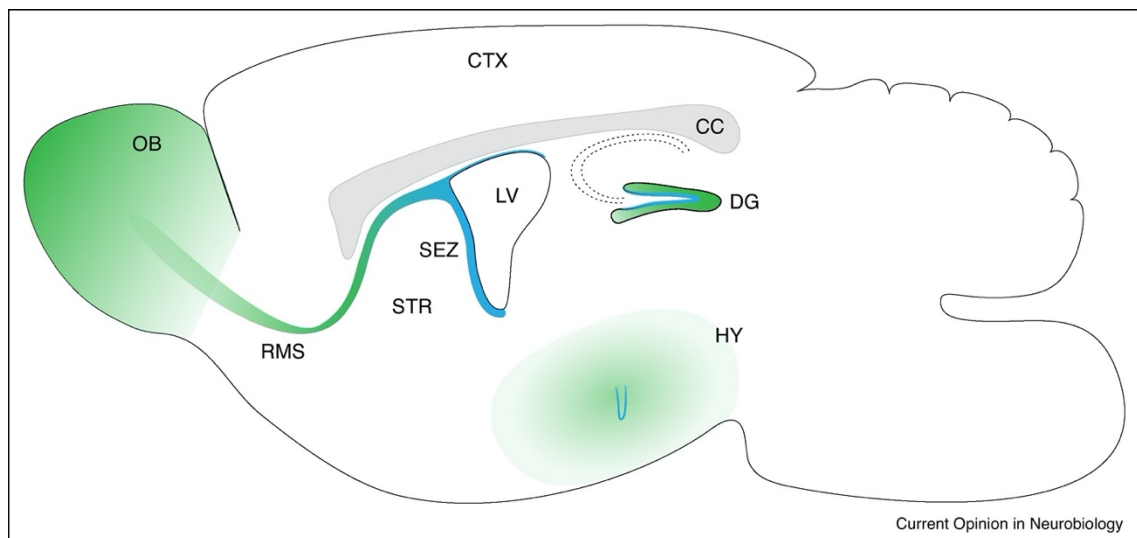


**Figure 2: Neural stem cell niches in the adult mammalian brain.**

Regions containing aNSCs are depicted in blue and regions of neurogenesis are shown in green. OB: olfactory bulb; RMS: rostral migratory stream; STR: striatum; SEZ: subependymal zone; LV: lateral ventricle; CTX: cortex; CC: corpus callosum; DG: dentate gyrus; HY: hypothalamus (Falk and Götz 2017, <https://doi.org/10.1016/j.conb.2017.10.025>, open access article published under the terms of the Creative Commons Attribution-NonCommercial-No Derivatives License (CC BY NC ND)).

As described above, NSCs are multipotent during development and generate all neurons, astrocytes, and oligodendrocytes. Because of their radial morphology connecting the apical and basal membrane, they are also known as radial glia cells (RGC) (Falk & Götz, 2017). In addition, RGCs, generate adult neural stem cells (aNSC) that maintain radial morphology and reside only in three defined regions within the adult mammalian brain, namely the subependymal zone (SEZ) of the lateral ventricle, the subgranular zone (SGZ) of the hippocampal dentate gyrus (DG) and the third ventricle in the hypothalamus (Figure 2) (Ninkovic & Götz, 2013). Interestingly, aNSCs share the expression of many proteins like GLAST (L-glutamate/L-aspartate transporter), GLT1 (excitatory amino acid transporter 2), S100 $\beta$ , Prominin1, and ALDH1L1 (aldehyde dehydrogenase 1 family, member L1) not only with RGCs but also with astrocytes (Anthony & Heintz, 2007; Dimou & Götz, 2014; Robel et al., 2011). Furthermore, reactive astrocytes in the cerebral cortex upregulate immature markers like GFAP, vimentin, and nestin, which are also shared with adult and embryonic NSCs (Robel et al., 2011). Nevertheless, only a very small fraction of reactive astrocytes can dedifferentiate and acquire stem cell

potential *in vitro* after TBI (Buffo et al., 2008; Sirko et al., 2013). Due to the similarities between NSCs and reactive astrocytes and their potential to acquire stem cell characteristics, it is worthwhile to examine the parallels of signaling cascades occurring in reactive astrocytes upon injury and the adult neural stem cell niches.

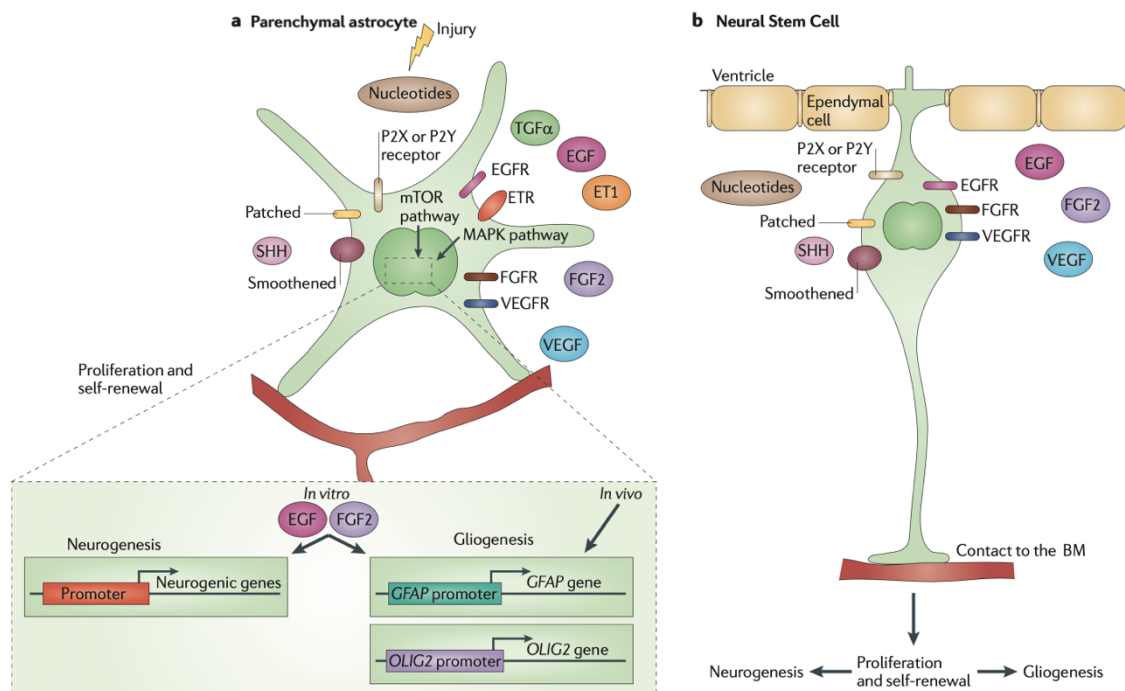


**Figure 3: Shared signals between reactive astrocytes after injury and neural stem cells in their niches.** (Adapted from Robel et al. 2011, <https://doi.org/10.1038/nrn2978>, License Number: 5270311314840)

TBI induces the release of the growth factors such as EGF (epidermal growth factor) and FGF2 (basic fibroblast growth factor) by different cell types and the upregulation of the respective receptors in astrocytes (Figure 3) (Robel et al., 2011). Additionally, it has been shown that FGF2 signaling induces the proliferation of reactive astrocytes not only *in vitro* but also *in vivo* (Gomez-Pinilla et al., 1995; Kang et al., 2014). Similar effects have been shown with EGF signaling on astrocytes *in vitro* (Chan et al., 2019). Both growth factor signaling pathways can activate the mammalian target of rapamycin (mTOR) and mitogen-activated protein kinase (MAPK) pathways (Figure 3) (Robel et al., 2011). It has been demonstrated that mTOR is upregulated in reactive astrocytes (Codeluppi et al., 2009). Furthermore, genetically overactivation of mTOR specifically in astrocytes by loss of PTEN (Phosphatase and tensin homolog) resulted in astrocyte reactivity and proliferation without inducing an injury (Fraser et al., 2004). Activation of the extracellular signal-regulated protein kinase (ERK) and Jun N-terminal kinase (JNK) pathways leads to the MAPK signaling pathway being upregulated in astrocytes upon injury and regulates GFAP expression and proliferation in reactive astrocytes (Gadea et al., 2008). Similar to the injury response, the growth factors EGF and FGF2 play a central role in orchestrating the proliferative activity of aNSCs (Doetsch et al., 2002; Frinchi et

al., 2008; Kuhn et al., 1997; Tao et al., 1997). Interestingly, EGF and FGF2 signaling are not only important for cell division but also linked to lineage decisions in the CNS. For example, the infusion of EGF into the lateral ventricles at the site of the SEZ stimulated aNSCs to an enhanced generation of astrocytes (Kuhn et al., 1997). In contrast, FGF2 administration induced enrichment of neurogenesis in the olfactory bulb, the region of neurogenesis of aNSCs located in the SEZ that migrate as neuroblasts via the rostral migratory stream to the olfactory bulb (Kuhn et al., 1997). Taken together, both growth factors are potential candidates to mediate the dedifferentiation of astrocytes upon TBI.

In addition to the growth factors mentioned, other signaling pathways are well-known regulators of aNSC behavior and some of them are upregulated upon TBI (Figure 3). For instance, sonic hedgehog (SHH) signaling is a key factor to maintain the proliferation of aNSC in both the SEZ and the DG of the hippocampus (Lai et al., 2003; Machold et al., 2003). SHH signaling is also increased upon invasive injury in the cerebral cortex and has been shown to regulate the proliferation of reactive astrocytes (Sirko et al., 2013). Of note, it was demonstrated that SHH originated from the cerebrospinal fluid, which might explain the fact that reactive astrocyte proliferation has been linked to BBB disruption (Burda & Sofroniew, 2014; Dimou & Götz, 2014; Sirko et al., 2013). Additionally, an increase of neurospheres has been observed, indicating that SHH does not only increase proliferation but also may regulate dedifferentiation of reactive astrocytes (Sirko et al., 2013). However, the deletion of SHH signaling in astrocytes did not fully abolish the stem cell potential of reactive astrocytes, suggesting further signaling pathways to be involved in the process of dedifferentiation. Also, the prominent wingless-type (Wnt) signaling, which is known for its fundamental roles during development, is involved in neurogenesis and aNSC self-renewal in the hippocampal SGZ and the SEZ via the canonical  $\beta$ -catenin pathway (Adachi et al., 2007; Knotek et al., 2020; Lie et al., 2005; Qu et al., 2010; Rim et al., 2022). Noteworthy, Wnt-dependent  $\beta$ -catenin signaling is upregulated in reactive astrocytes and associated with their proliferative status upon TBI (White et al., 2010). Yet, there are also differences observed between aNSCs and reactive astrocytes. For example, the bone morphogenic protein (BMP) signaling is recognized for its role in positively regulating neurogenesis in the aNSC niches by blocking the gliogenic fate (Colak et al., 2008). Conversely, BMP signaling after injury fosters astrocyte fate by synergistic effects together with STAT signaling (Robel et al., 2011). Interestingly, a recent study could demonstrate that diencephalic astrocytes proliferate *in vivo* and even form neurospheres *in vitro* without injury in a Smad4-dependent way, a downstream target of BMP signaling (Ohlig et al., 2021).

Furthermore, the reaction of aNSCs has also been intensively studied upon TBI in the CNS of species with high regenerative capacities such as the zebrafish (*Danio rerio*) (Barbosa et al., 2015; Baumgart et al., 2012; Di Giaimo et al., 2018; Kishimoto et al., 2012; Kroehne et al., 2011; Kyritsis et al., 2012; Sanchez-Gonzalez et al., 2022). It has been shown that the zebrafish CNS can regenerate brain tissue, including the replacement of lost neurons, which is referred to as restorative neurogenesis. (Barbosa et al., 2015; Baumgart et al., 2012; Di Giaimo et al., 2018; Kroehne et al., 2011; Kyritsis et al., 2012). Interestingly, restorative neurogenesis in the zebrafish brain is initiated by inflammation in response to injury (Kyritsis et al., 2012). Acute inflammation in the zebrafish brain starts with the accumulation of neutrophils and microglia at the injury site that is followed by activation of OPCs within 1 day post injury (Baumgart et al., 2012; Kroehne et al., 2011; Sanchez-Gonzalez et al., 2022). In the second phase, adult NSCs are activated and start to proliferate and generate new neurons (Di Giaimo et al., 2018; Kyritsis et al., 2012). Live imaging of aNSCs after an injury has shown that the generation of new neurons upon injury can also occur without prior proliferation of aNSCs and is referred to as direct conversion (Barbosa et al., 2015; Di Giaimo et al., 2018). Importantly, the aryl hydrocarbon receptor (AhR) has been identified as a key regulator for timing restorative neurogenesis and thus brain regeneration (Di Giaimo et al., 2018). Low levels of AhR signaling did promote proliferation and/or self-renewal of aNSCs a few days upon injury (Di Giaimo et al., 2018). High levels of AhR signaling at later stages post-injury did induce direct conversion of aNSCs into neurons (Di Giaimo et al., 2018). In addition, a recently published study demonstrated the importance of AhR signaling in aNSCs in an Alzheimer's Disease (AD) zebrafish model system that is based on the injection of A $\beta$ 42 into the ventricles (Siddiqui et al., 2021). In line with the work of Di Giaimo and others, the study could show that activation of AhR signaling reduces proliferation of aNSCs while antagonization of AhR and A $\beta$ 42 injection results in an increase in cell division (Siddiqui et al., 2021). Together, these studies have shown that AhR signaling is involved in brain regeneration as well as in the neuronal potential and proliferation of aNSCs in the zebrafish brain after injury. Of note, AhR expression has also been described in reactive astrocytes upon TBI and stroke in mouse models (Chen et al., 2019; Frik et al., 2018).

In conclusion, significant efforts have already been made to understand the process of dedifferentiation of reactive astrocytes and how they acquire stem cell capacities. Nonetheless, this highly complex phenotype is not yet fully understood, and more research needs to be done to provide potential novel regenerative therapies.

## 1.4 The aryl hydrocarbon receptor

As described above, AhR signaling is crucial for brain regeneration, promotes the neuronal potential of aNSCs, and is also expressed in reactive astrocytes. Therefore, AhR is a strong candidate to regulate astrocyte dedifferentiation and stem cell potential acquisition. AhR is a ligand-activated transcription factor (TF) that is part of the bHLH (basic helix-loop-helix) TF family, a domain that allows DNA binding (Figure 4) (Stockinger et al., 2014). The ligand-binding activity is ensured by the interaction of the AhR PAS domain (PER [period circadian protein], with ARNT [AhR nuclear translocator], SIM [single minded protein] domain), which is also crucial for dimerization processes (Stockinger et al., 2014). These interactions and AhR cellular localization determine the AhR signaling activity (Figure 5). If the signaling is inactive, AhR is bound in the cytoplasm to the chaperone protein HSP90 (heat shock protein 90) that interacts with the bHLH and PAS domain of AhR (Figure 4 and 5) (Antonsson et al., 1995; Denis et al., 1988; Perdew, 1988; Perdew & Bradfield, 1996). Importantly, this interaction with HSP90 retains the AhR in a conformational state allowing a high affinity for ligand-binding (Pongratz et al., 1992). Moreover, not only does HSP90 bind to AhR in the cytoplasm but also additional interactors like the AIP (AhR-interacting protein) and the cochaperone p23 (Stockinger et al., 2014). The interaction of AIP with the PAS domain of AhR and HSP90 stabilizes the protein complex and blocks ubiquitin-dependent degradation (Kazlauskas et al., 2000; Lees et al., 2003; Meyer & Perdew, 1999; Morales & Perdew, 2007). The co-chaperone p23, a member of the HSP90 machinery, binds to AhR and HSP90, and hence, blocks the unspecific activation of AhR in a ligand-independent manner (Kazlauskas et al., 1999, 2001).

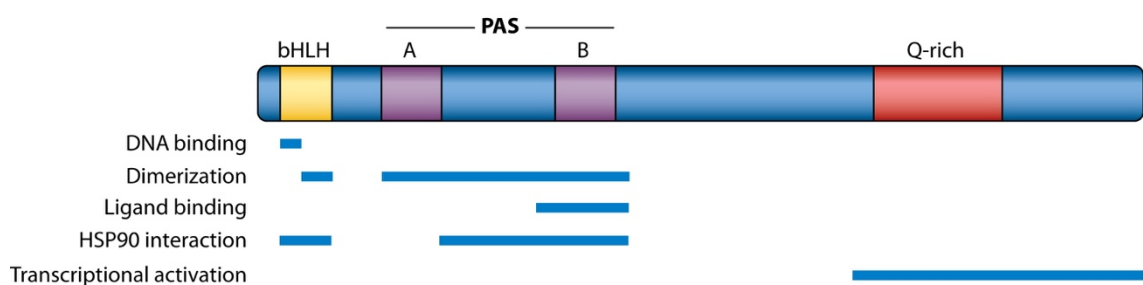


**Figure 4: Functional domains of AhR**

(Stockinger et al. 2014, <https://doi.org/10.1146/annurev-immunol-032713-120245>, License Number: 1201738-1, ISSN: 1545-3278)

The activation of AhR signaling follows ligand binding, which is postulated to result in a conformational change of AhR within the HSP90 chaperone complex leading to the exposure of the nuclear localization signal, that is recognized by importin  $\beta$  and ultimately regulates the translocation into the nucleus (Figure 5) (Stockinger et al., 2014). The HSP90 chaperone complex dissociates upon dimerization of AhR with the AhR nuclear translocator (ARNT) located in the nucleus (McGuire et al., 1994). The dimerization of both proteins is required for AhR to bind

genomic sequences containing a dioxin responsive element (DRE) and act as a transcriptional regulator (Denison et al., 1988a, 1988b; Fukunaga et al., 1995). Well-known target genes of this transcriptional activation are cytochrome P450 enzymes (e.g. CYP1A1, CYP1A2, and CYP1B1) and the AhR repressor (AhRR). Both types of proteins have a negative feedback mechanism by either metabolizing the AhR ligand or disrupting the AhR/ARNT complex due to higher binding affinity for ARNT, respectively (Figure 5) (Bergander et al., 2004; Mimura et al., 1999; Wincent et al., 2009). At last, AhR is degraded by the proteasome after activation (Davarinos & Pollenz, 1999).

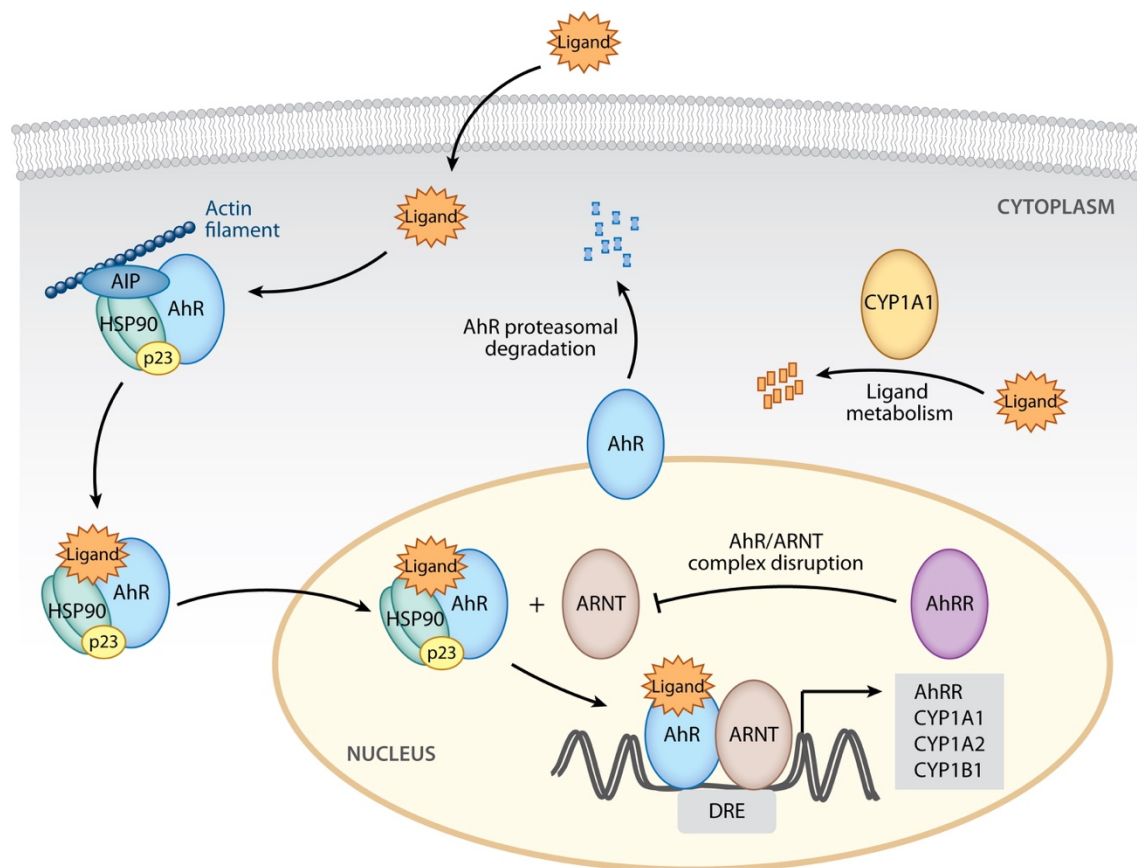


**Figure 5: AhR signaling pathway**

(Stockinger et al. 2014, <https://doi.org/10.1146/annurev-immunol-032713-120245>, License Number: 1201738-1, ISSN: 1545-3278)

One of the most prominent ligands of AhR signaling is TCDD (2,3,7,8-tetrachlorodibenzo-*p*-dioxin) due to its strong toxic effects and high affinity for AhR (Okey, 2007). Therefore, the role of AhR has been studied for a long time in the context of sensing xenobiotic chemicals. However, accumulating research in the past years changed their focus on physiological roles of the AhR signaling, and thus also on endogenous ligands (Okey, 2007; Rothhammer & Quintana, 2019; Stockinger et al., 2014). Metabolites of the essential amino acid tryptophan are known endogenous ligands of AhR (Stockinger et al., 2014). For example, bacterial degradation of tryptophan via tryptophanase follows the formation of various indoles, which have been shown to activate AhR in astrocytes (Rothhammer et al., 2016). Another

tryptophan metabolite often discussed as an AhR agonist is kynurenine, which is produced by indoleamine 2,3-dioxygenase (IDO) and tryptophan 2,3-dioxygenase (TDO) (Stockinger et al., 2014). In an additional enzymatic reaction, kynurenic acid can be formed that is not only an AhR agonist but also a well-known antagonist of ionotropic glutamate receptors and considered to be neuroprotective (Ostapiuk & Urbanska, 2022). The process of photolysis of tryptophan by visible and UV light ends in the formation of 6-formylindolo[3,2-b]carbazole (FICZ), a high-affinity ligand of AhR (Rannug et al., 1987; Wincent et al., 2009). Interestingly, in contrast to TCDD, the endogenous agonist FICZ is effectively metabolized by the AhR downstream target CYP1A1 (Bergander et al., 2004; Miniero et al., 2001; Wincent et al., 2009). Such a mechanism may give rise to prolonged AhR activation and consequently result in altered or ligand-specific outcomes of AhR signaling (Quintana & Sherr, 2013; Stockinger et al., 2014).

Initially, AhR function has been investigated in the nervous system mainly in the context of xenobiotic effects (Juricek & Coumoul, 2018). Growing evidence of research indicates a strong role of AhR in regulating stem cell self-renewal and differentiation (Casado, 2016; Di Giaimo et al., 2018; Gasiewicz et al., 2014; Mulero-Navarro & Fernandez-Salguero, 2016). Of particular interest for my thesis are studies investigating the role of AhR during neurogenesis in the adult mammalian system. For instance, AhR-deficiency in cerebellar granule neuron precursor cells led to a reduction in proliferation and increased differentiation into inhibitory granule neurons (Dever et al., 2016). In the adult organism, the knock-out of AhR causes reduced proliferation, differentiation, and cell survival in aNSCs of the hippocampal DG with the consequence of impaired memory functions (Latchney et al., 2013). Controversially, the activation of AhR signaling by exposure to TCDD had similar effects in wildtype mice, indicating that AhR needs to be tightly regulated to allow for proper neurogenesis (Latchney et al., 2013). Remarkably, the treatment with the endogenous ligand FICZ revealed an improvement of hippocampus-dependent behavioral tasks related to learning and memory (Keshavarzi et al., 2020). This was most likely due to an increase in neuronal differentiation in the DG (Keshavarzi et al., 2020). Improved neuronal differentiation in the adult hippocampus has also been described by the group of Sven Pettersson upon indole-dependent signaling mediated by AhR, which could not be reproduced by the application of kynurenine (Wei et al., 2021). In a stroke mouse model, an augmented proliferation of aNSCs has been noticed in the ipsilateral SEZ and hippocampal SGZ upon AhR knock-out in nestin-positive cells or AhR antagonization with 6,2',4'-trimethoxyflavone (Chen et al., 2019). Taken together, AhR plays a crucial role in regulating the behavior of adult neural stem cells, which in turn can influence animal behavior.

In the last years, AhR signaling has also become the center of attention regarding CNS insult and inflammation (Di Giaimo et al., 2018; Rothhammer & Quintana, 2019). It has been

shown that AhR mediates anti-inflammatory effects via type I interferons and indoles of metabolized dietary tryptophan in astrocytes (Rothhammer et al., 2016). These anti-inflammatory effects were key in reducing the EAE disease scores of the animals, resulting in a loss of hind limb paralysis (Rothhammer et al., 2016). Acute focal insult in a stroke mouse model causes upregulation of AhR expression in astrocytes and microglia (Chen et al., 2019). Strikingly, AhR knock-out in a nestin-dependent manner or systemic antagonization of AhR leads to a reduced infarct area (Chen et al., 2019). Furthermore, it has been reported that AhR expression is highest in juxtavascular astrocytes upon traumatic brain injury, the astrocyte population that preferentially proliferates (Frik et al., 2018). As already stated in section 1.3, the AhR pathway has central regulatory functions in zebrafish brain regeneration by inducing proliferation of aNSCs when AhR signaling is decreased and increasing differentiation into neurons when AhR signaling is elevated (Di Giaimo et al., 2018; Siddiqui et al., 2021). Noteworthy, the AhR agonist  $\beta$ -naphthoflavone (BNF), used by Di Giaimo and others, also disrupts astrocyte differentiation in a C6 glioma cell line, which is used as an *in vitro* model for astrocyte differentiation, indicating that AhR signaling is important in cell fate decisions (Takanaga et al., 2004). Finally, the first therapeutical approaches targeting AhR in multiple sclerosis have been made using laquinimod, which did result in reduced brain atrophy and was to some extent facilitated by astrocytes (Vollmer et al., 2014).

In conclusion, AhR signaling is activated upon ligand binding triggering nuclear translocation and transcriptional regulation. AhR plays a crucial role in stemness function in mice and regulates brain regeneration in zebrafish. Furthermore, the notion that AhR is highly expressed by the main population of proliferating reactive astrocytes upon TBI makes AhR a strong candidate gene being involved in the process of fate decision of reactive astrocytes.

## 1.5 Aims

Understanding the process of dedifferentiation of reactive astrocytes is important to develop new strategies for regenerative therapies. Our lab has shown that AhR signaling is crucial for brain regeneration and the neuronal potential of aNSCs in zebrafish (Di Giaimo et al., 2018). In addition, multiple studies have shown that AhR is important in aNSC fate decision and the response of astrocytes to CNS damage in mice. Therefore, AhR is a potential regulator of the dedifferentiation of reactive astrocytes upon TBI.

The main goal of my thesis was thus to investigate whether AhR signaling is involved in the dedifferentiation and gain of stem cell potential of reactive astrocytes after injury. The second aim was to study the effects of AhR in astrocytes in the context of CNS injury response *in vivo*. To work towards these two objectives, I exploited a combinatorial approach of transgenic mouse models, primary cell culture systems, western blot, and immunohistochemistry.

In addition, I focused on the cell-autonomous effects of the AhR pathway in astrocytes exposed to injury. Since AhR signaling results in transcriptional activation of its target genes, cell-autonomous changes can be detected on the mRNA level. Furthermore, only a subset of reactive astrocytes dedifferentiates upon injury. Thus, my third aim was to explore bioinformatically the heterogeneity and cell-autonomous changes of astrocytes with and without AhR knock-out by using single-cell transcriptomics of sorted astrocytes.



## 2 Results

### 2.1 The aryl hydrocarbon receptor knock-out system

For my PhD thesis, I utilized the Cre/loxP-system to induce a conditional knock-out of the aryl hydrocarbon receptor (AhR) by modifying the genomic DNA. The Cre/loxP-system uses the bacterial Cre recombinase that allows site-specific recombination of floxed DNA sequences. The floxed DNA sequence is defined by two flanking loxP sites, which consist of 34 bp, and based on their orientation define the recombination event. The floxed DNA sequence is excised if the flanking loxP sites are in the same orientation. If they are in the opposite direction, the floxed sequence is inverted (R. Feil, 2007).

Here, the second exon of *AhR* is floxed by two loxP sites in the same orientation in the *Ahrfx* mouse line (Walisser et al., 2005). The Cre-dependent excision of exon 2 of *AhR* leads to a premature stop codon at the beginning of exon 3 and thereby to a knock-out of AhR. To prove the knock-out model, I used the *Emx1<sup>Cre</sup>* mouse line due to the strong Cre activity in empty spiracle homeobox 1 (*Emx1*) expressing cells during cortical development (Gorski et al., 2002). The *Emx1<sup>Cre</sup>* mouse line was crossed to our *Ahrfx* mouse line including a GFP (green fluorescent protein) reporter with a floxed premature stop codon under the control of a CAG promoter (CAG-GFP) (Figure 6A). For this experiment proteins from cortex punches with a diameter of 2.5 mm were extracted (Figure 6B) and a subsequent western blot (WB) was performed to detect the AhR protein (Figure 6C). Indeed, a definite band of AhR at about 90kDa in all wildtype (wt; *AhR<sup>wt/wt</sup>*) and heterogeneous (*AhR<sup>wt/fl</sup>*) animals was identified. Importantly, this band was no longer detectable in AhR deficient (*AhR<sup>fl/fl</sup>*) animals (Figure 6C) leading to a knock-out at the protein level.

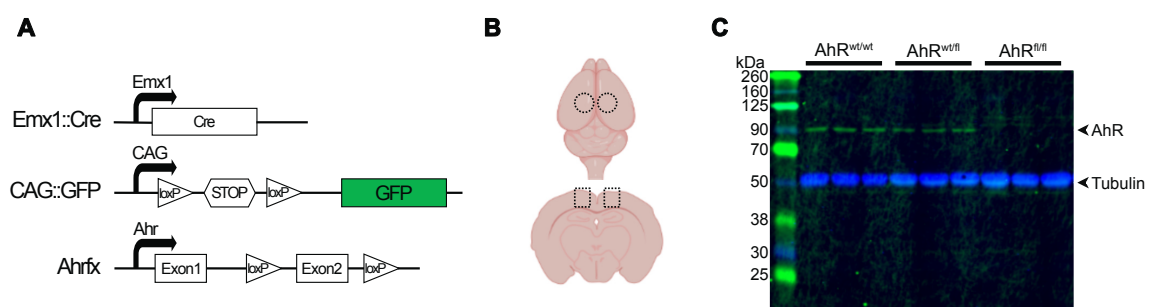


**Figure 6: AhR knock-out upon Cre-dependent recombination**

**(A)** Strategy of the experimental mouse model used to knock out AhR in a cell type-specific manner. **(B)** Mouse brain scheme depicting the location of punches (dotted lines) used for Western Blot (WB) experiments. Created with BioRender. **(C)** Full-length WB image against AhR (green) and Tubulin (blue). The prominent band of AhR in the *AhR<sup>wt/wt</sup>* and *AhR<sup>wt/fl</sup>* samples is lost in the *AhR<sup>fl/fl</sup>* knock-out condition. Each lane represents one animal with  $n = 3$ .

## 2.2 The role of AhR in acquiring stem cell potential

To study the effects of AhR deficiency in astrocytes, I used the  $Glast^{CreERT2} \times Ahr^{fl/fl} \times CAG-GFP$  mouse line (Figure 7A). The astrocyte-specific L-glutamate/L-aspartate transporter (GLAST, *Slc1a3*) dependent expression of Cre fused to a mutant estrogen ligand-binding domain (CreERT2) that is activated upon tamoxifen binding, allowed me to knock out AhR in a time- and astrocyte-specific manner and report the CreERT2 activity by GFP expression (S. Feil et al., 2009; Mori et al., 2006). The tamoxifen-induced recombination is, however, limited to a few astrocytes within the cortex, and thus did not allow for validating the knock-out using WB experiments as shown above. Unfortunately, none of the tested antibodies used in immunohistochemistry (IHC) experiments resulted in convincing staining of AhR in the hippocampus or cortex (data not shown). It has been shown that the half-life of the AhR protein is below 20 h (Swanson & Perdew, 1993). Therefore, I induced the AhR knock-out by application of tamoxifen (TAM) 14 days prior to stab wound injury of the somatosensory cortex to ensure full AhR-deficiency in astrocytes (Figure 7B).

Brain injury in mice does not only stimulate the proliferation of astrocytes *in vivo* but also leads to their dedifferentiation and acquisition of stem cell capacities *in vitro* (Buffo et al., 2008; Sirko et al., 2009, 2013). The peak of proliferation *in vivo* and the yield of neurospheres *in vitro* is highest at 5 days post injury (5 dpi) (Frik et al., 2018; Sirko et al., 2013). Hence, I carried out the neurosphere assay at 5 dpi to investigate the stem cell potential of AhR deficient astrocytes (Figure 7B). When comparing neurospheres at 14 days *in vitro* (14 div) from control animals (Ctr), which includes animals having at least one wt allele of *Ahr* ( $AhR^{wt/wt}$  or  $AhR^{wt/fl}$ ), with AhR knock-out ( $AhR^{fl/fl}$ ) animals, no morphological differences in respect to their size were observed (Figure 7C). Quantification of neurospheres did not result in differences between the number of non-recombined (GFP<sup>-</sup>) neurospheres derived from Ctr or  $AhR^{fl/fl}$  animals (Figure 7D). Conversely, when comparing GFP<sup>+</sup> recombined neurospheres, I observed about 30 % of GFP<sup>+</sup> neurospheres in the Ctr condition and none when AhR was knocked-out in astrocytes (Figure 7, C to E).

Nonetheless, it cannot be excluded that the  $AhR^{fl/fl}$  animals had low recombination rates and thus I might not detect any GFP<sup>+</sup> recombined neurospheres derived from AhR-deficient animals. Since I performed unilateral injuries and the injured hemisphere was used for the neurosphere assay, I stained the contralateral hemisphere with an anti-GFP antibody and counted the GFP<sup>+</sup> cells in the somatosensory cortex to control for possible differences in recombination rates. Importantly, the recombination rate did show a linear correlation with the percentage of GFP<sup>+</sup> neurospheres in the Ctr animals ( $R^2 = 0.8566$ ; Figure 7H). As indicated by the representative images, no differences in the recombination rate between the Ctr and  $AhR^{fl/fl}$

animals have been observed that could explain the loss of GFP<sup>+</sup> recombined neurospheres upon AhR knock-out (Figure 7, F and G).

To validate whether the effect of AhR on neurosphere formation is astrocyte-specific, I generated neurospheres from the neural stem cell niche located at the later ventricle, the subependymal zone (SEZ). Since GLAST is also expressed in adult neural stem cells (aNSC), I made use of the same mouse line (Glast<sup>CreERT2</sup> x Ahrfx x CAG-GFP) to study the role of AhR knock-out in the neurosphere forming capacity of aNSCs. Neurospheres at 7 div were not different in shape or number in Ctr or AhR<sup>fl/fl</sup> condition (Figure 7, I and J). Interestingly, no differences have been observed within the recombined GFP<sup>+</sup> neurospheres when comparing both conditions (Figure 7, J and K).

In conclusion, as already shown by Buffo and others Glast<sup>+</sup> astrocytes can dedifferentiate after traumatic brain injury and form neurospheres *in vitro* (Buffo et al., 2008). This acquisition of stemness in reactive astrocytes was lost upon AhR knock-out, as they could not form neurospheres. Interestingly, AhR-deficiency did not affect the neurosphere forming capacity of aNSCs, suggesting that AhR signaling is specific for the dedifferentiation process of reactive astrocytes to acquire stem cell potential. However, it doesn't regulate the sphere-forming capacity of already undifferentiated cells (stem cells and progenitors in the SEZ). It is, thus interesting to investigate how AhR regulates the astrocyte fate upon injury.

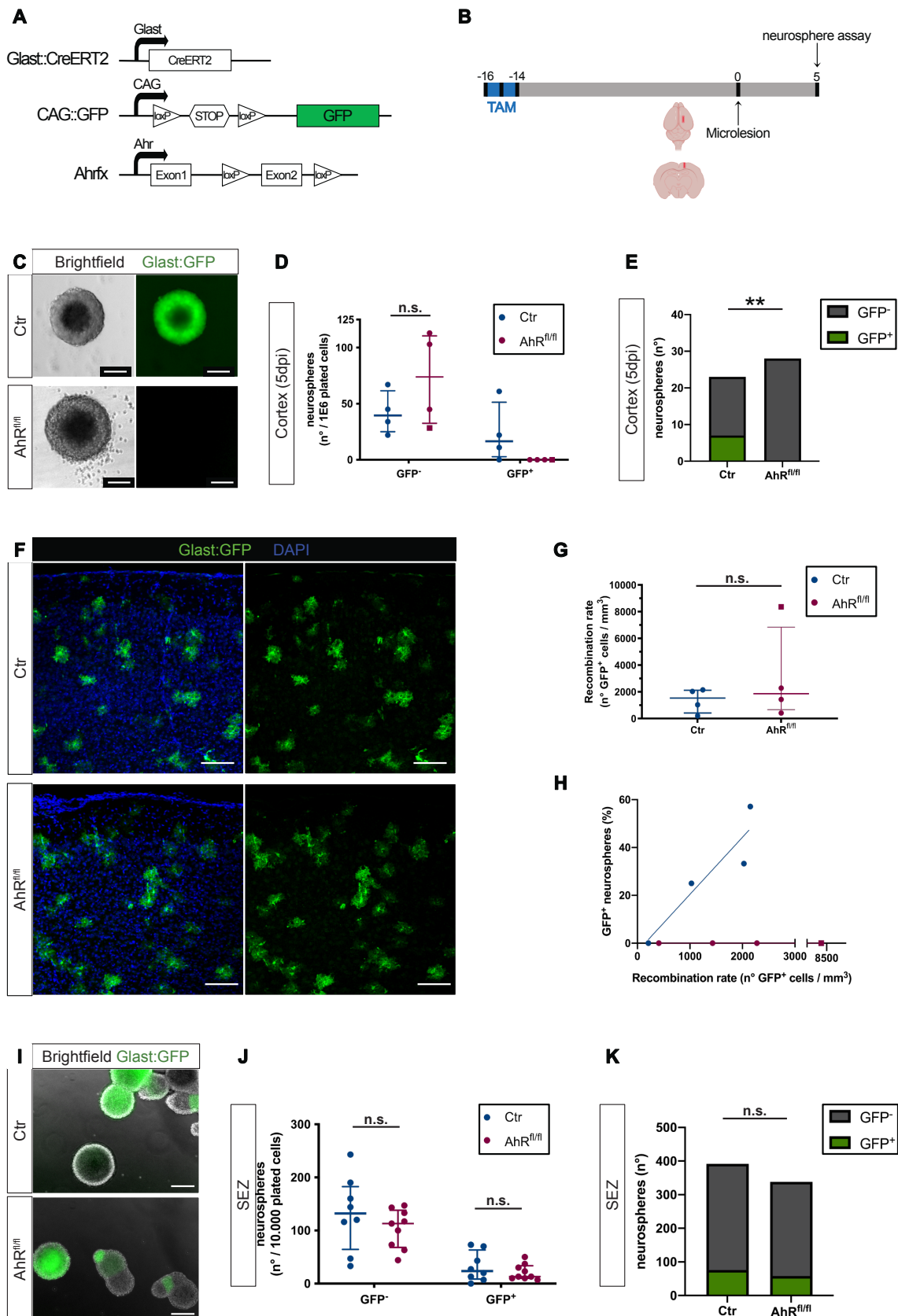


**Figure 7: AhR knock-out in astrocytes results in loss of neurosphere-forming capacity after injury**

(A) Strategy of the experimental mouse model used to knock out AhR in astrocytes in a time-specific manner. (B) Experimental timeline used to knock out AhR in astrocytes by i.p. injection of tamoxifen (TAM) at 3 consecutive days 14 days before injury (microlesion). The neurosphere assay was performed 5 days post injury (5 dpi). Created with BioRender. (C) Representative images of cortical neurospheres (brightfield) with GFP expression (green) derived from Ctr (AhR<sup>wt/wt</sup> or AhR<sup>wt/fl</sup>) and AhR knock-out (AhR<sup>fl/fl</sup>)

animals. **(D)** Quantification of non-recombined (GFP<sup>-</sup>) and recombined neurospheres (GFP<sup>+</sup>) normalized to the number of plated cells. **(E)** Contingency graph of all counted non-recombined (GFP<sup>-</sup>) and recombined cortical neurospheres in Ctr (number of plated cells: 391,000) and AhR<sup>fl/fl</sup> (number of plated cells: 455,500) mice. **(F)** Representative images of the contralateral cortex of injured animals showing the recombined astrocytes (green). **(G)** The recombination rate is calculated based on the amount of GFP<sup>+</sup> cells normalized to the volume in the cortex. **(H)** Correlation of GFP<sup>+</sup> neurospheres and recombination rate in Ctr (blue) and AhR<sup>fl/fl</sup> (red) neurospheres. Line represents the linear regression for Ctr (blue, R<sup>2</sup> = 0.8566) and AhR<sup>fl/fl</sup> (red, R<sup>2</sup> = 1.0). **(I)** Representative composite images of subependymal zone (SEZ) derived neurospheres from Ctr and AhR<sup>fl/fl</sup> animals with recombined neurospheres (green). **(J)** Quantification of counted SEZ-derived non-recombined (GFP<sup>-</sup>) and recombined (GFP<sup>+</sup>) neurospheres normalized to the number of plated cells. **(K)** Contingency graph of all counted non-recombined (GFP<sup>-</sup>) and recombined (GFP<sup>+</sup>) neurospheres from the SEZ in Ctr (number of plated cells: 24,000) and AhR<sup>fl/fl</sup> (number of plated cells: 27,000) mice. Scale bars represent 200 μm (C and I) and 100 μm (F). Each point represents one animal with n = 4 (D, G and H) and n = 8-9 (J). Squared data point (D, G, and H) indicates the TAM protocol from Figure 11A. Data are shown as median with IQR (D, G, and J). Significance was calculated using the Mann-Whitney test (D, G, and J) and Fisher's exact test (E and K). \*p < 0.05, \*\*p < 0.01.

### 2.3 AhR signaling does not regulate astrocytes proliferation upon injury

A correlation between proliferating astrocytes and their acquisition of stem cell potential after TBI has been observed in previous studies (Dimou & Götz, 2014; Sirko et al., 2013). This correlation is supported by the fact that both phenotypes are at their peak at 5 dpi and decline with age (Frik et al., 2018; Heimann et al., 2017; Sirko et al., 2013). Proliferating astrocytes are predominantly located with their soma at blood vessels, so-called juxtavascular astrocytes (Bardehle et al., 2013; Frik et al., 2018; Heimann et al., 2017). In addition, the majority of astrocytes with high expression of AhR were juxtavascular astrocytes (Frik et al., 2018). Hence, I hypothesized that AhR signaling would also decrease or even abolish the proliferative response of astrocytes *in vivo* upon injury.

To test this hypothesis the proliferation of astrocytes at 5 dpi was assessed by labeling cycling cells in S-phase with the thymidine analogs, 5-bromo-2'-deoxyuridine (BrdU) and 5-ethynyl-2'-deoxyuridine (EdU). BrdU was administered by water for 5 days after injury to label all proliferating cells induced by injury (Figure 8A). EdU was injected 50 minutes before sacrificing the animal to detect cells entering the cell cycle at the peak of astrocyte proliferation at 5 dpi (Figure 8A). GFP<sup>+</sup> – and thus recombined – astrocytes in a radial distance of 150 μm to the injury site were analyzed in Ctr and AhR<sup>fl/fl</sup> animals (Figure 8B). About 45 % of the recombined astrocytes were BrdU<sup>+</sup> in both conditions, and on average, 3 % of GFP<sup>+</sup> astrocytes did proliferate shortly before sacrifice at 5 dpi based on the EdU incorporation in Ctr and AhR<sup>fl/fl</sup> mice (Figure 8, C to E). These results suggest a comparable proliferative capacity of Ctr and AhR knock-out cells throughout the period of 5 dpi, as well as at the peak of proliferation at 5 dpi. And thus, AhR signaling may not be involved in regulating the proliferation of reactive astrocytes. Nevertheless,

both analogs – BrdU and EdU – are incorporated into the DNA during the S-phase of the cell cycle, thus leaving the possibility that the analog labeled astrocytes got stuck in S-phase without fully completing the cell cycle. To exclude this possibility, an immunohistochemical (IHC) staining against Ki67 (marker of proliferation Ki-67, *Mki67*) was carried out (Figure 9A). Ki67 is a widely established marker of cell proliferation that is expressed throughout the cell cycle and absent in resting ( $G_0$ ) cells (Bruno & Darzynkiewicz, 1992). Comparable to the results above, the analysis of Ki67<sup>+</sup> recombined astrocytes resulted in no differences between Ctr and AhR-deficient mice at the injury site (Figure 9D). Since a major fraction of proliferating astrocytes are juxtavascular and those are reported to express AhR, I decided to further investigate whether this particular subpopulation of astrocytes is affected by the AhR knock-out (Bardehle et al., 2013; Frik et al., 2018; Heimann et al., 2017). However, when separating juxtavascular and non-juxtavascular GFP<sup>+</sup> astrocytes, no altering patterns of proliferation have been observed (Figure 9B, C, and E).

It can be concluded that the perturbation of AhR in GLAST<sup>+</sup> astrocytes did not lead to any changes in their proliferative behavior upon injury. This is in contradiction with the hypothesis suggested above and with the correlation of proliferating astrocytes and neurosphere forming astrocytes observed in the past (Sirko et al., 2013). It thus opens the question, of whether reactive astrocytes dedifferentiate after they proliferate or whether both processes are unrelated to each other after injury.

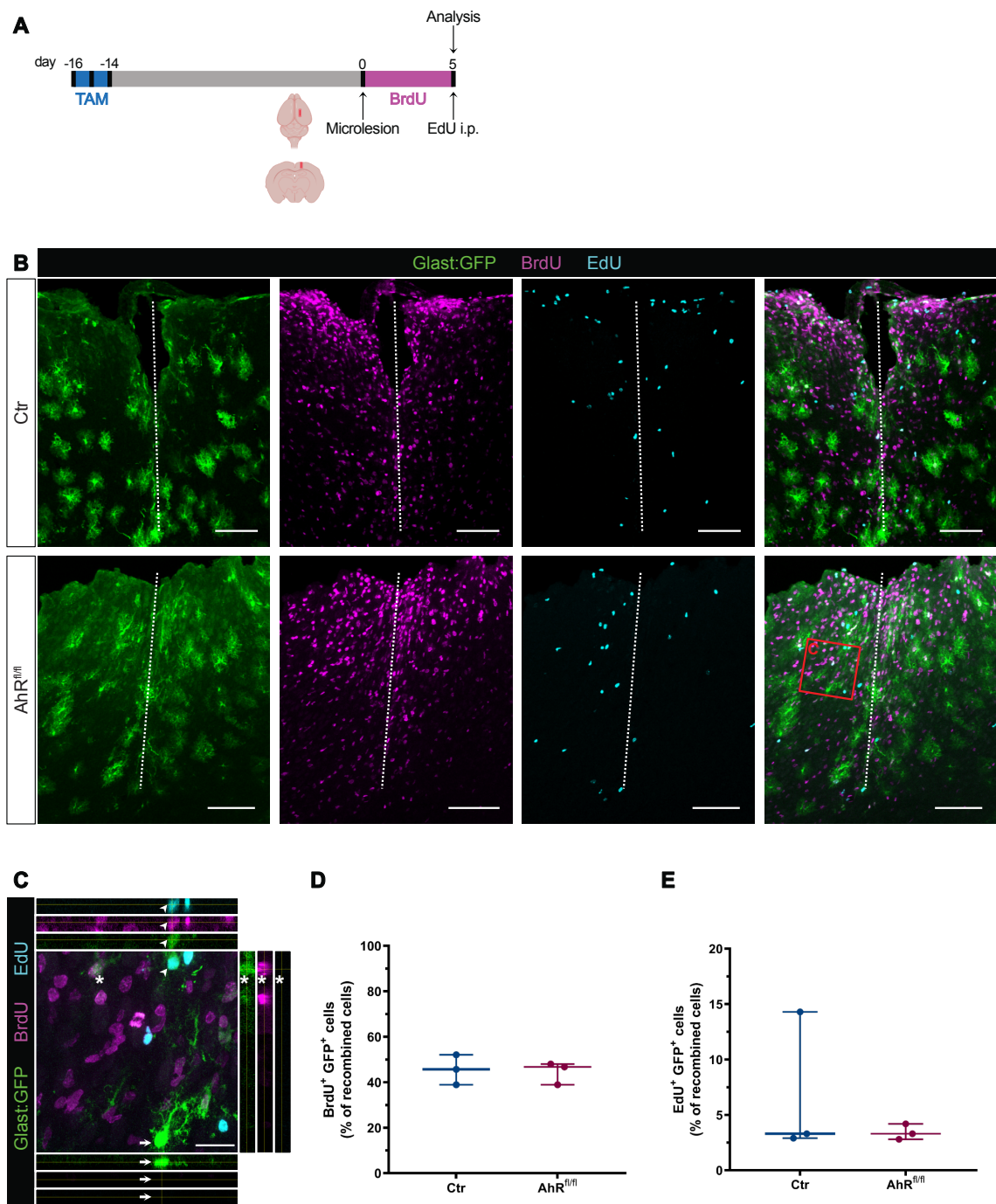


**Figure 8: AhR knock-out does not alter proliferation of astrocytes at the injury site**

(A) Experimental timeline used to knock out AhR in astrocytes by i.p. injection of tamoxifen (TAM) at 3 consecutive days 14 days before injury (microlesion). Labeling of proliferating cells for 5 consecutive days after injury with BrdU water and cells proliferating at 5 dpi with EdU injection (i.p.). Created with BioRender. (B) Representative images at the injury site of Ctr and AhR<sup>fl/fl</sup> animals show recombined astrocytes (green), BrdU labeled cells (magenta) and EdU labeled cells (cyan). (C) Magnification image including orthogonal projection to show recombined astrocytes that are BrdU<sup>+</sup> EdU<sup>+</sup> (arrowhead), BrdU<sup>+</sup> EdU<sup>-</sup> (asterisk), and BrdU<sup>-</sup> EdU<sup>-</sup> (arrow). (D) Quantification of BrdU<sup>+</sup> recombined astrocytes over all recombined astrocytes at the injury site. (E) Quantification of EdU<sup>+</sup> recombined astrocytes over all recombined astrocytes at the injury site. Each dot represents one animal with n = 3. Scale bars represent 100  $\mu$ m (B) and 20  $\mu$ m (C).

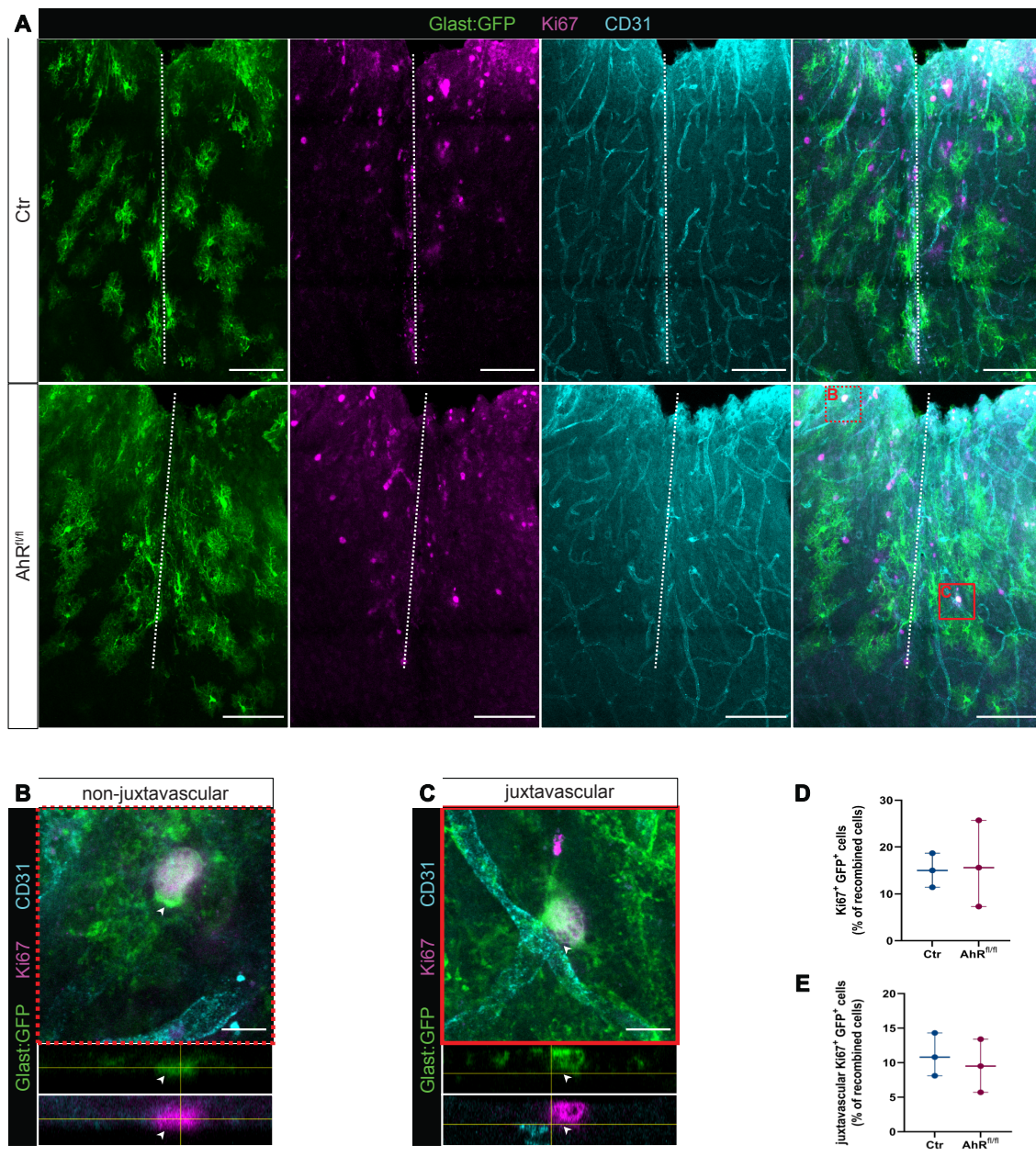


**Figure 9: AhR knock-out does not alter proliferation of heterogeneous populations of astrocytes at the injury site**

**(A)** Representative images at the injury site of Ctr and AhR<sup>fl/fl</sup> animals showing recombined astrocytes (green), Ki67<sup>+</sup> cells (magenta), and CD31<sup>+</sup> blood vessels (cyan). **(B)** Magnification image including orthogonal projection to show recombined non-juxtavascular astrocytes that are Ki67<sup>+</sup> and not closely located to a blood vessel. **(C)** Magnification image including orthogonal projection to show recombined juxtavascular astrocytes that are Ki67<sup>+</sup> and closely located at a blood vessel. **(D)** Quantification of Ki67<sup>+</sup> recombined astrocytes over all recombined astrocytes at the injury site. **(E)** Quantification of juxtavascular Ki67<sup>+</sup> recombined astrocytes over all recombined astrocytes at the injury site. Each dot represents one animal with n = 3. Scale bars represent 100  $\mu$ m (A) and 20  $\mu$ m (B and C)

## 2.4 Is leukocyte extravasation upon injury affected by the astrocytic AhR-deficiency?

The observed phenotype that the astrocyte-specific AhR knock-out prevents the acquisition of stem cell properties suggests a cell-autonomous effect. Nevertheless, it cannot be excluded that cell non-autonomous effects are responsible for the change of astrocyte fate after injury. It has been demonstrated that astrocytes block leukocyte extravasation, a process in which immune cells invade the parenchyma after brain insult (Frik et al., 2018). This infiltration of leukocytes is known to inhibit proliferation and self-renewal of reactive astrocytes upon injury (Frik et al., 2018; Lange Canhos et al., 2021). In addition, AhR signaling blocks Ccl2 expression in astrocytes, an essential mediator of leukocyte extravasation (Frik et al., 2018; Rothhammer et al., 2016). I hence investigated whether AhR-deficient astrocytes alter leukocyte infiltration upon injury, which then might result in cell-nonautonomous changes observed in the neurosphere assay.

For this experiment, I used IHC staining against Iba1 (ionized calcium-binding adapter molecule, *Aif1*), a marker of brain resident microglia, and CD45 (cluster of differentiation 45), a marker for leukocytes (Figure 10A). The staining against Iba1 was necessary to differentiate between microglia that upregulate CD45 (Iba1<sup>+</sup> and CD45<sup>+</sup>) and invading leukocytes (CD45<sup>+</sup> and Iba1<sup>-</sup>) (Figure 10B). Quantifications of CD45<sup>+</sup> Iba1<sup>-</sup> invading leukocytes resulted in no changes between Ctr and AhR<sup>fl/fl</sup> animals (Figure 10C).

In summary, the similar numbers of extravasating leukocytes observed in animals with an astrocyte-specific knock-out of AhR and in Ctr mice suggest that the loss of stem cell potential in the AhR-deficient astrocytes is not attributed to this cell non-autonomous effect. Supported by these results, I was intrigued to investigate the cell-autonomous effects of AhR knock-out within astrocytes upon injury to understand how AhR regulates astrocyte fate.

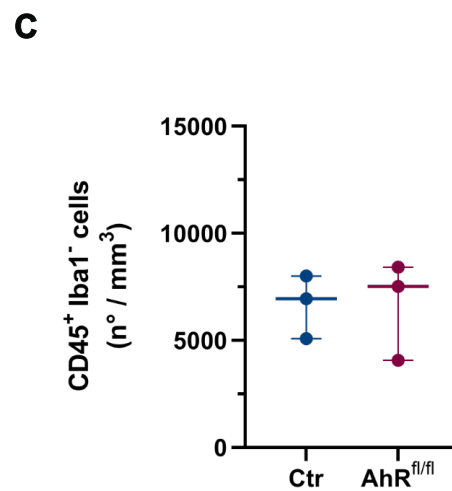
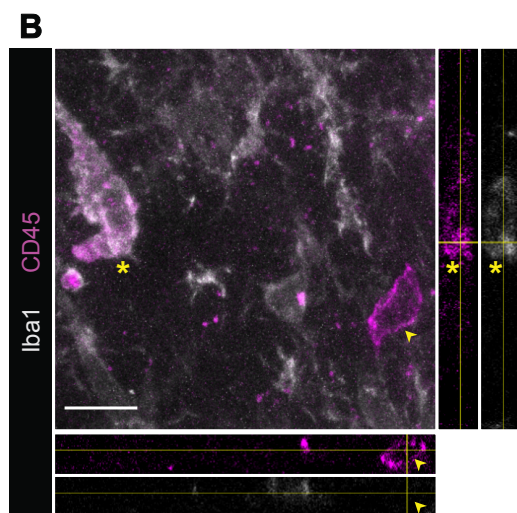
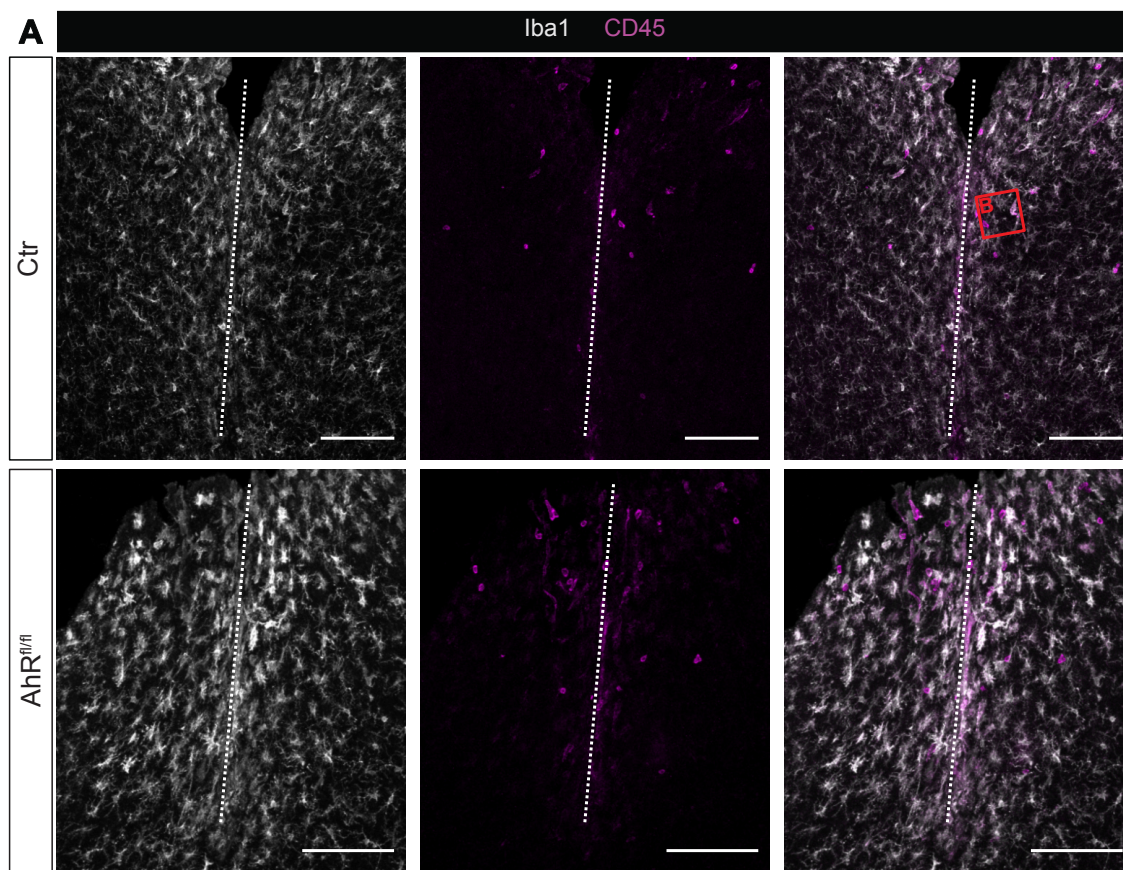


**Figure 10: Leukocyte extravasation upon injury**

**(A)** Representative images at the injury site of Ctr and AhR<sup>fl/fl</sup> animals showing Iba1<sup>+</sup> labeled microglia (white) and CD45<sup>+</sup> labeled cells (magenta). **(B)** Magnification image including orthogonal projection to show Iba1<sup>+</sup> microglia upregulating CD45 (asterisk) and CD45<sup>+</sup> Iba1<sup>-</sup> leukocytes invading the brain parenchyma (arrowhead). **(C)** Quantification of CD45<sup>+</sup> Iba1<sup>-</sup> invading leukocytes at the injury site in Ctr and AhR<sup>fl/fl</sup> animals. Each dot represents one animal with n = 3. Scale bars represent 100  $\mu$ m (A) and 20  $\mu$ m (B).

## 2.5 Elucidating the role of AhR in astrocytes after injury using single-cell RNA sequencing

The results described above implied that the phenotype observed in the neurosphere assay is likely caused by loss of AhR signaling in reactive astrocytes (sections 2.2 to 2.4). This initiated the question of how AhR signaling is regulating the astrocyte fate upon injury. Since AhR activation instructs transcriptional activation and only a small fraction of astrocytes are reported to dedifferentiate and acquire stem cell potential, I choose to address this subject using single-cell RNA sequencing (scRNAseq). Single-cell transcriptomics allows investigating the heterogeneity of various cell types like astrocytes in further detail, which would not be possible in bulk RNA sequencing experiments (X. Li & Wang, 2021). Moreover, the observed outcome that astrocytes maintain their proliferative behavior *in vivo* after injury raised the question, of whether the processes of proliferation and dedifferentiation of astrocytes are connected, as suggested previously (Dimou & Götz, 2014; Sirko et al., 2013). To elucidate this aspect I also made use of the scRNAseq data by using velocity analysis, which enables to resolve transient cell states (Bergen et al., 2020).

For this experiment, the protocol to induce Cre-dependent recombination in astrocytes was altered to achieve higher yields of recombined astrocytes by injecting 2 cycles of tamoxifen each for 5 consecutive days in the period of three weeks (Figure 11A). The animals have been injured at both hemispheres – to reduce the number of animals – 14 days after the last day of induction and sacrificed at 5 dpi (Figure 11A). Furthermore, only  $\text{Glast}^{\text{CreERT2}} \times \text{AhR}^{\text{fl/fl}} \times \text{CAG-GFP}$  animals were used to study the cell-autonomous effects of AhR by comparing recombined  $\text{GFP}^+$  AhR-deficient astrocytes (KO) to non-recombined  $\text{GFP}^-$  astrocytes (NR) (Figure 11B). To enrich astrocytes, I performed magnetic-activated cell sorting (MACS) using anti-ACSA-2 (astrocyte cell surface antigen-2) MicroBeads (Figure 11B) as previously described (Batiuk et al., 2017; Kantzer et al., 2017; Ohlig et al., 2021). To reduce the number of animals used in this experiment, I performed the  $\text{ACSA-2}^+$  MACS sorting without a myelin removal step upon dissociation, which has been suggested to increase the purity of sorted cells but would increase the number of animals required for this experiment (Batiuk et al., 2017). Subsequently, single-cell transcriptome libraries were prepared following the 10x Genomics protocol, sequenced, and analyzed in-depth in the following sections of this thesis (Figure 11B).

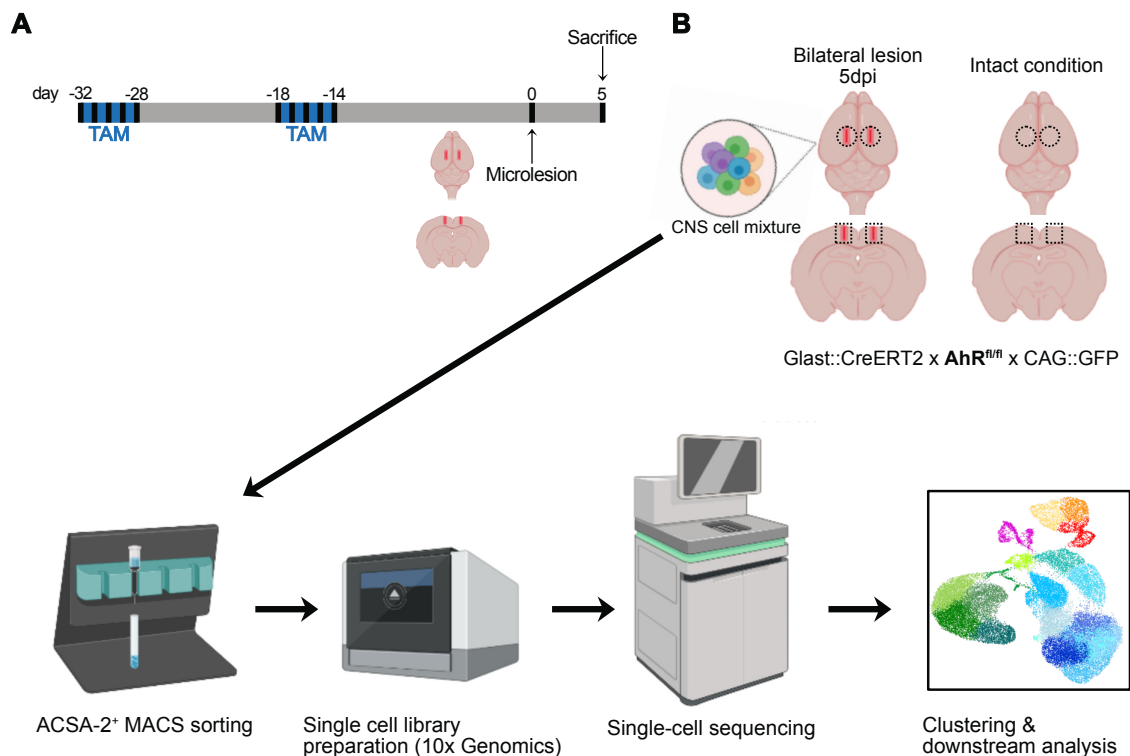


**Figure 11: Setup for scRNAseq experiment**

**(A)** Experimental paradigm used to knock out AhR in astrocytes by i.p. injection of tamoxifen (TAM) for 2 cycles for 5 consecutive days in the period of three weeks. The last injection of TAM was done 14 days before injury (microlesion). **(B)** Scheme depicting the strategy to enrich sequenced cells for astrocytes by ACSA-2<sup>+</sup> MACS sorting of brain punches from intact or injured animals. Subsequently, the 10X Genomics protocol has been carried out, and libraries were sequenced using Novaseq 6000 and analyzed by a custom Python pipeline. Created with BioRender.

### 2.5.1 Quality control of sequenced cells

For both conditions, intact and injured (5 dpi), I split the MACS sorted cells into two samples and loaded both separately on the 10x Chromium Chip to increase the number of sequenced cells. Before proceeding with the analysis of the single-cell transcriptomic data, I had to make sure that the quality of the samples is acceptable and that the different samples are comparable. The quality of the sequenced libraries was examined by comparing the correlation of the counts and genes per cell, which is depicted in the joint plot and shows that most cells have about 1,800 to 3,600 genes and 3,000 to 13,500 counts per cell in the intact and injured (5 dpi) condition (Figure 12, A and D). In addition, there is also a population of cells with lower expression of genes ranging from 500 to 1,200 genes and 1,000 to 3,000 counts per cell in both conditions (Figure 12, A and D). I observed that mainly cells with low count numbers (500 to 5,000 counts) and low gene numbers (100 to 1,000 genes) had high mitochondrial gene fractions, which indicates dying or low-quality cells (Figure 12, B and E). After filtering out of these cells, 20,932 cells in the intact and 18,324 cells in the 5 dpi condition remained for the analysis, and their distribution in the scatter plot was similar to each other (Figure 12, C and F).

Overall, the quality of the sequenced samples was acceptable, and no striking differences between both conditions have been observed. Hence, I continued with the analysis with the filtered cells.

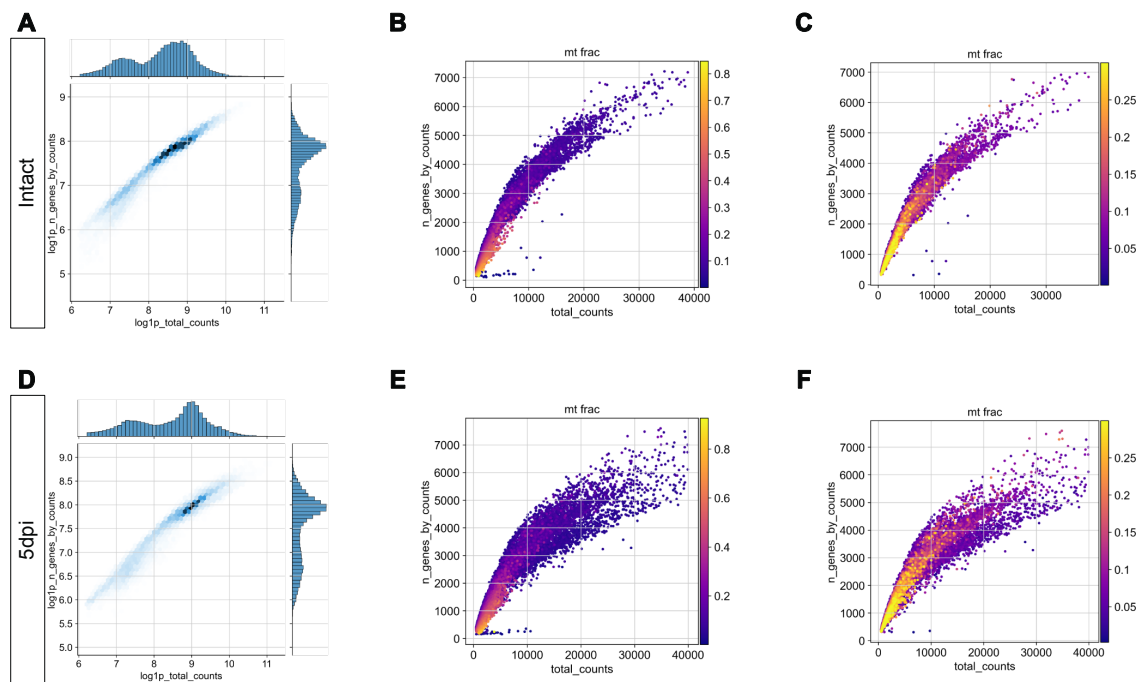


**Figure 12: Quality Control of scRNAseq experiment**

(A) Joint plot depicting the distribution of the log-transformed total number of counts to the log-transformed number of genes expressed before filtering of bad quality cells, that are derived from the intact condition. (B and C) Scatter plot depicting the distribution of a total number of counts to the number of genes expressed before (D) and after (E) filtering out bad quality cells, that are derived from the intact condition. The scale bar represents the fraction of mitochondrial-associated genes. (D) Joint plot depicting the distribution of the log-transformed total number of counts to the log-transformed number of genes expressed before filtering of bad quality cells, that are derived from the injured (5 dpi) condition. (E and F) Scatter plot depicting the distribution of a total number of counts to the number of genes expressed before (E) and after (F) filtering out bad quality cells, that are derived from the 5 dpi condition. The scale bar represents the fraction of mitochondrial-associated genes.

### 2.5.2 ACSA-2+ MACS sorting enriched for astrocytes and oligodendrocytes

Following the quality control (section 2.5.1), altogether 39,256 cells with a total of 15,406 genes were used for the analysis of the ACSA-2<sup>+</sup> MACS isolated cells. To study the heterogeneity of these cells a principal component analysis (PCA) using 2,000 highly variable genes (HVG) was performed. Seven dimensions of the PCA data with 30 local neighbors were used to compute a uniform manifold approximation and projection (UMAP) based on the k-nearest neighbor algorithm. Subsequently, Leiden clustering with a resolution of 1.0 revealed 20 different clusters (Figure 13A). To identify the cell type of each cluster the top 100 expressed genes per cluster were used and cross-referenced with the Linnarson lab database (Zeisel et al., 2018). Interestingly, not only astrocytes were identified, but also oligodendrocytes,

oligodendrocyte precursor cells (OPC), microglia, neurons, pericytes, and endothelial (Figure 13A). In addition, I validated these results by examining the expression of marker genes for astrocytes (homeostatic: *Sox9*, *Aldh1l1*, *Atp1b2*, *Slc1a3*, *Aldoc*, *Aqp4*; and reactive: *Vim*, *Gfap*), oligodendrocytes (*Sox10*, *Mag*, *Mog*, *Mbp*), OPCs (*Pddgfra*, *Cspg4*, *Gpr17*), microglia (*Aif1*, *P2ry12*, *Cx3cr1*), neurons (*Rbfox3*, *Slc17a7*, *Gabra1*, *Bcl11b*, *Foxp2*, *Cck*), pericytes (*Pecam1*, *Pdgfrb*, *Rgs5*, *Kcnj8*, *Flt1*) and endothelial cells (*Cldn5*, *Cdh5*, *Abcb1a*, *Vwf*) for each cluster (Figure 13B). These sets of genes have further been used to calculate a cell type-specific score to comprehend the distribution of each cell type on the UMAP (Figure 13, C to I). The distribution of astrocytes on the UMAP showed that this cell type was the most abundant (56.06 %) of all cells (Figure 13C). Additionally, 31.02 % of the identified cells were classified as oligodendrocytes (Figure 13D). The percentage of identified cell types did vary compared to previously performed scRNAseq using ACSA-2<sup>+</sup> dependent MACS isolation from diencephalic tissue (Ohlig et al., 2021). A possible explanation for the discrepancy may be that I included tissue from the injured cortex at 5 dpi as well as the fact, that no myelin removal step previous to the ACSA-2 labeling was performed.

To analyze effects based on the condition, an embedding density score, which depicts the distribution of cells, was calculated and plotted on the UMAP for each condition (Figure 13J). Indeed, most cells in the intact condition were assigned to the astrocyte clusters. Nonetheless, the remaining clusters of the other cell types did also include cells from the intact condition (Figure 13J), suggesting that the myelin removal step was crucial for Ohlig and others to gain higher purity of astrocytes (Ohlig et al., 2021). Furthermore, the cells from the injured (5 dpi) condition were distributed across all clusters with high abundance in oligodendrocyte and astrocyte clusters (Figure 13J). Additionally, the main fraction of microglia was attributed to cells from the injured brain (Figure 13J). Taken together, these results show that the injury and the left-out myelin removal step affect the purity of the ACSA-2<sup>+</sup> MACS isolation of astrocytes. However, with 15,012 and 6,995 astrocytes from the intact and injured conditions respectively, I had enough cells to continue with the analysis of sub-clustered astrocytes.

As stated above, only *Glast*<sup>CreERT2</sup> x *AhR*<sup>fl/fl</sup> x CAG-GFP animals have been used for this experiment and non-recombined AhR-abundant (NR) cells were separated in the bioinformatic analysis from the recombined AhR-deficient (KO) cells based on their *GFP* expression. The distribution of NR and KO cells showed that most KO cells are in the astrocyte clusters (Figure 13K). This pattern indeed corresponds to the expression of the GLAST gene *Slc1a3* which was used as a driver of Cre-dependent recombination and thus also of *GFP* expression (Figure 13L).

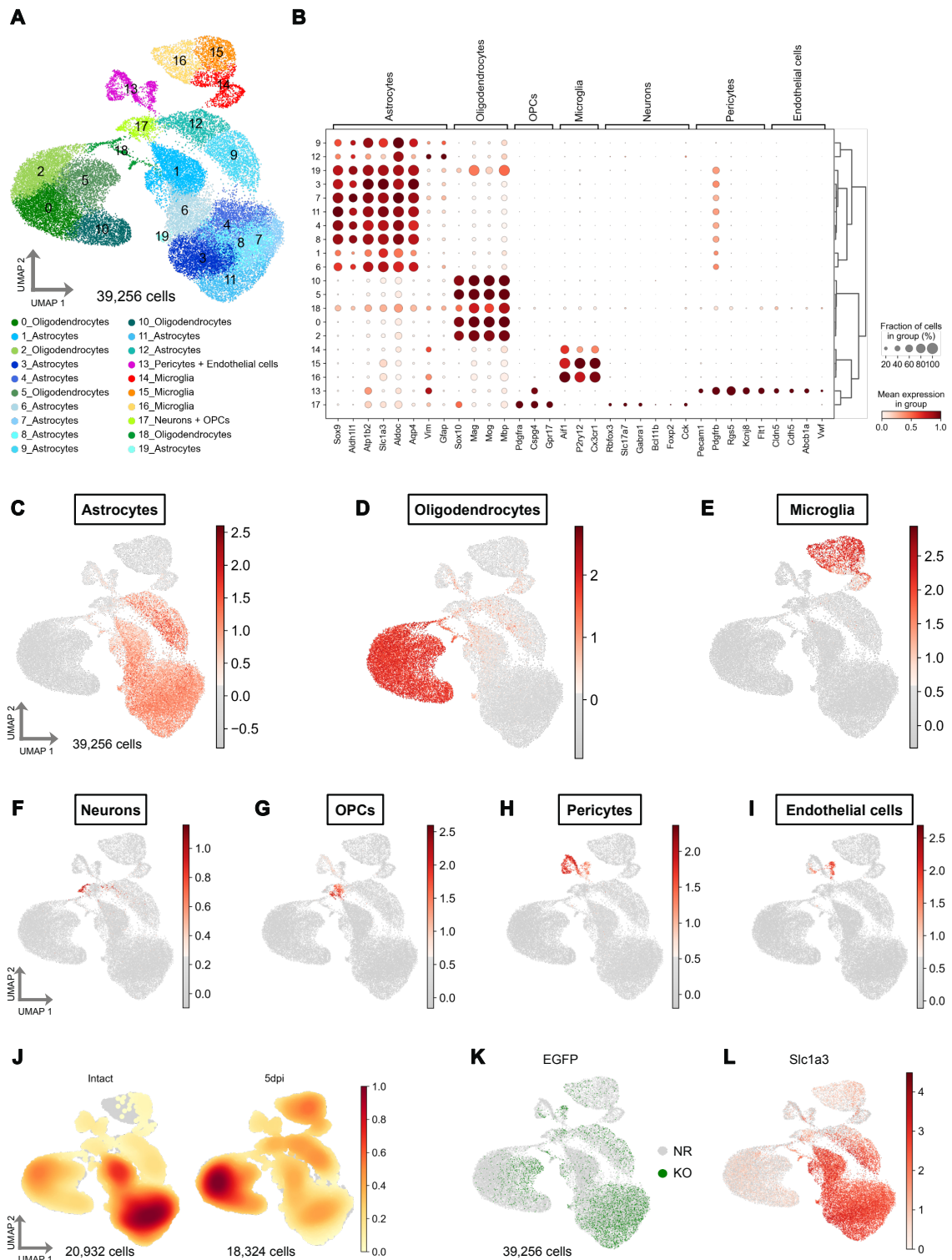


**Figure 13: Defining cell types identified in scRNAseq experiment**

(A) Clustering of all sequenced cells based on their transcriptome from injured (5 dpi) and intact samples. Color code for their cell type identity was used. (B) Dot plot depicting the expression of cell type-specific genes for each cluster. The scale bar represents a standardized scale between 0 and 1 for each gene. (C to I) UMAPs depict a cell type-specific score calculated based on the cell type-specific genes from the dot plot (D). Scale bars represent gene expression scores for each cell type. (J) UMAP depicting the computed embedding density of cells in the intact or injured (5 dpi) condition. The scale bar represents the density score. (K) Distribution of recombined Ahr-KO (KO) cells (green) and non-recombined (NR) cells (grey). (L) UMAP depicts gene expression of two genes *Slc1a3* (GLAST). The scale bar represents log transformed gene expression. Each dot represents a single cell in the UMAPs. OPCs = Oligodendrocyte progenitor cells

To conclude, not only astrocytes were identified in the scRNAseq analysis, but also various other brain-associated cell types such as oligodendrocytes, microglia, and neurons. Furthermore, differences in the distribution of intact and 5 dpi cells were observed, however, enough cells in both conditions have been identified as astrocytes for subsequent analysis of this cell type. Importantly, AhR-KO cells can be separated from NR cells by their *GFP* expression.

### 2.5.3 Non-recombined astrocytes show heterogeneity in their expression profiles

To examine the differences between NR and AhR-KO astrocytes, I first had to understand the heterogeneity of NR astrocytes in the intact and injured conditions. Hence, I subclustered the annotated astrocytes and selected the NR fraction based on the absence of *GFP* expression (Figure 13, A and K). Following PCA using 2,000 HVGs a UMAP was constructed utilizing 9 dimensions of the PCA data set and 30 local neighbors for the k-nearest neighbor algorithm (Figure 14A). Leiden clustering with a resolution of 0.45 resulted in 7 unique subclusters of NR astrocytes (Figure 14A). The top five expressed genes indicated that reactive astrocytes are found in cluster 5\_NR with increased expression of *Gfap* and *Vim* compared to the other subclusters (Figure 14B). A calculated reactive astrocyte score based on enriched genes in A1, A2, and pan reactive astrocytes from Liddelow and colleagues confirmed this result (Figure 14C) (Liddelow et al., 2017). However, when looking into the distribution of *Gfap* and *Vim* on a single cell level, also cluster 2\_NR, 6\_NR, and partially 1\_NR had cells with high gene expression (Figure 14D). In addition, a cell cycle score has been calculated based on genes associated with the S and G<sub>2</sub>/M phase (Tirosh et al., 2016), which showed that the main population of cycling cells was in clusters 2\_NR and 5\_NR (Figure 14E). Actively proliferating astrocytes in the G<sub>2</sub>/M phase were in cluster 5\_NR and astrocytes in the S phase were mostly in cluster 2\_NR (Figure 14E). This was confirmed when looking at the proliferation marker genes *Mki67* and *Cdk1*, which were expressed mainly in cluster 5\_NR (Figure 14F). Furthermore, the number of 5 dpi astrocytes was increased in clusters 2\_NR, 5\_NR, and 6\_NR, whereas astrocytes from the intact brain were more abundant in clusters 0\_NR, 1\_NR, 3\_NR, and 4\_NR (Figure 14, G and H). Taken together, all mentioned parameters suggest that homeostatic astrocytes are found in clusters 0\_NR, 1\_NR, 3\_NR, and 4\_NR (blue) and reactive astrocytes are in clusters 2\_NR, 5\_NR, and 6\_NR (red) (Figure 14A).

To further investigate the heterogeneity of NR astrocytes, the gene ontology (GO) of biological processes (BP) of significantly upregulated differentially expressed genes (DEG) with a threshold of adjusted p-value < 0.05 and log<sub>2</sub> fold change > 1 per cluster have been explored. The 20 most significant biological processes with at least 3 genes per BP and a fold enrichment > 2 are depicted in the dot plots (Figure 15). The homeostatic astrocytes in cluster 0\_NR had many enriched biological processes related to cell signaling but also show a negative

regulation of inflammatory response and positive regulation of angiogenesis and thus might be involved in anti-inflammatory processes (Figure 15A). Cluster 1\_NR astrocytes showed enrichment of biological processes related to the extracellular matrix modulation (Figure 15B). Reactive astrocytes in cluster 2\_NR were characteristic of their enriched biological processes related to immunity and inflammation (Figure 15C) The upregulation of chemokines such as *Ccl2*, *Ccl3*, and *Ccl4* suggests that these cells attract leukocytes and act as pro-inflammatory upon traumatic brain injury (Middleton et al., 2002). The cluster 3\_NR astrocytes showed a general enrichment of transcriptional activity, whereas 4\_NR cells had enriched biological processes related to short-term memory, peptide signaling, and NO signaling indicating a potential role in regulating neuronal activity and neurovascular coupling (Figure 15, D and E) (Muñoz et al., 2015; Verkhratsky et al., 2016). As already shown by the scRNAseq analysis (Figure 14, E and F), the cluster 5\_NR reactive astrocytes had enriched GO terms related to proliferation, but also innate immunity and oxidative stress (Figure 15F). This reactive cluster showed thus a strong indication to be involved in anti-inflammatory processes by astrocyte border formation (Sofroniew, 2020). Finally, cluster 6\_NR had many GO terms enriched that are linked to synapse regulation, suggesting that these astrocytes interact directly with neurons at the synapse (Figure 15G).

In conclusion, the analysis of the NR astrocytes resulted in seven different subclusters and each of them has been characterized as either homeostatic or reactive astrocytes, indicating heterogeneous functions of astrocytes. Indeed, with the GO term analysis I could identify subpopulations of astrocytes that show a strong pro- and anti-inflammatory response to traumatic brain injury, but also homeostatic subpopulations were involved in different aspects of homeostasis like extracellular matrix modulation and regulation of neuronal activity.

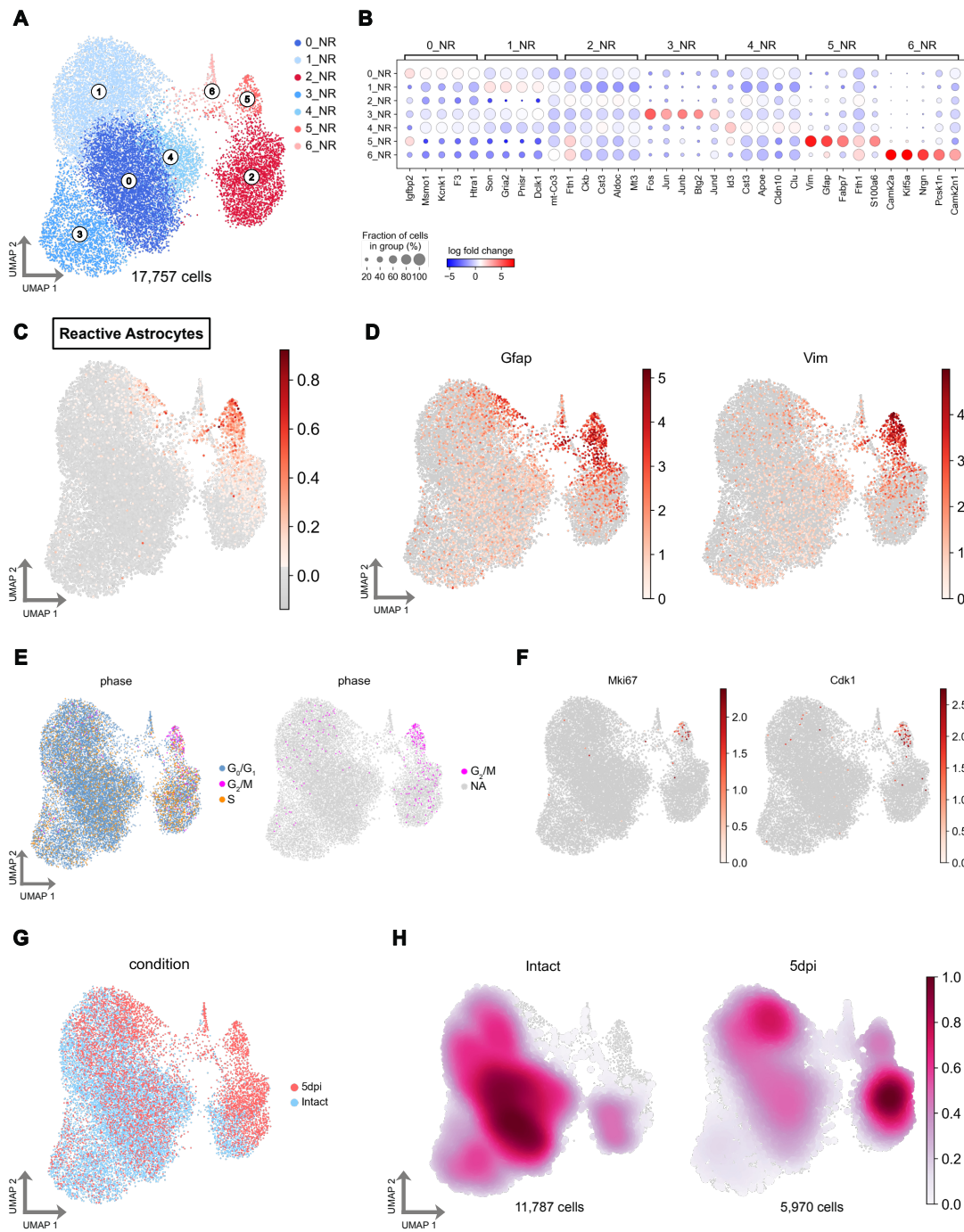


**Figure 14: Characterization of subclustered non-recombined astrocytes**

(A) UMAP of subclustered non-recombined (NR) astrocytes from intact and injured (5 dpi) animals. Cells are colored by their subcluster identity. (B) Dot plot of the top 5 enriched genes in each NR astrocyte cluster. The scale bar represents the log fold change of each gene compared to the other clusters. (C) UMAP depicts the reactive astrocyte score calculated from genes enriched in reactive astrocytes (Liddelow et al., 2017). The scale bar represents the gene expression score. (D) UMAP depicts gene expression of two genes, *Gfap* and *Vim*, that are characteristic of reactive astrocytes. The scale bar represents log transformed gene expression. (E) UMAP depicts the distribution of cells in different cell cycle states  $G_0/G_1$  (blue),  $G_2/M$  (magenta), and S phase (orange). Cells in the  $G_2/M$  phase are highlighted in the right UMAP. (F) UMAP depicts gene expression of two genes, *Mki67* and *Cdk1*, that are characteristic of proliferation. The scale bar represents log transformed gene expression. (G) UMAP depicting the distribution from both intact (blue) and 5 dpi (red) samples. (H) UMAP depicting the computed embedding density of cells in the intact or 5 dpi condition. The scale bar represents the density score. Each dot represents a single cell in the UMAPs.

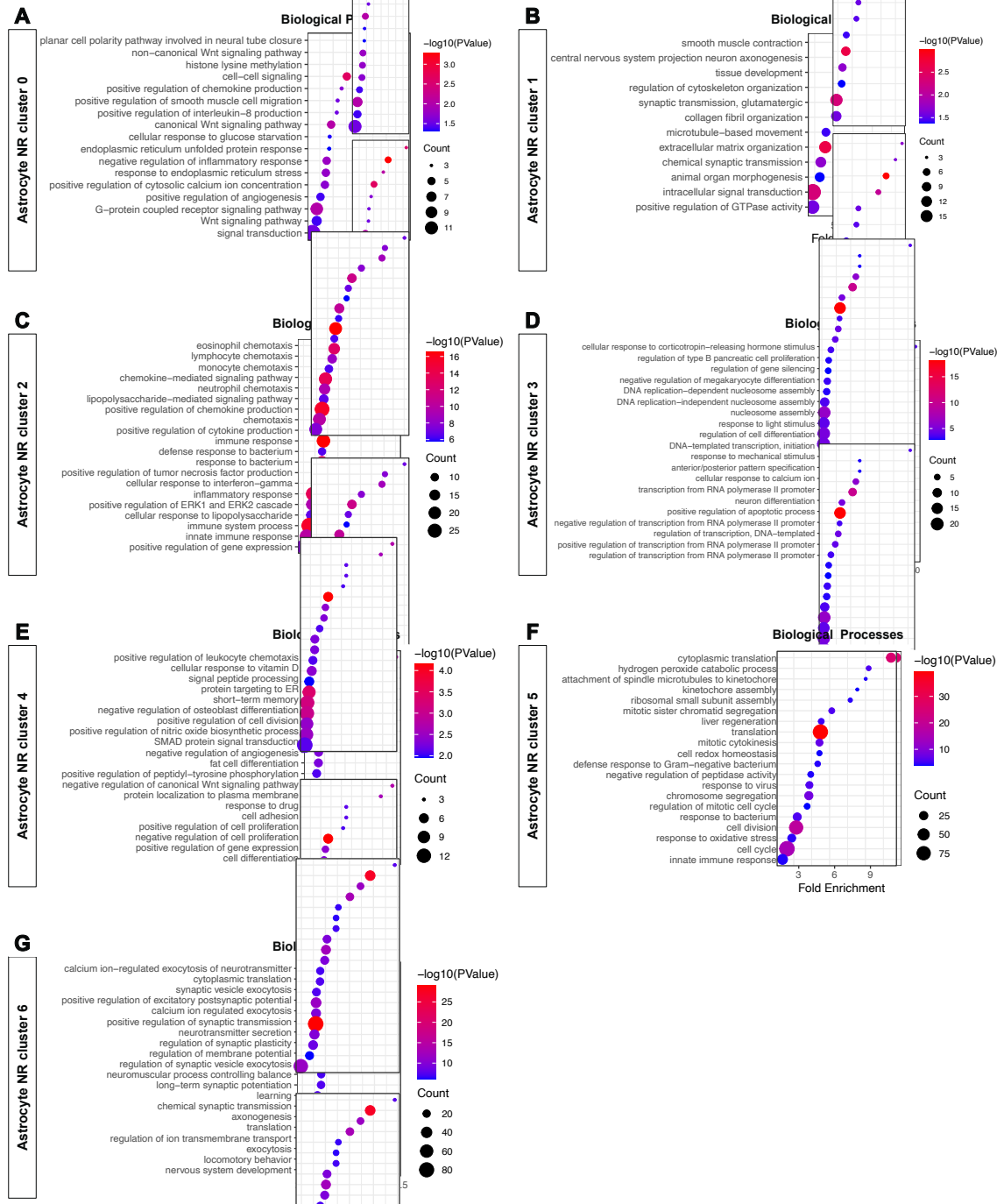


**Figure 15: GO term-based characterization of NR subclustered astrocytes**

(A to G) Dot plots depicting representative Biological Processes enriched by upregulated differentially expressed genes in each subcluster of NR astrocytes. Cluster 0\_NR (A), 1\_NR (B), 2\_NR (C), 3\_NR (D), 4\_NR (E), 5\_NR (F), and 6\_NR (G). Scale bars represent the negative  $\log_{10}$  p-value calculated by GO term analysis (DAVID).

## 2.5.4 AhR-deficient astrocytes maintain heterogeneous functions

As I identified multiple subclusters of non-recombined astrocytes, I asked the question, which of those would be affected by the deletion of AhR. Therefore, I subclustered only the AhR-KO astrocytes based on the annotation of astrocytes and their *GFP* expression (Figure 13, A and K). Principal component analysis with 2,000 HVGs was performed and by the use of 9 dimensions a UMAP was constructed based on the k-nearest neighbor algorithm with 30 local neighbors (Figure 16A). Six unique subclusters of KO astrocytes have been identified following Leiden clustering with a resolution of 0.5 (Figure 16A). Similar to the NR astrocytes a reactive astrocyte cluster within the KO astrocytes (5\_KO) was identified by the top five expressed genes due to increased expression of *Gfap* and *Vim* (Figure 16B). This was also confirmed by the reactive astrocyte score (for definition see section 2.5.3) and the distribution of *Gfap* and *Vim* expressing KO astrocytes, which also revealed some cells expressing those two genes in clusters 3\_KO and 4\_KO (Figure 16, C and D). As in the analysis of NR astrocytes, the proliferating cells in the G<sub>2</sub>/M phase were in cluster 5\_KO, and cluster 4\_KO included mainly cells in the S phase (Figure 16E). Expression profiles of proliferation marker genes *Mki67* and *Cdk1* corroborated the cell cycle score analysis (Figure 16F). In addition, reactive astrocytes were enriched in clusters 4\_KO and 5\_KO, and homeostatic astrocytes from the intact tissue were more abundant in clusters 0\_KO to 3\_KO (Figure 16, G and H). In summary, within the KO subclustered astrocytes I was able to distinguish between reactive (red clusters) and homeostatic (blue clusters) astrocytes (Figure 16A).

To study whether clusters from AhR-KO subclustered astrocytes were different from NR astrocyte subclusters, a similarity matrix has been computed based on the top 100 expressed genes per cluster (Figure 16I). Remarkably, all clusters from KO astrocytes had high correlation scores to at least one NR astrocyte cluster (Figure 16I). This result correlated with the following GO term analysis that has been performed on differentially expressed genes (DEG) with a threshold of adjusted p-value < 0.05 and log<sub>2</sub> fold change > 1 per cluster. Noteworthy to mention that the number of DEGs was highly reduced overall in the KO clusters and thus did not allow for the study of biological processes in all subclusters that are AhR-deficient. For the GO term analysis, I highlighted the 20 most significant biological processes (BP) with at least 3 genes per BP and a fold enrichment > 2 (Figure 17). The biological processes enriched in the homeostatic 2\_KO astrocyte cluster were related to overall transcriptional activity and gene regulation (Figure 17A), which was also observed in the corresponding cluster 3\_NR (Figure 15D, Figure 16I). Moreover, a strong overlap of enriched biological processes has been observed in the reactive subclusters 4\_KO and 5\_KO with their corresponding subclusters of non-recombined astrocytes (Figure 16I, Figure 17, B and C). I thus could identify pro-inflammatory astrocytes

within cluster 4\_KO by the enrichment of inflammation and immune system-related GO terms and upregulation of chemokines such as *Ccl3* and *Ccl4*, similar to cluster 3\_NR (Figure 15C, Figure 17B). Also, proliferating reactive astrocytes have been identified in cluster 5\_KO based on their cell cycle phase (G<sub>2</sub>/M) (Figure 16H) and the enrichment of proliferation-associated GO terms (Figure 17C). The enriched biological processes related to protein translation, synaptic processes, innate immunity, and cell division in 5\_KO astrocytes and the similarity matrix (Figure 16I, Figure 17C) suggest that this cluster contains cells that are similar to the subclusters 5\_NR and 6\_NR of non-recombined astrocytes. This is likely due to the reduced cell number of AhR-KO astrocytes compared to NR astrocytes and thus does not allow more defined clustering.

Taken together, the loss of AhR in astrocytes resulted in a reduced number of differentially expressed genes in each subcluster, indicating that AhR is transcriptionally active in NR astrocytes. However, the analysis of AhR-KO and NR astrocytes showed that AhR-deficient and NR control astrocytes react similarly to injury, as was already observed in the *in vivo* analysis in sections 2.3 and 2.4. In addition, I was not able to identify differences between AhR-KO and NR astrocytes that would explain the loss of dedifferentiation in AhR-deficient astrocytes and their subsequent inability to form neurospheres as observed in section 2.2.

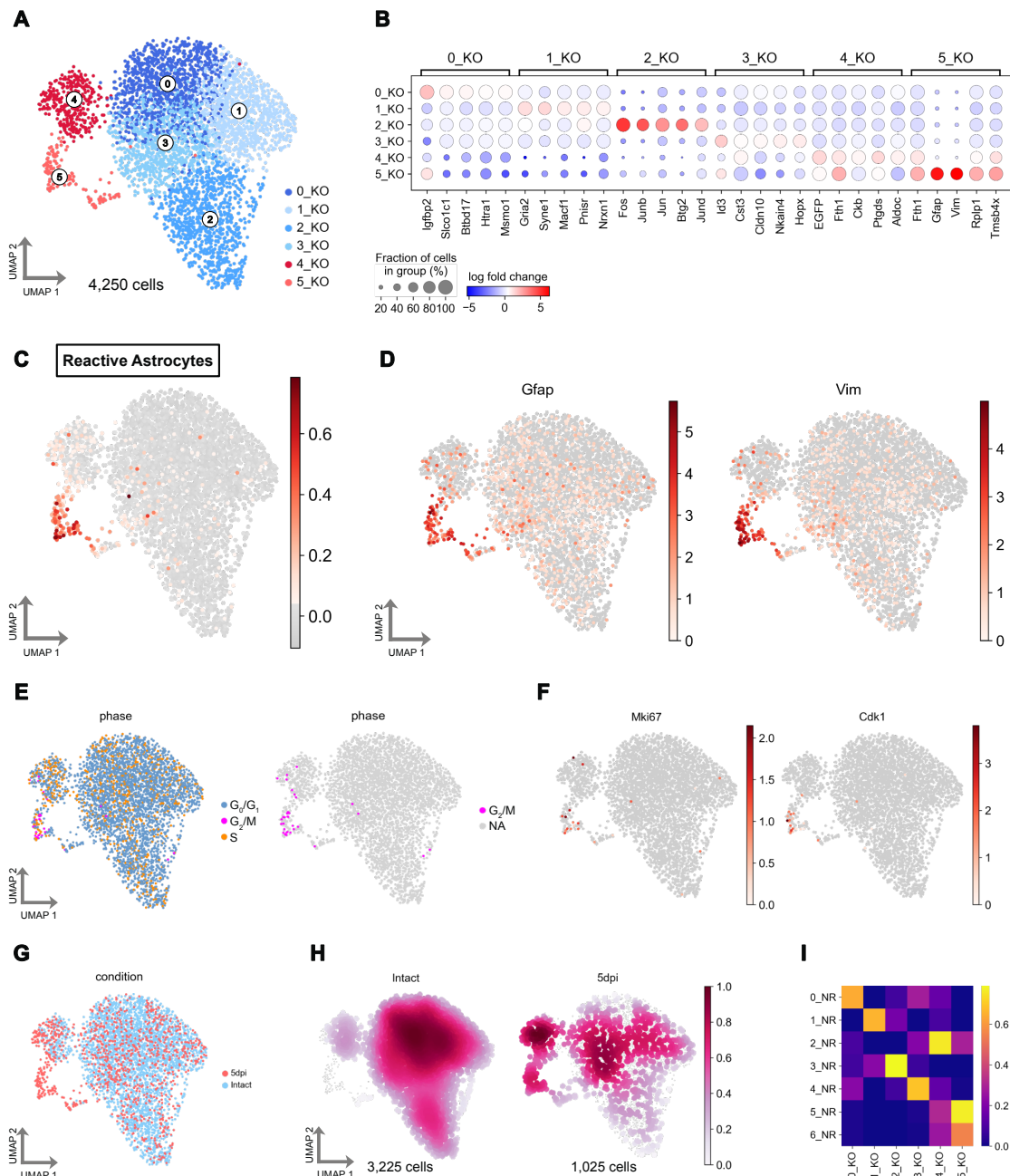


**Figure 16: Characterization of subclustered recombined AhR-KO astrocytes**

(A) UMAP of subclustered recombined AhR-KO (KO) astrocytes from intact and injured (5 dpi) animals. Cells are colored by their subcluster identity. (B) Dot plot of the top 5 enriched genes in each KO astrocyte cluster. The scale bar represents the log fold change of each gene compared to the other clusters. (C) UMAP depicts the reactive astrocyte score calculated from genes enriched in reactive astrocytes (Liddelow et al., 2017). The scale bar represents the gene expression score. (D) UMAP depicts gene expression of two genes *Gfap* and *Vim* that is characteristic of reactive astrocytes. The scale bar represents log transformed gene expression. (E) UMAP depicts the distribution of cells in different cell cycle states  $G_0/G_1$  (blue),  $G_2/M$  (magenta), and S phase (orange). Cells in the  $G_2/M$  phase are highlighted in the right UMAP. (F) UMAP depicts gene expression of two genes, *Mki67* and *Cdk1*, that are characteristic of proliferation. The scale bar represents log transformed gene expression. (G) UMAP depicting the distribution from both intact (blue) and 5 dpi (red) samples. (H) UMAP depicting the computed embedding density of cells in the intact or 5 dpi condition. The scale bar represents the density score. (I) Heatmap depicting the correlation between the KO and NR astrocyte clusters based on the top 100 enriched genes per cluster. The scale bar represents the fraction of overlapping genes. Each dot represents a single cell in the UMAPs.

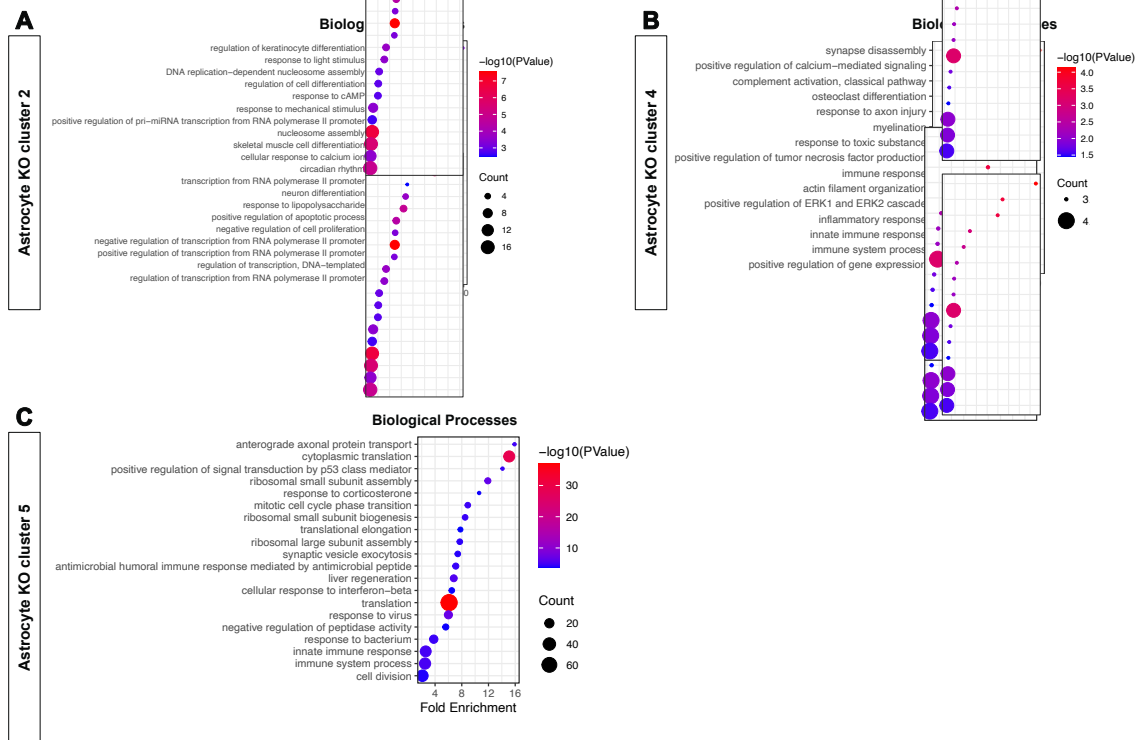


**Figure 17: GO term-based characterization of AhR-KO subclustered astrocytes**

(A to C) Dot plots depict representative Biological Processes enriched by upregulated differentially expressed genes in each subcluster of AhR-KO astrocytes. Cluster 2\_KO (A), 4\_KO (B), and 5\_KO (C). Scale bars represent the negative  $\log_{10}$  p-value calculated by GO term analysis (DAVID).

### 2.5.5 Analysis of injured astrocytes reveals a subpopulation of astrocytes with stem cell characteristics

Given that the analysis described above did not provide any conclusion about how the loss of neurosphere forming capacity in AhR-KO astrocytes is regulated, I used yet another approach. Since dedifferentiation and thus the acquiring of stem cell potential of astrocytes is injury dependent, I focused on the astrocytes derived from the injured mice. Therefore, I subclustered all astrocytes originating from the injured brain, including AhR-deficient (KO) and non-recombined (NR) cells, which allows direct comparison between both types of astrocytes. For this approach, a principal component analysis was performed with 2,000 HVGs and a UMAP was constructed using 8 dimensions of the PCA data set and 30 local neighbors for the k-nearest neighbor algorithm (Figure 18A). Leiden clustering with a resolution of 0.5 resulted in 7 unique groups of astrocytes derived from the injured cortex (Figure 18A). The top 5 genes per cluster revealed that two clusters (4\_5dpi and 5\_5dpi) had enrichment of the reactive astrocyte marker *Gfap* (Figure 18B). The reactive astrocyte score (for definition see section 2.5.3) confirmed the presence of an additional cluster (5\_5dpi) containing reactive astrocytes compared to the NR astrocyte clustering (Figure 18C). The marker genes *Gfap* and *Vim* were also expressed in the cluster 2\_5dpi and 6\_5dpi (Figure 18D). The cell cycle score indicated that most cells in the S

phase were in cluster 2\_5dpi and proliferating cells in the G<sub>2</sub>/M phase were mainly in cluster 4\_5dpi but also cluster 2\_5dpi (Figure 18E). The marker genes for proliferation *Mki67* and *Cdk1* showed that the main proliferating cells are indeed located in cluster 4\_5dpi (Figure 18F). When comparing the top 100 genes of the clusters from the injured brain to the NR clusters using a similarity matrix, most of the 5 dpi clusters showed high similarities to one of the NR clusters except to 4\_NR (Figure 18G). The reactive clusters from NR astrocytes (2\_NR, 5\_NR, and 6\_NR) had high similarity scores to the reactive astrocyte clusters 2\_5dpi, 4\_5dpi, and 6\_5dpi, respectively (Figure 18G). A similar correlation has also been found comparing the injured astrocytes with the KO subclustered astrocytes (Figure 18H). However, cluster 5\_5dpi did not show any correlation with one of the NR or KO astrocyte clusters (Figure 18, G and H). This is of interest because, based on the similarity matrices (Figure 18, G and H), it showed that the cluster 5\_5dpi is an injury-specific cluster and thus may contain dedifferentiated astrocytes.

As described in section 2.2 the AhR-deficient astrocytes were not able to dedifferentiate and form neurospheres. Therefore, I investigated the distribution of AhR-KO versus NR astrocytes and observed that NR astrocytes were present in all seven different clusters (Figure 19, A to C). KO astrocytes, however, were mainly located in clusters 0\_5dpi, 2\_5dpi, 3\_5dpi, and 4\_5dpi (Figure 19, A and B). When quantifying the percentages of NR and KO cells within each cluster to all NR and KO astrocytes from the injured brain, respectively, it appeared that KO astrocytes were enriched in clusters 0\_5dpi and 3\_5dpi (Figure 19C). Interestingly, the two clusters that had a depletion of KO astrocytes were 1\_5dpi and 5\_5dpi, while the clusters 4\_5dpi and 6\_5dpi were unchanged between NR and KO astrocytes (Figure 19C). Since cluster 5\_5dpi appeared to be injury specific and AhR-KO cells were highly depleted in this cluster, I analyzed their distribution in the UMAP of NR and AhR-KO astrocytes from the analysis above (Figure 19D). Interestingly, the NR 5\_5dpi astrocytes did cluster mainly within cluster 1\_NR, whereas the KO cells of the 5\_5dpi cluster were more spread within clusters 0\_KO and 3\_KO (Figure 19D).

Summarizing the first results of this part revealed four reactive (red) and three homeostatic (blue) astrocyte clusters within the 5 dpi astrocytes (Figure 19A). Furthermore, cluster 5\_5dpi is emerging when investigating astrocytes only from the injured brain and AhR-KO cells are depleted in this cluster.

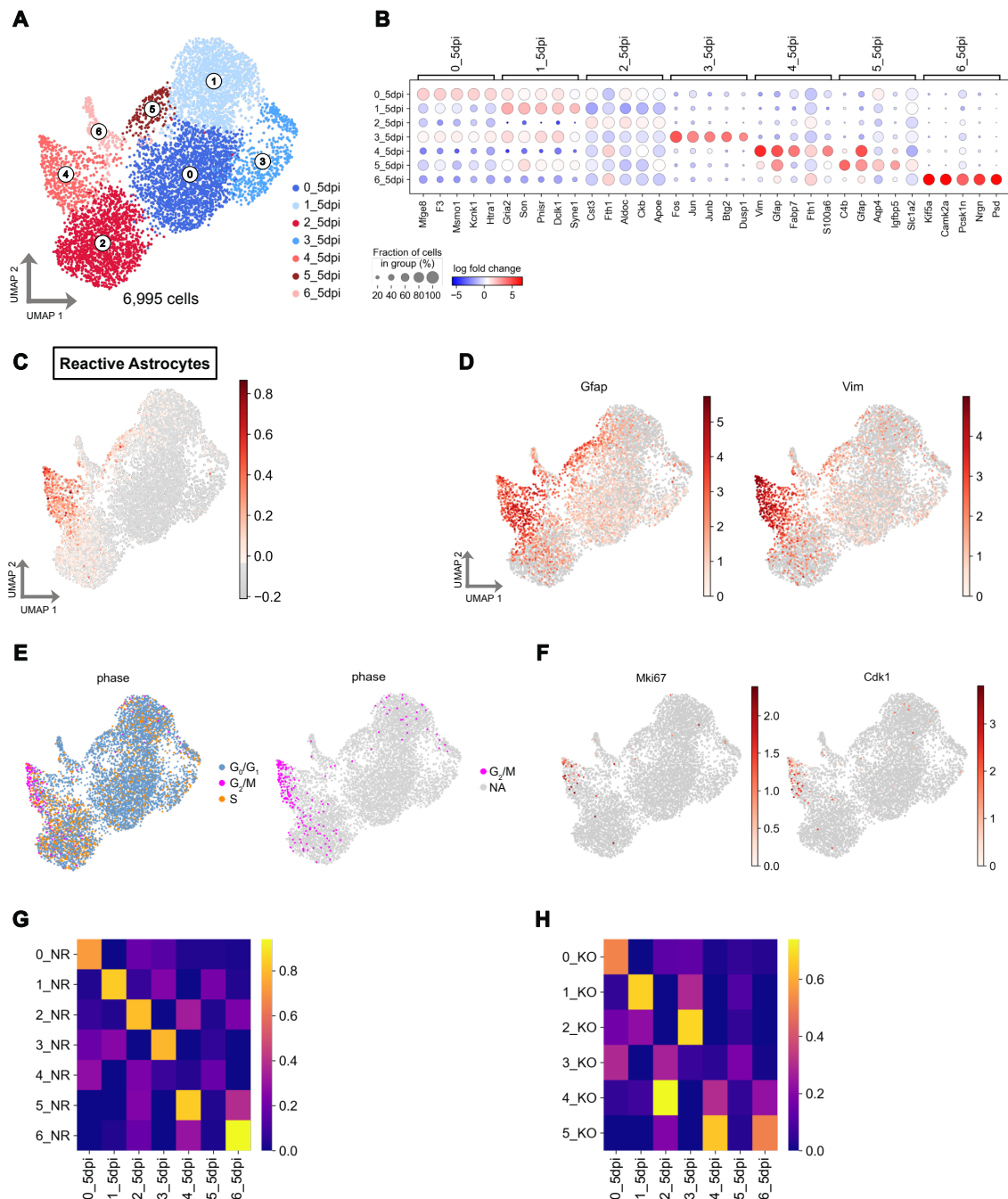


**Figure 18: Characterization of subclustered astrocytes from injured brain**

(A) UMAP of subclustered astrocytes (NR and KO) from injured (5 dpi) animals. Cells are colored by their subcluster identity. (B) Dot plot of the top 5 enriched genes in each KO astrocyte cluster. The scale bar represents the log fold change of each gene compared to the other clusters. (C) UMAP depicts the reactive astrocyte score calculated from genes enriched in reactive astrocytes (Liddelow et al., 2017). The scale bar represents the gene expression score. (D) UMAP depicts gene expression of two genes *Gfap* and *Vim* that is characteristic of reactive astrocytes. The scale bar represents log transformed gene expression. (E) UMAP depicts the distribution of cells in different cell cycle states  $G_0/G_1$  (blue),  $G_2/M$  (magenta), and S phase (orange). Cells in the  $G_2/M$  phase are highlighted in the right UMAP. (F) UMAP depicts gene expression of two genes, *Mki67* and *Cdk1*, that are characteristic of proliferation. The scale bar represents log transformed gene expression. (G and H) Heatmaps depicting the correlation between the 5 dpi and NR astrocyte clusters (G) and between 5 dpi and KO astrocyte clusters (H) based on the top 100 enriched genes per cluster. The scale bar represents the fraction of overlapping genes. Each dot represents a single cell in the UMAPs.

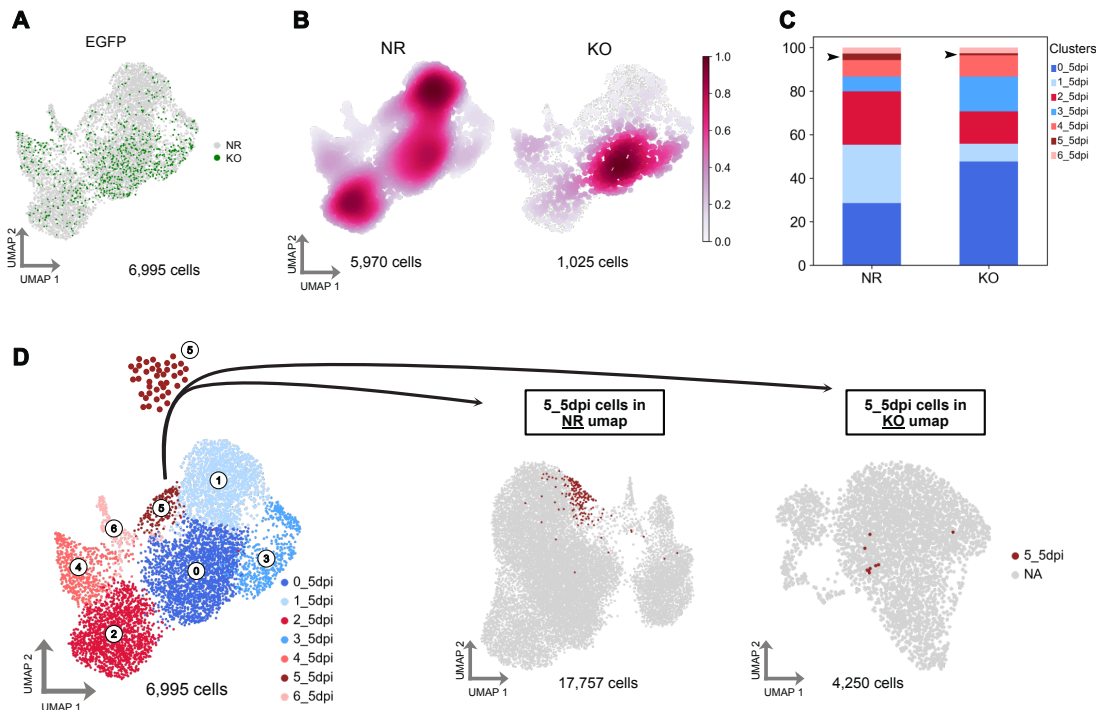


**Figure 19: Comparison of NR and KO astrocytes of subclustered astrocytes from injured brain**

(A) UMAP depicting the distribution of recombined AhR-KO (KO) cells (green) and non-recombined (NR) cells (grey). (B) UMAPs depict the computed embedding density of NR and KO astrocytes. The scale bar represents the density score. (C) Stacked bar plot depicting the percental fractions of cells per cluster in NR and KO astrocytes at 5 dpi. Scale in percentage. Each cluster is color-coded by its identity (Figure 18A). Arrowheads highlighting cluster 5\_5dpi. (D) UMAPs depicting the localization of cluster 5\_5dpi cells (dark red) in the UMAPs of NR and KO astrocytes. Each dot represents a single cell in the UMAPs.

Since AhR-deficient astrocytes did not form neurospheres after injury *in vitro* (section 2.2), I expected a cluster that showed a depletion of reactive AhR-KO astrocytes. In addition, clusters that showed high expression of proliferation markers were excluded because I did not observe any differences between AhR<sup>fl/fl</sup> and Ctr astrocytes regarding their proliferative behavior (section 2.3). Due to these reasons, I further investigated cluster 5\_5dpi as it was the only cluster of reactive astrocytes that showed a depletion of KO cells and emerged upon injury.

To get a first impression of the regulated genes in cluster 5\_5dpi astrocytes, I performed GO term analysis of significantly upregulated differentially expressed genes (adjusted  $p < 0.05$ ,  $\log_2$  fold change  $> 1$ ) of cluster 5\_5dpi compared to the remaining six clusters (Figure 20, A and B). The 35 most significant biological processes with at least 7 genes (to reduce redundant GO terms) and a fold enrichment  $> 2$  are depicted in the dot plots (Figure 20A). Interestingly, GO terms related to bone morphogenetic protein (BMP) and wingless-type (Wnt) signaling pathway were enriched in biological processes as well as a positive regulation of mitogen-activated protein kinase (MAPK) cascade, which are all important signaling pathways important in neural stem cell maintenance and differentiation (see section 1.3) (Figure 20A). Additionally, biological processes such as multicellular organism development and neuron differentiation were

enriched (Figure 20A). To complement the GO terms, KEGG (Kyoto Encyclopedia of Genes and Genomes) pathway analysis was performed. Plotting all significant enriched KEGG pathways resulted in an enrichment of signaling pathways regulating pluripotency of stem cells that include BMP and Wnt signaling (Figure 20, B and C; Figure 21, A, C, and D). The upregulated genes in cluster 5\_5dpi in this KEGG pathway are receptor molecules and downstream targets of their signaling (Figure 20C; Figure 21A). Moreover, the receptors of EGF (*Egfr*) and FGF2 (*Fgfr1* and *Fgfr3*) signaling, important for the neurosphere formation *in vitro*, were significantly upregulated in cluster 5\_5dpi (Figure 20D).

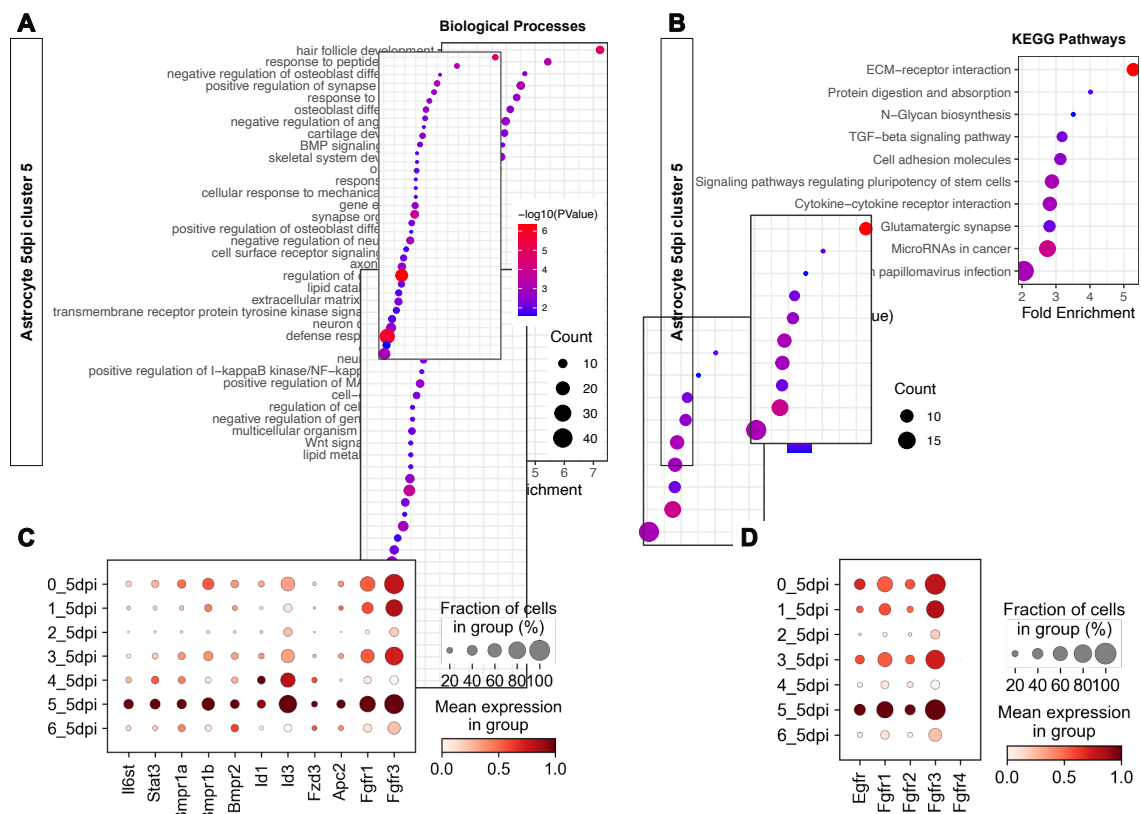


**Figure 20: Cluster 5\_5dpi astrocytes show stem cell characteristics**

(A and B) The dot plots depict representative Biological Pathways (A) and KEGG Pathways (B) enriched by upregulated genes in cluster 5 of 5 dpi (5\_5dpi) subclustered astrocytes. Scale bars represent the negative  $\log_{10}$  p-value calculated by GO term analysis (DAVID). (C) The dot plot depicts genes from the KEGG pathway “Signaling pathways regulating pluripotency of stem cells” in 5 dpi astrocyte subclusters. (D) The dot plot depicts EGF and FGF2 receptor genes expressed in 5 dpi astrocyte subclusters. The scale bars represent a standardized scale between 0 and 1 for each gene (C and D).

However, for signaling pathways it is important that not only the receptors and some downstream targets are upregulated but also the remaining genes of each pathway need to be expressed to allow the signaling mechanism to function and regulate cellular processes such as dedifferentiation. I thus further explored the expression of genes involved in the KEGG pathway “Signaling pathways regulating pluripotency of stem cells” (Figure 21). The differentially expressed genes of each signaling cascade related to stem cell maintenance are highlighted in

red (Figure 21A). From all four pathways the ligand molecules *Bmp4*, *Wnt*, *Fgf2*, and *Lif* were very low expressed, suggesting that the activation of these pathways is initiated from a different cell type than astrocytes (Figure 21, B to E). Many genes involved in the BMP signaling, including the downstream targets *Id1* to *Id4*, were highly expressed in cluster 5\_5dpi (Figure 21B). Also, genes involved in the Wnt signaling cascade including membrane receptors, signal amplifying and effector molecules like *Tcf3* were expressed in cluster 5\_5dpi (Figure 21C). In addition, genes involved in the FGF2 signaling were also detected in 5\_5dpi astrocytes (Figure 21D). In contrast, the effector molecules of the LIF mediated pathways such as *Klf4*, *Myc*, and *Tbx3* were barely expressed in 5\_5dpi astrocytes (Figure 21E). Hence, these results suggest a potential role of BMP, Wnt, and FGF2 signaling in the dedifferentiation process of reactive astrocytes upon injury. To complete this analysis, the target genes of the stem cell regulating pathways have been investigated and one of the highest expressed target genes within cluster 5\_5dpi astrocytes was the transcription factor *Pax6* (Figure 21F).

Since transcription factors regulate the gene expression of a variety of genes and thus are highly important in controlling cellular processes, I wanted to investigate, which transcription factors (TF) are the most relevant to regulating the gene expression in this subcluster. To perform this analysis I collaborated with Pawel Smialowski, who developed a pipeline to analyze TF activity based on differentially expressed gene sets with a cut-off of the adjusted p-value < 0.05 (Angerilli et al., 2018). The top 15 transcription factors from this ranking are depicted in a network, which is based on the STRING database with a confidence cutoff of 0.4 (Figure 22A). It has been hypothesized that reactive astrocytes upregulate developmental signaling cascades that are important in stem cell maintenance and differentiation and thus allow them to dedifferentiate (Robel et al., 2011). Interestingly, the transcription factor *Pax6*, which is known to play a crucial role during brain development and is also upregulated in reactive astrocytes (Robel et al., 2011), was enriched in this analysis (Figure 22A). This was also supported by the significant upregulation of *Pax6* with a  $\log_2$  fold change of 0.96 in 5\_5dpi astrocytes (Figure 21F, Figure 22A). Of note, the transcription factor Achaete-scute homolog 1 (*Ascl1*) was among the top 15 TFs in this analysis, as well as among the differentially upregulated genes in cluster 5\_5dpi (Figure 22, A and B). *Ascl1* has shown to be crucial for efficient reprogramming of astrocytes to inhibitory neurons (Heinrich et al., 2010; Kempf et al., 2021; Masserdotti et al., 2015). In addition, Wnt (*Tcf4*) and BMP (*Id1*, *Id3*, and *Id4*) signaling were also enriched by the TF ranking analysis (Figure 22, A and B). Interestingly, the upregulation and enriched activity of *Stat* transcription factors has been observed in cluster 5\_5dpi (Figure 22, A and B). The expression of *Stat1* and *Stat2* is regulated by interferon I (IFN-I) signaling in reactive astrocytes, which is accompanied by an upregulation of the interferon regulatory factor 9 (*Irf9*) (Rothhammer et al., 2016). *Irf9* was also enriched in cluster 5\_5dpi astrocytes with a z-score of

2.2 and a  $\log_2$  fold change of 1.2 (Figure 22B). IFN-I signaling is important during neuroinflammation and AhR is known to mediate its signaling in reactive astrocytes (Rothhammer et al., 2016). Hence, the emergence of stem cell characteristics in dedifferentiated reactive astrocytes for example by activation of PAX6 might be induced by IFN-I signaling that is mediated by AhR.

In conclusion, I could show that the cluster 5\_5dpi astrocytes had enriched stem cell signatures based on their differentially expressed genes. Furthermore, the analysis revealed a potential link between neuroinflammation and upregulation of transcription factors that are important during brain development such as *Pax6*. I could also demonstrate that receptors for EGF and FGF2 signaling, which are important in the neurosphere assay were upregulated in 5\_5dpi cells. Therefore, these astrocytes are strong candidates to dedifferentiate upon injury and subsequently form neurospheres *in vitro*.



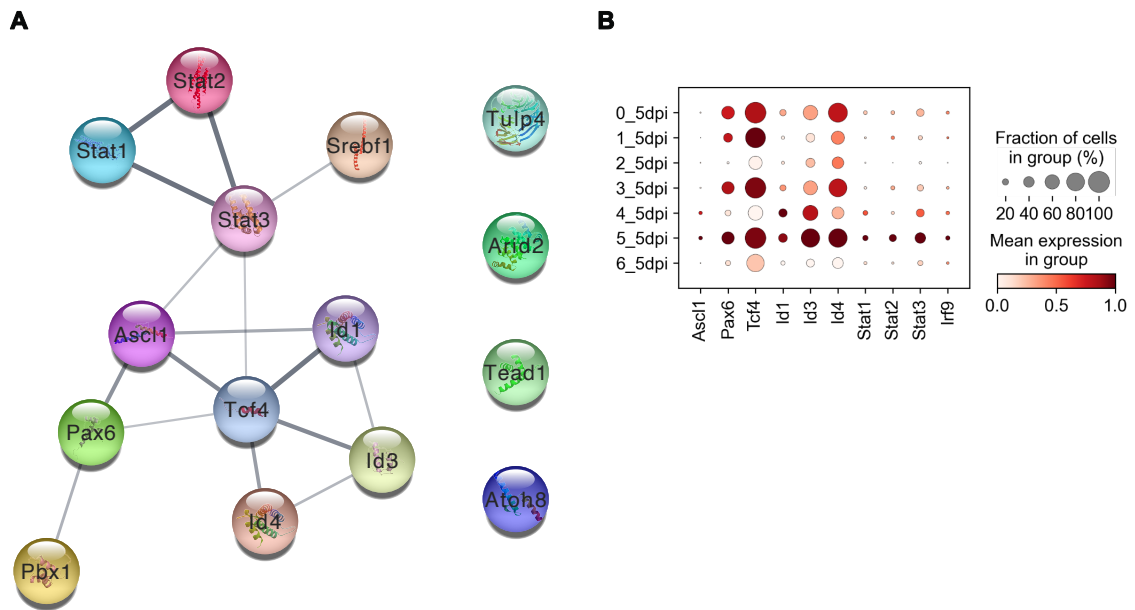


**Figure 22: Transcription factor ranking of cluster 5\_5dpi astrocytes**

**(A)** Top 15 TFs from transcription factor network analysis detecting active TFs in cluster 5\_5dpi. Interactions are calculated based on the STRING database. The strength of known interactions is indicated by the thickness of connecting lines. **(B)** Dot plot depicting a selection of ranked TFs and *Irf9* in 5 dpi astrocyte subclusters. Scale bars represent standardized scales between 0 and 1 for each gene

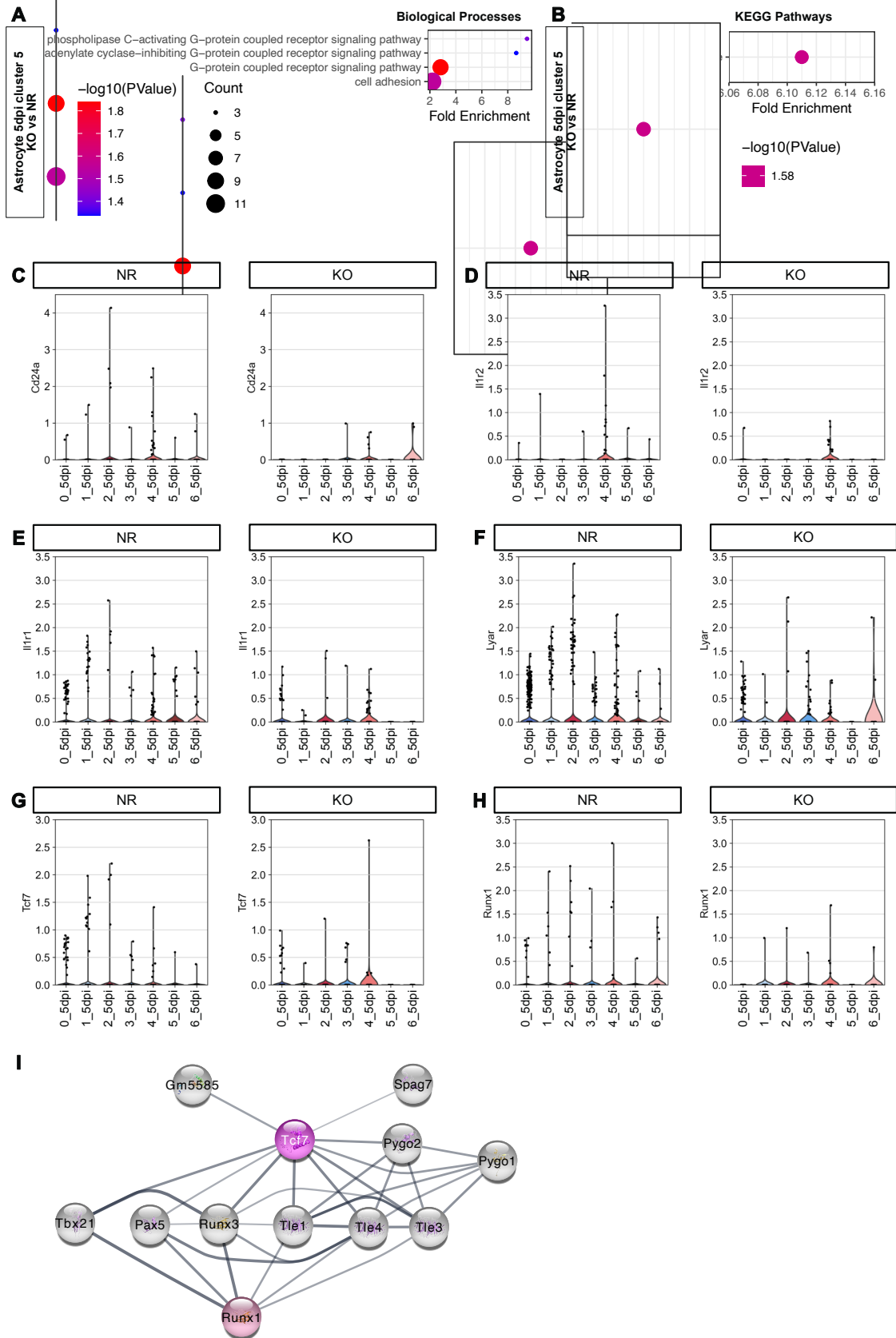
### 2.5.6 What are the AhR-dependent processes regulated in 5\_5dpi astrocytes with stem cell characteristics?

As described in the section above (2.5.5), the astrocytes in cluster 5\_5dpi are strong candidates for defining the subpopulation of reactive astrocytes that dedifferentiate upon injury and acquire stem cell potential. Because AhR-deficient astrocytes did not form neurospheres *in vitro* (see section 2.2), I assessed the differences between NR and AhR-KO astrocytes in cluster 5\_5dpi by differential gene expression analysis using the Wald test. Subsequently, I used the 203 differentially expressed genes that were downregulated in AhR-KO astrocytes to perform GO term and KEGG pathway analysis (Figure 23, A and B). The biological processes showed a reduction of G-protein coupled receptor signaling pathway and cell adhesion in AhR-KO astrocytes in cluster 5\_5dpi (Figure 23A). The GO term related to cell adhesion did consist of *Cd24a*, among other genes, which is known to be expressed in the neuronal stem cell lineage and thus might be a potential candidate explaining the loss of stem cell potential acquisition in AhR-deficient astrocytes (Pruszek et al., 2009). Moreover, *Cd24a* showed to be lower expressed across all 5 dpi clusters in KO astrocytes compared to NR cells from the injured brain (Figure 23C). In addition, the KEGG pathway “Hematopoietic cell lineage” was enriched within the downregulated genes in 5\_5dpi KO astrocytes (Figure 23B). The downregulated genes in this pathway were *Cd24a* and *Il1r2* next to others. Furthermore, *Il1r2* – a non-signaling receptor of interleukin 1 (IL-1) (Colotta et al., 1993) – was lower expressed in most KO astrocytes derived

from injured mice (Figure 23D). This trend was not observed by the IL-1 signaling receptor gene *Il1r1* (Figure 23E). Interestingly, the IL-1 receptors are potential direct downstream targets of AhR activation (Hanieh, 2014). Noteworthy, *Lyar* was within the top 10 downregulated genes in KO astrocytes based on the mean expression within NR and KO astrocytes. LYAR is a nucleolar protein essential to maintaining the self-renewal of embryonic stem cells (H. Li et al., 2009). When comparing the gene expression levels of *Lyar* across all 5 dpi subclusters, I observed that this gene was absent only in KO astrocytes in cluster 5\_5dpi (Figure 23F). The differential gene expression analysis between AhR-deficient and non-recombined astrocytes with subsequent GO term and KEGG pathway analysis resulted thus in three potential candidates that might be responsible for the loss of dedifferentiation in AhR-KO astrocytes.

As stated in section 2.5.5, transcription factors are crucial in regulating gene expression and with those also cellular processes. Therefore, I used the transcription factor ranking analysis based on the differentially expressed genes with a cut-off of q-value < 0.5 to have enough genes to construct a TF-based network, which was performed by Pawel Smialowski (Angerilli et al., 2018). The analysis resulted in two downregulated transcription factors *Tcf7* and *Runx1* (Figure 23I). A network with these two TFs was calculated based on the STRING database (confidence cutoff 0.4) and extended by ten additional interactors (grey) (Figure 23I). The network revealed that *Tcf7* and *Runx1* share 6 common interactors, among the 10 top interactors, that are also transcription factors and thus may regulate partially overlapping gene expressions (Figure 23I). Furthermore, *Tcf7* and *Runx1* were also significantly downregulated in 5\_5dpi KO astrocytes (Figure 23, G and H). Interestingly, both transcription factors are associated with the Wnt signaling pathway (Jeannet et al., 2010; Medina et al., 2016).

In conclusion, the direct comparison of AhR-deficient and NR astrocytes resulted in five potential candidates that might explain the loss of neurosphere formation directly based on the differential gene expression analysis. However, the enrichment of Wnt signaling in 5\_5dpi astrocytes and the specific downregulation of downstream target genes of this signaling pathway in 5\_5dpi AhR-KO astrocytes strongly suggest that Wnt signaling is important during dedifferentiation and stem cell potential acquisition in an AhR-dependent manner.



represents log transformed gene expression; each dot represents a single cell. (I) Repressed transcription factors (colored) in KO astrocytes in cluster 5\_5dpi from transcription factor network analysis. Interactions are calculated based on the STRING database and the network is expanded by 10 interactors (grey). The strength of known interactions is indicated by the thickness of connecting lines.

### 2.5.7 Are dedifferentiated astrocytes derived from proliferating astroglia?

In section 2.3 I described that no differences between AhR-deficient and Ctr astrocytes had been found regarding their proliferation upon injury *in vivo*. Until now it was suggested that proliferation and dedifferentiation of reactive astrocytes are linked with each other (Dimou & Götz, 2014; Sirko et al., 2013). So far, the scRNAseq analysis in section 2.5.5 also supports the concept that different astrocyte clusters proliferate and form neurospheres. To further investigate, whether the proliferative reactive astrocytes are linked to the astrocytes exhibiting stem cell potential, I made use of RNA velocity analysis. RNA velocity is based on the ratio between spliced and unspliced mRNA transcripts and was successfully used to analyze developmental stages (Bergen et al., 2020). The rationale behind this analysis lies in the fact that unspliced pre-mRNA is spliced in the process of mRNA maturation and thus allows to indicate the direction of cell differentiation.

The velocity analysis was performed on non-recombined and AhR-KO astrocytes derived from the injured (5 dpi) brain, respectively. The top 2,000 highly variable genes were used to calculate the velocity, which was then embedded on the UMAP of 5 dpi astrocytes (Figure 24, A to D). The velocity analysis of 5 dpi NR astrocytes showed that cells from the clusters 2\_5dpi, 4\_5dpi, and 6\_5dpi had a directionality towards the stem cell-associated cluster 5\_5dpi (Figure 24, A and B). Cluster 4\_5dpi has been shown to contain mainly reactive proliferating astrocytes (see section 2.5.5), and thus a connection between proliferating and dedifferentiation astrocytes could be established. Interestingly, only cluster 6\_5dpi but not 2\_5dpi and 4\_5dpi astrocytes maintained the direction towards 5\_5dpi cells in the AhR-KO condition (Figure 24, C and D). Furthermore, KO cells in cluster 5\_5dpi lost their north-east directionality observed in NR astrocytes within this cluster (Figure 24, B' and D').

Together, these results suggest a possible link between proliferating and dedifferentiating reactive astrocytes. Furthermore, the velocity analysis implies that some of the proliferating astrocytes can fully dedifferentiate and acquire stem cell potential upon injury. To complement this analysis, I identified important genes in NR astrocytes that may explain the velocity in 4\_5dpi astrocytes (Figure 24E). Interestingly, transferrin (*Trf*) was among the top ten important genes (Figure 24E). Additionally, *Trf* was expressed in 5\_5dpi cells in its spliced mature mRNA form (Figure 24E). Transferrin expression is known to be regulated by hypoxia which induces oxidative stress and an increase of reactive oxygen species (McGarry et al., 2018; Rolfs

et al., 1997). Notably, oxidative stress is a key barrier to direct neuronal reprogramming of astrocytes (Gascón et al., 2016).

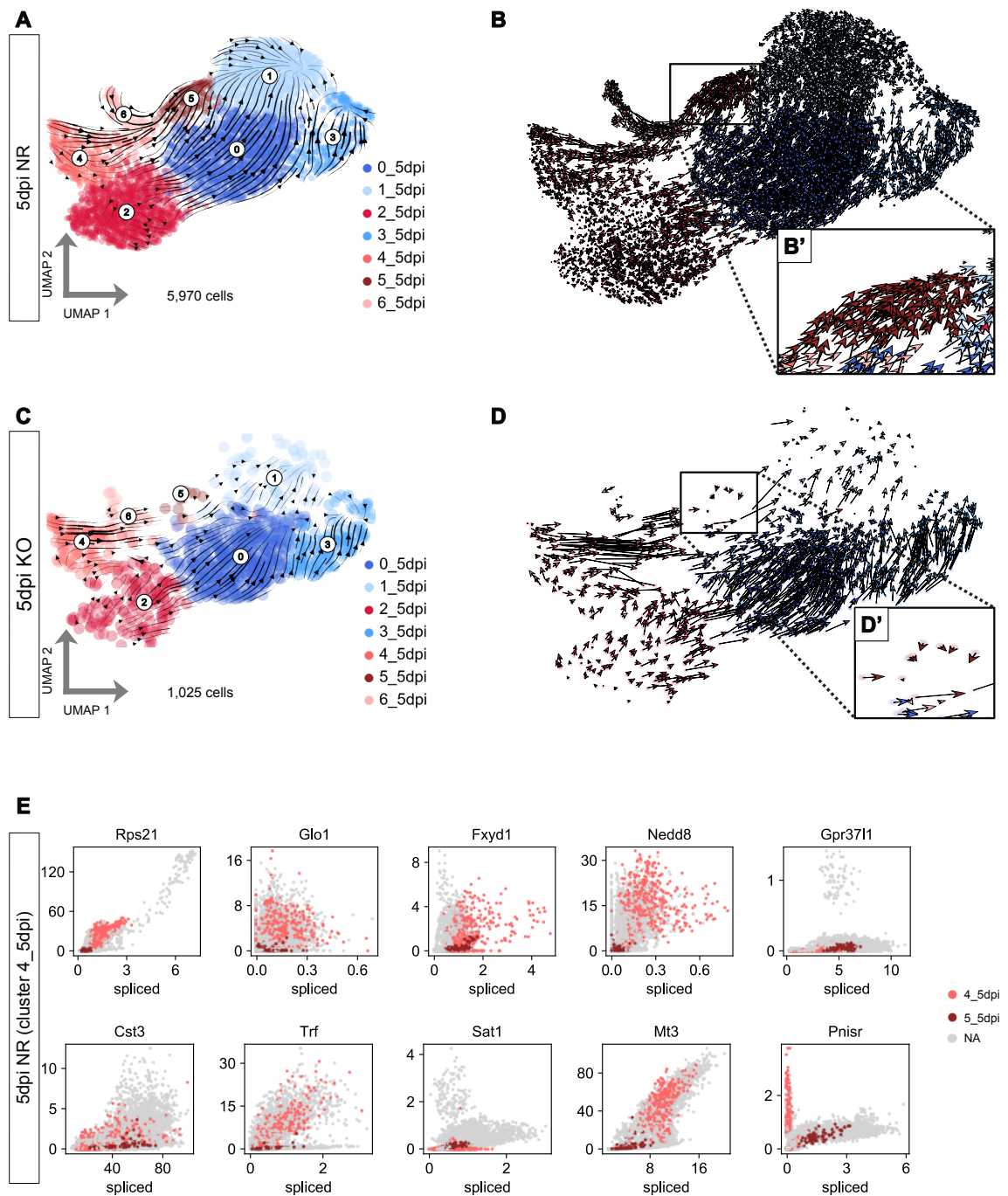


**Figure 24: Velocity analysis of injured astrocytes**

**(A)** Stream plot of velocity analysis on the UMAP of non-recombined (NR) injured (5 dpi) astrocytes. **(B)** Scatter plot of velocity analysis on the UMAP of NR 5 dpi astrocytes including a magnification of cluster 5\_5dpi (B'). **(C)** Stream plot of velocity analysis on the UMAP of AhR-KO injured (5 dpi) astrocytes. **(D)** Scatter plot of velocity analysis on the UMAP of KO 5 dpi astrocytes including a magnification of cluster 5\_5dpi (D'). Arrows in the velocity analysis indicate the direction and speed of movement of cells. **(E)** Scatter plots of top ten ranked genes defining velocities in cluster 4\_5dpi NR astrocytes. Non-recombined cells in cluster 4\_5dpi (light red) and 5\_5dpi (dark red) are highlighted. Each dot in the scatter plots and UMAPs represent a single cell.



### 3 Discussion

Replacement of lost neurons after central nervous system (CNS) injury is at the center of regenerative therapy. The acquisition of stem cell properties of a subpopulation of astrocytes after injury gives a promising target population for direct reprogramming into neurons. It is, however, important to understand the underlying mechanisms of astrocyte dedifferentiation not only to facilitate the process of reprogramming into desired neuronal fates but also more immature astrocytes might have additional neuroprotective aspects, like the support of synapse formation and neurite outgrowth. The aryl hydrocarbon receptor (AhR) has been implicated with brain regeneration by promoting neuronal potential of adult neural stem cells (aNSC) and is also expressed in reactive astrocytes (Chen et al., 2019; Di Giaimo et al., 2018; Frik et al., 2018; Siddiqui et al., 2021). Therefore, AhR is an interesting candidate to regulate astrocyte dedifferentiation upon injury and I investigated the neural stem cell response of the subpopulation of cortical astrocytes after injury regarding the AhR signaling. My work shows, that the AhR signaling is necessary for the dedifferentiation of astrocytes and their neurosphere forming capacity. None of the AhR-deficient cerebral cortex astrocytes formed a neurosphere after injury. Interestingly, the AhR-KO did not result in differences in astrocyte proliferation *in vivo* upon stab wound injury. Hence, these results suggest that proliferation and dedifferentiation of reactive astrocytes might not be interconnected processes. However, the velocity analysis of single-cell transcriptome data of injured astrocytes could indicate that proliferating reactive astrocytes dedifferentiate to acquire stem cell capacities. With the single-cell RNA sequencing (scRNAseq) analysis, I was able to find different subpopulations of astrocytes and identified a subpopulation that may have dedifferentiated with the potential to form neurospheres *in vitro*. Furthermore, my analysis suggests the reduction in Wnt (wingless-type) signaling in AhR-KO astrocytes within the dedifferentiated astrocyte subpopulation giving a potential mechanism explaining the loss of neurosphere formation.

#### 3.1 The aryl hydrocarbon receptor is necessary for the dedifferentiation of astrocytes after injury

AhR-deficient astrocytes lost the capacity to form neurospheres, and thus their stem cell potential after injury *in vitro*. Recently it has been shown that aNSCs in the zebrafish telencephalon increase their proliferation rate upon injury by downregulating AhR activity. Conversely, the enhancement of the AhR signaling leads to increased neuronal differentiation (Di Giaimo et al., 2018). A study investigating the effects of AhR signaling in the DG showed that deletion of AhR or its activation led to reduced neurogenesis (Latchney et al., 2013). However, this study did lack a defined tool since they used a full knock-out system for AhR and systemic

activation via 2,3,7,8-tetrachlorodibenzo-*p*-dioxin (TCDD), and thus, the observed effects might result from indirect effects on neural precursor cells in the dentate gyrus. Using a full knock-out of AhR did also result in a pluripotent phenotype in embryonic stem cells, which was accompanied by overexpression of the pluripotency factors OCT4 and NANOG, and enhanced glycolytic metabolism during early mouse embryo development (Nacarino-Palma et al., 2021). In addition, antagonizing the AhR signaling leads to an expansion of human HSCs (Boitano et al., 2010). The pivotal role of AhR in hematopoiesis has been also examined in mice and led to the conclusion that a conditional AhR-KO in HSCs and AhR antagonization led to increased proliferation of murine HSCs (Vaughan et al., 2021). Taken together, the low levels of AhR promoted stemness in several somatic stem cells. Therefore, it would be expected that AhR-KO would promote stemness in astrocytes after injury and increase neurosphere formation upon conditional AhR-KO in astrocytes. This discrepancy might be explained by the fact that the studies mentioned above did look at stem cells. However, astrocytes in the cortex are post-mitotic cells without stem cell characteristics in intact conditions. To acquire stem cell potential, astrocytes need to dedifferentiate. The astrocyte de-differentiation shares some features with the cancer initiation and induction of the cancer stem cells (CSC) from somatic, differentiated cells. CSCs are known for their capacity to self-renew and emerge either from adult stem cells or from somatic cells by dedifferentiation (Friedmann-Morvinski et al., 2012; Friedmann-Morvinski & Verma, 2014; Hanahan, 2022). This process has also been observed in astrocytes after deletion of the tumor suppressors p16<sup>INK4a</sup> and p19<sup>ARF</sup> in combination with EGF signaling (Bachoo et al., 2002). Interestingly, the role of AhR in CSCs has been investigated in choriocarcinoma and did result in a decrease of spheroids, and thus, in reduced stem cell-like characteristics upon AhR knockdown using short hairpin RNA (shRNA) (C. Wu et al., 2018). The shRNA-mediated knockdown of AhR led also to a suppressed tumorigenesis *in vivo* using a xenograft model (C. Wu et al., 2018). Furthermore, it is widely accepted that Wnt signaling, a signaling pathway that we identified in the AhR-deficient astrocytes, plays a crucial role in the process of dedifferentiation in cancer (Hanahan, 2022). Thus, AhR signaling may have opposing roles in stem cell maintenance and acquiring stem cell potential in the process of dedifferentiation.

This concept is further strengthened by the observation that the conditional AhR-KO does not alter the neurosphere formation capacity of progenitors and aNSCs from the subependymal zone (SEZ). Moreover, AhR-deficient *Nestin*<sup>+</sup> aNSCs in the SEZ and DG increase their proliferation after stroke (Chen et al., 2019). Similar results have been obtained by antagonizing AhR in the same study.

### 3.2 The astrocyte-specific AhR does not alter the proliferation of astrocytes and infiltration of leukocytes

It has been suggested that reactive astrocytes that acquire stem cell potential *in vitro* upon injury are a subpopulation of *in vivo* proliferating reactive astrocytes (Buffo et al., 2008; Sirko et al., 2013). For both phenotypes, astrocytes need to dedifferentiate toward an earlier developmental state that resembles features of NSCs. Recently it has been shown that the proliferation of astrocytes was increased when infiltration of leukocytes into the parenchyma was impaired in a C-C motif chemokine receptor 2 (CCR2) deficient mouse model (Frik et al., 2018). In addition, the aryl hydrocarbon receptor nuclear translocator 2 (ARNT2), an important partner protein of AhR to form a heterodimer for transcriptional activation, was enriched in the cortical parenchyma at 5 days post injury (dpi) based on mass spectrometry in CCR2-KO animals (Frik et al., 2018). AhR deficiency in astrocytes in multiple sclerosis (MS) mouse model systems was associated with a pro-inflammatory state of astrocytes and resulted in an increase of infiltrating monocytes (Rothhammer et al., 2016). Together, these studies suggest that AhR signaling is associated with proliferation of reactive astrocytes and their anti-inflammatory role upon injury. In this work, however, I did not observe any differences in the proliferation behavior of astrocytes or the extravasation of leukocytes in an AhR-dependent manner. But it cannot be excluded that the number of AhR-KO astrocytes was too low to observe any non-cell-autonomous, astrocyte-mediated regulation of leukocytes infiltration. The use of an astrocyte-specific mouse line expressing constitutively Cre in combination with the *Ahrfx* mouse line (Walisser et al., 2005) would help to study the effects on leukocyte extravasation after injury. Nonetheless, it can be concluded that the infiltration of leukocytes into the parenchyma after injury did not affect the dedifferentiation of astrocytes. In this study, I did not observe any differences in the proliferation of AhR-KO astrocytes after injury compared to control astrocytes based on both immunohistochemical and scRNAseq analysis. As cell cycle regulation is a cell-autonomous feature, my results support no role of AhR in regulating the proliferation of astrocytes after brain injury. This data also raises the question, of whether fully dedifferentiated astrocytes with stem cell properties in the neurosphere assay are indeed a subpopulation of proliferating astrocytes. It is possible, that dedifferentiation towards early developmental stages occurs after entering the cell cycle, and thus, effects of the AhR-KO in astrocytes cannot be observed on proliferating astrocytes but only when examining the stem cell capacities. This hypothesis would be supported by the velocity analysis performed on the scRNAseq data of injured astrocytes. Another, yet plausible, explanation would be that the processes of proliferation and dedifferentiation are independent of each other and AhR signaling is only required for the acquisition of stem cell capacities by dedifferentiation. To address this topic,

BrdU labeling of proliferating cells would not be sufficient due to its diluting nature after each cell division, which occurs multiple times in the process of neurosphere formation from a single cell. Hence, a system would be required to fate map proliferating cells in adult animals. The group of Hans Clevers generated a mouse line expressing CreERT2 in a Ki67-dependent manner (Basak et al., 2018). Crossing this mouse line with the CAG-CAT-EGFP reporter mouse line (Nakamura et al., 2006) would enable us to study whether cortical-derived neurospheres are indeed a subpopulation of proliferating astrocytes.

### 3.3 Heterogeneity of astrocytes observed by scRNAseq

It is widely accepted that astrocyte heterogeneity exists among different brain regions (Sofroniew & Vinters, 2010; Verkhratsky & Nedergaard, 2018). A well-established heterogeneity lies between astrocytes located in grey and white matter, which are referred to as protoplasmic and fibrous astrocytes, respectively (Verkhratsky & Nedergaard, 2018). Increasing evidence has shown that cortical astrocytes are heterogeneous within the same brain region, not only in their gene expression profile at single-cell level but also in physiological properties (Batiuk et al., 2020; Bayraktar et al., 2020). Furthermore, the response to CNS insult is heterogeneous among astrocytes (Sofroniew, 2020). An important feature is to discriminate between proliferating and non-proliferating reactive astrocytes (Sofroniew, 2020). Non-proliferating reactive astrocytes undergo gene expression and morphological changes but retain cellular interactions and supportive functions in neural tissue (Sofroniew & Vinters, 2010; Sofroniew, 2009; Zamanian et al., 2012). Proliferating reactive astrocytes contribute to the astrocyte border forming process separating the insulted area from the healthy CNS, which in the brain is also accompanied by non-proliferating reactive astrocytes (Frik et al., 2018; Sofroniew, 2020). In addition, it has been shown that the location of proliferating astrocytes is preferential juxtavascular (Bardehle et al., 2013; Frik et al., 2018). This astrocyte population downregulates the inward rectifying  $K^+$  channel  $K_{ir}4.1$  resulting in changes in their electrophysiological properties after traumatic brain injury (TBI) compared to non-juxtavascular astrocytes (Götz et al., 2021). Therefore, it was interesting to see different states of cortical astrocytes in the scRNAseq data. Not only reactive and homeostatic astrocytes have been identified, but also various states of astrocytes that might explain their wide range of diverse functions, such as metabolic support, synaptic plasticity, and regulation of inflammatory processes. For example, proliferative reactive astrocytes identified by scRNAseq analysis are known to serve anti-inflammatory purposes by reforming the BBB (Bush et al., 1999; Frik et al., 2018). In addition, astrocytes with a pro-inflammatory signature were found in the single-cell transcriptomic data. Interestingly, it has been shown that acute inflammation is critical for regenerative processes and neurogenesis upon TBI in zebrafish telencephalon (Kyritsis et al., 2012, 2014). Furthermore, a cluster of astrocytes showed an

upregulation of immediate-early genes like *Fos* and *Jun*. Immediate-early genes are transcription factors (TF) and are recognized for their rapid response to a broad range of signaling molecules. This is of importance in neurons during synaptic processes and vital for brain functions (Kim et al., 2018). Recently, it has been demonstrated that the immediate-early gene c-Fos is also upregulated in a pre-state of reactive astrocytes in a mouse model of MS (Groves et al., 2018). The abundance of the so-called immediate-early astrocytes did correlate with MS severity in these mice (Groves et al., 2018). It would be interesting to study whether this astrocyte state is also present after TBI in mice.

As indicated by the presented work and also by other publications, astrocytes that acquire stem cell capacities after TBI are yet another subpopulation (Buffo et al., 2008; Sirko et al., 2013). It remained difficult to find a marker gene for this particular astrocyte subpopulation. Sonic hedgehog (SHH) signaling in reactive astrocytes showed to be important for proliferation and stem cell properties after TBI (Sirko et al., 2013). However, ablation of SHH signaling did not lead to a complete loss of neurosphere formation of reactive astrocytes (Sirko et al., 2013). Remarkably, diencephalic astrocytes have NSC potential, which was observed by neurosphere formation *in vitro* (Ohlig et al., 2021). A key regulator of the NSC potential was Smad4, a downstream mediator of TGF $\beta$ /BMP signaling. BMP signaling is also active in aNSCs and is required for their progression towards the neurogenic lineage (Colak et al., 2008). Remarkably, BMP signaling was also upregulated in the dedifferentiated astrocyte cluster, which was associated with stem cell functions. Although no differences between AhR-KO and NR astrocytes regarding the BMP signaling were observed in this study, it cannot be excluded that BMP signaling may also play a crucial role in acquiring stem cell properties. Nonetheless, this study provided clear evidence that AhR signaling is required for neurosphere formation, and thus AhR activity may be the marker for this subpopulation of astrocytes. AhR activity can be reported in mice *in vivo* by use of the *Cyp1a1* (Cytochrome P450 family 1 subfamily a member 1) fate reporter, which works in a Cre recombinase-dependent manner (Henderson et al., 2015; Schiering et al., 2017). The *Cyp1a1* gene is a well-known downstream target of the AhR signaling. Yet another mouse line reporting AhR activity exists, which uses the transgenic expression of a chimeric construct consisting of the human *CYP1A1* gene fused to a *GFP* reporter gene (Operaña et al., 2007). Such reporter mouse lines might allow to label dedifferentiated astrocytes that acquired stem cell capacities after TBI. Furthermore, scRNAseq experiments with these mice would then also enable us to verify the results obtained in the presented work.

### 3.4 Downstream targets of AhR signaling involved in the acquisition of stem cell properties of reactive astrocytes

Interestingly, a cluster with stem cell characteristics emerged when studying injured astrocytes on a single cell transcriptomic level. In addition, AhR-KO astrocytes were almost absent in this cluster. As a result, it strongly suggests that astrocytes within this cluster did dedifferentiate and acquired NSC potential. Hence, I was motivated to study the differences between AhR-KO and NR astrocytes within this cluster to better understand the role of AhR signaling in the process of dedifferentiation. Various genes have been identified as being downregulated upon AhR-KO in dedifferentiated astrocytes. One of the candidates that might explain the loss of stem cell capacities upon AhR deficiency is *Cd24a*. CD24 is expressed in the neuronal stem cell lineage and plays an important role in self-renewal capacities of chemoresistant tumor cells (Lee et al., 2011; Pruszek et al., 2009). However, CD24 is upregulated by each step of differentiation of NSCs and is negatively regulating cell proliferation in aNSCs in the DG and SEZ; thus, is not the strongest candidate to explain the phenotype observed in AhR-deficient astrocytes (Belenguer et al., 2021; Belvindrah et al., 2002; Pruszek et al., 2009). Two other candidates that were differentially regulated in AhR-KO astrocytes located in the cluster with stem cell characteristics were *Il1r2* and *Lyar*.

The IL1R2 is a non-signaling receptor binding IL1 molecules (Colotta et al., 1993). Chronic IL1 signaling leads to loss of self-renewal in hematopoietic stem cells (HSC) mediated by IL1R1 (Pietras et al., 2016). Therefore, it might be possible that AhR-KO astrocytes are lacking the expression of IL1R2, which might be important to allow reactive astrocytes to dedifferentiate and acquire self-renewal capacities. Both IL1 receptors also contain dioxin responsive elements (DRE) in upstream sequences, and thus are potential downstream targets of AhR transcriptional activation (Hanieh, 2014).

One of the top 10 downregulated genes in AhR-KO astrocytes was *Lyar* (Ly1 Antibody Reactive). LYAR is a nucleolar protein and is highly expressed in undifferentiated embryonic stem cells (ESC) (H. Li et al., 2009). Knock-down experiments have shown that LYAR is essential to maintaining the self-renewal of ESCs and their full differentiation potential (H. Li et al., 2009). LYAR expression is driven by IFN- $\beta$ , a type I interferon that also activates AhR signaling in astrocytes (Rothhammer et al., 2016; Yang et al., 2019). AhR signaling and LYAR expression have not yet been linked, but it is plausible that AhR activation directly or indirectly leads to LYAR expression in an IFN- $\beta$  dependent mechanism, and thus, leads to dedifferentiation of reactive astrocytes.

The differentially regulated genes in AhR-KO astrocytes in the stem cell-associated cluster were used for a transcription factor ranking analysis (Angerilli et al., 2018). This analysis revealed that the two transcription factors *Tcf7* and *Runx1* were downregulated in AhR-KO astrocytes. Both TFs are interesting candidates since both are reported to have important roles in stem cell functions. The transcription factor TCF1 (encoded by *Tcf7*) is a nuclear effector of the canonical Wnt signaling and known for its role in maintaining stem cell-like functions in CD8<sup>+</sup> T cells (Jeannet et al., 2010; Shan et al., 2021; Zhou et al., 2010). The transcription factor RUNX1 is linked to neurosphere formation of neural stem or progenitor cells and does affect their differentiation and proliferation potential (Logan et al., 2015). Strikingly, the RUNX1 did not only have six out of ten common interactors with TCF1, but is also linked to Wnt signaling (Q. Li et al., 2019; Medina et al., 2016). In addition, it has been reported that TCF1 and RUNX1 bind each other's promoter regions, suggesting synergetic transcriptional regulation (J. Q. Wu et al., 2012). Hence the fact that the Wnt signaling pathway was upregulated in the astrocyte cluster with stem cell characteristics and downregulated in AhR-KO astrocytes of the same cluster, strongly indicates that Wnt signaling is affected by AhR activity. Indeed, it has been shown that Wnt signaling was upregulated upon AhR activation during zebrafish fin regeneration and in the embryonal carcinoma cell line P19 (Mathew et al., 2009; Zhu et al., 2012). Therefore, it may be worthwhile to further investigate the role of the AhR-Wnt axis during the dedifferentiation of reactive astrocytes upon traumatic brain injury. This could be performed by application of Wnt activators *in vivo* and/or *in vitro* using the *Glast<sup>CreERT2</sup> x Ahrfx x CAG-GFP* mouse line. A more sophisticated experiment would include the genetic overexpression of TCF1 and/or RUNX1 in AhR-deficient astrocytes.

### 3.5 Concluding remarks

Collectively, I showed for the first time the requirement of AhR signaling in the process of dedifferentiation of cortical reactive astrocytes to acquire stem cell potential after TBI. Furthermore, I provided evidence of downstream signaling mechanisms that may explain the loss of stem cell capacity acquisition in AhR-KO astrocytes. This work also provides new thoughts about the concept that reactive astrocytes acquiring stem cell potential upon injury are a subpopulation of proliferating reactive astrocytes.

A future aspect of interest is the ligand specificity of AhR signaling. It has been postulated that the outcome of AhR signaling is dependent upon specific exogenous and endogenous ligands (Quintana & Sherr, 2013; Safe et al., 2018). A human-based study revealed different concentration levels of AhR-specific ligands such as kynurenine, tryptophan, and quinolinic acid in the blood and cerebrospinal fluid (CSF) (Raison et al., 2010). This might also be

an important factor explaining the differences observed in neurosphere formation capacity of AhR-KO astrocytes, which start proliferation and dedifferentiation upon BBB rupture while aNSCs are located at the third ventricle with direct access to the CSF. A recently published work by the group of Conacci-Sorrell linked AhR signaling with an increase in protein synthesis by regulating genes involved in ribosome biogenesis and protein translation (Lafita-Navarro et al., 2018). In addition, it has been shown that the regulation of protein translation is crucial for differentiation processes in aNSCs (Baser et al., 2019). Therefore, it might be critical to investigate the effects of AhR signaling not only on a transcriptomic level but also on the post-transcriptional consequences. In the last year, new methods have been developed to study the translome on a single cellular level (Brannan et al., 2021; VanInsberghe et al., 2021).

Although the exact mechanisms of AhR signaling regulating the dedifferentiation and acquisition of neural stem cell potential remain to be validated and further investigated, the presented work is an important step toward future potential therapeutic strategies facilitating stem cell potential of astrocytes in patients affected by traumatic brain injuries.

## 4 Material and Methods

### 4.1 Materials

#### 4.1.1 Reagents and solutions

Description	Source
10 % running gel	Rotiphorese® Gel (3.3 ml), 4X Stacking Gel Buffer (2.5 ml), H <sub>2</sub> O (4.2 ml), TEMED (10 µl), APS (100 µl)
10% Tween 20	BioRad
10X Electrophoresis Buffer (TGS)	Tris (0.5 M), Glycine (1.9 M), SDS (1 %), fill up with diH <sub>2</sub> O
10X PBS	NaCl (400 g), KCl (10 g), KH <sub>2</sub> PO <sub>4</sub> (10 g), Na <sub>2</sub> HPO <sub>4</sub> (58.75 g), adjust to pH 7.4 and fill up to 5 l diH <sub>2</sub> O
10X PO <sub>4</sub> buffer (0.25 M)	NaH <sub>2</sub> PO <sub>4</sub> * 2 H <sub>2</sub> O (65 g), NaOH (15 g), adjust to pH 7.4 and fill up to 400 ml diH <sub>2</sub> O
10X TBST	Tris (60 g), NaCl (87.7 g), adjust to pH 7.6, Tween-20 (10 ml), fill up to 1 l diH <sub>2</sub> O
10X Transfer Buffer	Glycine (144.2 g), Tris (30.2 g), SDS (2 g), fill up to 1 l with diH <sub>2</sub> O
1X Transfer Buffer	10X Transfer Buffer (100 ml), MeOH (200 ml), diH <sub>2</sub> O (700 ml)
2-Propanol	Roth
4 % stacking gel	Rotiphorese® Gel (1.3 ml), 4X Stacking Gel Buffer (2.5 ml), H <sub>2</sub> O (6.2 ml), TEMED (10 µl), APS (100 µl)
4X Running Gel Buffer	Tris base (1.5 M), SDS (0.4 %), adjust to pH 8.8 and fill up with diH <sub>2</sub> O
4X SDS solution	Tris (110 mM), Glycerol (40 %), SDS (4 %), DTT (40 mM), Bromphenol blue (0.1 %), adjust to pH 6.8 and fill up with diH <sub>2</sub> O
4X Stacking Gel Buffer	Tris base (0.5 M), SDS (0.4 %), adjust to pH 6.8 and fill up with diH <sub>2</sub> O
50X TAE buffer	Tris base (242 g), acetic acid (57.1 ml), EDTA (50 mM), adjust to pH 8.0 and fill up with 1 l diH <sub>2</sub> O
Acetic acid	Sigma-Aldrich
Agarose (LE) for tissue embedding	Biozym
Agarose for DNA electrophoresis	Serva
Ammonium persulfate (APS)	Roth

Aqua (H <sub>2</sub> O)	B. Braun
Aqua-Poly/Mount	Polysciences
AR6 buffer (10X)	PerkinElmer
Atipazole (Atipamezole hydrochloride, 5 mg/ml)	Prodivet
B27 serum-free supplement (50X)	Gibco (Thermo Fischer Scientific)
Bepanthen Augen- und Nasensalbe 5 g (eye ointment)	Bayer
Blotting grade (Powdered milk)	Roth
Borate buffer (0.1 M)	Na <sub>2</sub> B <sub>4</sub> O <sub>7</sub> (20.1 g), adjust to pH 8.5 and fill up to 1 l diH <sub>2</sub> O
Bovine serum albumin (BSA)	Sigma-Aldrich
BrdU (5-Bromo-2'-deoxyuridine)	Sigma-Aldrich
Bromphenol blue	Sigma-Aldrich
Buffer EB (elution buffer)	Qiagen
Chameleon™ Duo Pre-stained Protein Ladder	LI-COR
cOmplete™ protease inhibitor cocktail	Roche
Corn oil	Sigma-Aldrich
D-(+)-Glucose	Sigma-Aldrich
D-Sucrose	Sigma-Aldrich
DAPI solution	DAPI (2 mg), Tris (2 ml), fill up to 500 ml with 1X PBS
Disodium phosphate (Na <sub>2</sub> HPO <sub>4</sub> )	Roth
Dissociation medium	Solution I (10 ml), Trypsin (7 mg), Hyaluronidase (7 mg)
Dithiothritol (DTT)	Applichem
DMEM/F-12, no glutamine	Gibco (Thermo Fischer Scientific)
DMEM/F-12+GlutaMAX™	Gibco (Thermo Fischer Scientific)
DNA lysis buffer	Tris (1 M), EDTA (5 mM), SDS (0.2 %), NaCl (200 mM), adjust to pH 8,5 and fill up with diH <sub>2</sub> O
dNTP Set, PCR Grade (100 mM)	Qiagen
Dormicum® (Midazolam, 5 mg/ml)	Roche
EBSS, no calcium, no magnesium (1X)	Gibco (Thermo Fischer Scientific)
EdU (5-ethynyl-2'-deoxyuridine)	Invitrogen (Thermo Fisher Scientific)
EGF-Stock (10 µg/ml)	EGF (100 µg), DMEM-F12 (no glutamine; 10 ml), D-Glucose (100 µl), P/S (100 µl)
Epidermal growth factor (EGF)	Gibco (Thermo Fischer Scientific)
Ethanol (EtOH)	Roth
Ethidium bromide solution (1 %)	Roth
Ethylenediaminetetraacetic acid (EDTA)	Roth
Ethylenglycol	AppliChem

Fentanyl (Fentanyl citrate, 0.1 mg/ml)	Janssen
FGF-Stock (10 µg/ml)	FGF (10 µg), DMEM-F12 (no glutamine; 1 ml), D-Glucose (10 µl), P/S (10 µl)
Fibroblast growth factor basic (FGF2)	Gibco (Thermo Fischer Scientific)
Flumazenil-hameln (Flumazenil, 0.1 mg/ml)	Hameln pharma
GeneRuler DNA Ladder (100 bp, 1 kb)	Thermo Fischer Scientific
Glycerol	Sigma-Aldrich
Glycine	Roth
Goat serum	Gibco (Thermo Fischer Scientific)
HBSS with calcium and magnesium (10X)	Gibco (Thermo Fischer Scientific)
HBSS with calcium and magnesium (1X)	Gibco (Thermo Fischer Scientific)
HBSS-HEPES (10 mM)	HEPES (5 ml), HBSS (500 ml)
HEPES (1M)	Gibco (Thermo Fischer Scientific)
Hyaluronidase from bovine testes (750-3,000 U/mg)	Sigma-Aldrich
Hydrochloric acid (HCl, 37 %)	Roth
Isotonic saline solution (NaCl, 0.9 %)	B.Braun
Ketamine-Xylazine solution	Ketamine (1 ml), Xylazine (1 ml), NaCl solution 0.9 % (8 ml)
Low TE Buffer (10 mM Tris-HCl pH 8.0, 0.1 mM EDTA)	Invitrogen (Thermo Fisher Scientific)
Melosus® suspension for oral application	CP-pharma
Metacam® injection solution	Boehringer Ingelheim
Methanol (MeOH)	Roth
Neurosphere medium	P/S (500 µl), HEPES (400 µl), B27 (1 ml), FGF-Stock (50 µl), EGF-Stock (50 µl), DMEM/F-12+GlutaMAX™ (up to 50 ml)
Nuclease-free Water	Ambion
Paraformaldehyde (PFA)	Roth
Penicillin/Streptomycin (P/S; 10,000 U/ml)	Gibco (Thermo Fischer Scientific)
PFA solution (4 %)	PFA stock (50 ml), 1X PBS (200 ml), both filtered
PFA stock solution (20 %)	Na <sub>2</sub> HPO <sub>4</sub> (58.75 g), PFA (400 g), adjust to pH 7.4 with NaOH pellets and fill up to 2 l diH <sub>2</sub> O
Ponceau S solution	Sigma-Aldrich
Potassium chloride (KCl)	Sigma-Aldrich
Potassium phosphate monobasic (KH <sub>2</sub> PO <sub>4</sub> )	Sigma-Aldrich
Primary antibody staining solution	Triton® X-100 (0.5 %), goat serum (10 %), primary antibodies (1:X dilution), fill up with 1X PBS
Proteinase K	Roth
Proxylaz® (Xylazine, 20 mg/ml)	Bela-pharm
RIPA buffer	Sigma-Aldrich

RNaseZAP™	Sigma-Aldrich
Rotiphorese® Gel 30 (37.5:1)	Roth
Secondary antibody staining solution	Triton® X-100 (0.5 %), secondary antibodies (1:1000), fill up with 1X PBS
Sedin® (Medetomidine hydrochloride, 1 mg/ml)	Pharma-Partner
Sodium chloride (NaCl)	Roth
Sodium dodecyl sulfate (SDS)	Sigma-Aldrich
Sodium hydroxide (NaOH)	Sigma-Aldrich
Sodium phosphate monobasic dihydrate (NaH <sub>2</sub> PO <sub>4</sub> * 2 H <sub>2</sub> O)	Sigma-Aldrich
Sodium tetraborate (Na <sub>2</sub> B <sub>4</sub> O <sub>7</sub> )	Sigma-Aldrich
Solution I (HBSS-Glucose)	HBSS (10X; 50 ml), D-Glucose (9 ml), HEPES (7.5 ml), diH <sub>2</sub> O (433.5 ml), pH 7.5
Solution II (Sucrose-HBSS)	HBSS (10X; 25 ml), D-Sucrose (154 g), diH <sub>2</sub> O (575 ml), pH 7.5
Solution III (BSA-EBSS-HEPES)	BSA (20 g), HEPES (10 ml), EBSS (490 ml), pH 7.5
SPRIselect Reagent Kit	Beckman Coulter
Storing solution	diH <sub>2</sub> O (150 ml), 10X PO <sub>4</sub> buffer (50 ml), Glycerol (150 ml), Ethylenglycol (150 ml)
Tamoxifen	Sigma-Aldrich
Tamoxifen solution	Tamoxifen (20 mg/ml), EtOH (10 %), fill up then with corn oil and dissolve using ultrasonic bath for 2x 10 min
TE buffer (pH 8.0)	Qiagen
TEMED	Sigma-Aldrich
Temgesic® (Buprenorphine hydrochloride, 0.3 mg/ml)	Essex
Tris	Roth
Tris base	Sigma-Aldrich
Triton® X-100	Roth
Trypan Blue Solution (0.4 %)	Gibco (Thermo Fischer Scientific)
Trypsin from bovine pancreas (7,500 BAEE U/mg)	Sigma-Aldrich
Tween-20	Sigma-Aldrich
Ursotamin® (Ketamine, 100 mg/ml)	Serumwerk Bernburg

#### 4.1.2 Laboratory equipment

Description	Source
2100 Bioanalyzer Laptop Bundle	Agilent
8-Strip PCR Tube (0.2 ml)	STARLAB Group
Axio Observer.Z1 inverted Microscope (with an EC Plan-NEOFLUAR® 10x/0.3 objective)	Zeiss
Biopunch Handstanze (2.5 mm)	Plano
Biosphere® plus Filter Tips (10 - 1000 µl)	Sarstedt
Capsulotomy Scissor	Geuder
Cell Strainer (70 µm)	Sarstedt
Cell Strainer Adapter	Sarstedt
CELLSTAR® tubes (15 ml, 50 ml)	Greiner Bio-One
Centrifuge 5420	Eppendorf
Centrifuge 5427 R	Eppendorf
Chromium™ Controller	10x Genomics
Conical Tubes (25 ml)	Eppendorf
Cover Slips	Roth
Digital Monochrom Thermal Printer (P95)	Mitsubishi
Digital Stereotaxic Frame	World Precision Instruments
Disposable syringe (50 ml)	Mediware
DM IL LED Microscope	Leica
DNA LoBind® Tube (1.5 ml)	Eppendorf
Dumont #5 Forceps	Fine Science Tools
E-BOX - Gel Documentation Imaging	PEQLAB Biotechnologie
Elmasonic S 40 H	Elma
Extra Fine Graefe Forceps	Fine Science Tools
Extra Fine Graefe Forceps - round	Fine Science Tools
Filter paper (Selecta)	Schleicher & Schüll
Filtropur BT25/V50	Sarstedt
FlowSafe® B-[MAxPro] <sup>2</sup> -160	Berner
FLUOVIEW FV1000 confocal laser-scanning microscope (with UPlanApo 10x/0.4 and UPlanSApo 20x/0.85 W, 60x/1.2 W objectives)	Olympus
Galaxy® 170 R/S incubator	Eppendorf
gentleMACS™ C Tubes	Miltenyi Biotec
gentleMACS™ Octo Dissociator	Miltenyi Biotec
Hemocytometer (Neubauer Zählkammer)	Roth
Heraeus Megafuge™ 8R Centrifuge	Thermo Fisher Scientific
High Speed Stereotaxic Drill	Bilaney Consultants GmbH
Horizontal Gel Systems	PEQLAB Biotechnologie
HXP 120 C lighting unit	Zeiss
LSM 710 Confocal Microscope (with Plan-NEOFLUAR® 10x/0.3, 25x/0.8, 63x/1.3 objectives)	Zeiss

M50 Stereo Microscope	Leica
MACS® MultiStand	Miltenyi Biotec
MACS® SmartStrainers (70 µm)	Miltenyi Biotec
Microscope Slides	Thermo Fischer Scientific
Microwave	Severin
Mini Trans-Blot Electrophoretic Transfer Cell	BioRad
Mini-100 Orbital Genie™	Scientific Industries
Mini-Centrifuge	Biozym
MINIPULS® 3 Peristaltic Pumps	Gilson
MS Column	Miltenyi Biotec
NovaSeq™ 6000 Sequencing System	Illumina
NovaSeq™ Flow cell Type S2	Illumina
OctoMACS™ Separator	Miltenyi Biotec
ODYSSEY CLx	LI-COR
Omnican® 50 (0.5 ml)	B. Braun
Omnifix® (10 ml)	B. Braun
Omnifix®-F (1 ml)	B. Braun
PCR Tube Strips (0.2 ml)	Eppendorf
Peel-A-Way® Embedding Mold	Polysciences
peqPOWER	PEQLAB Biotechnologie
Petri Dishes	Greiner Bio-One
Pipette Controller Pipetus®	Hirschmann
PowerPac™ Basic	BioRad
ProFlex™ PCR System	Applied Biosystems (Thermo Fisher Scientific)
Protein LoBind® Tube (1.5 ml)	Eppendorf
Qubit™ 3 Fluorometer	Invitrogen (Thermo Fisher Scientific)
Razor blades	Wilkinson Sword
Reagent Reservoirs	Vistalab
Research® plus Pipettes (2.5 - 1000 µl)	Eppendorf
Rotilabo®-syringe filters (0.22 µm)	Roth
S1000™ Thermal Cycler	BioRad
Safe-lock tube (5 ml)	Eppendorf
Serological Pipettes (5 ml, 10 ml, 25 ml)	Sarstedt
SevenCompact™ pH meter S220	Mettler Toledo
Standard Patteren Forceps	Fine Science Tools
Steamer	Braun
Sterican® cannula (0.45x25, 26 Gx1")	B. Braun
Student Fine Scissors	Fine Science Tools
Student Halsey Needle Holder	Fine Science Tools
Student Tissue Forceps	Fine Science Tools
Sugi® Sponge Points	Kettenbach
Supported Nitrocellulose Membrane	BioRad

Surgical Disposable Scalpels	B. Braun
Surgical Scissors - Sharp-Blunt	Fine Science Tools
TC plate, 24-well, flat bottom	Sarstedt
ThermoMixer C	Eppendorf
TipOne® Graduated Tips (10µl, 200 µl, 1000 µl)	STARLAB Group
TubeOne® Microcentrifuge tubes (1.5 ml, 2 ml)	STARLAB Group
U-RFL-T-200 Mercury Burner	Olympus
V-Lance knife (19 G)	Alcon
Vibratome (LeicaVT1000 S)	Leica
Vicryl SH1-Plus (4-0 Gauge, antibacterial wound closure suture)	Ethicon
Vortex	STARLAB Group
Waterbath WNB	Memmert

#### 4.1.3 Kits

Description	Source
Adult Brain Dissociation Kit, mouse and rat	Miltenyi Biotec
Agilent High Sensitivity DNA Kit	Agilent
Anit-ACSA-2 MicroBead Kit, mouse	Miltenyi Biotec
Chromium Next GEM Chip G Single Cell Kit, 48 rxns	10x Genomics
Chromium Next GEM Single Cell 3' GEM, Library & Gel Bead Kit v3.1, 4 rxns	10x Genomics
Chromium™ Accessory Kit	10x Genomics
Click-iT™ EdU Cell Proliferation Kit for Imaging, Alexa Fluor™ 647 dye	Invitrogen (Thermo Fisher Scientific)
Qubit™ dsDNA HS Assay Kit	Invitrogen (Thermo Fisher Scientific)
Taq DNA Polymerase Kit (1000 units)	Qiagen

#### 4.1.4 Antibodies and dyes

Antibody	Source	Dilution	Pretreatment	Experiment
Mouse anti-AhR	Santa Cruz (sc-398877)	1:100		Western Blot
Rabbit anti-alpha Tubulin	abcam (ab18251)	1:2000		Western Blot
Donkey anti-Mouse (IRDye® 800CW)	LI-COR (926-32212)	1:5000		Western Blot
Donkey anti-Rabbit (IRDye® 680RD)	LI-COR (926-68073)	1:5000		Western Blot
Chicken-anti-GFP	Aves Labs (GFP-1020)	1:500		IHC
Mouse anti-BrdU	Sigma-Aldrich (B2531)	1:1000	4N HCl	IHC
Rabbit anti-Ki67	Thermo Fischer Scientific (MA-14520)	1:100		IHC
Mouse anti-CD31	BD Biosciences (550274)	1:100		IHC

Rat anti-CD45	BD Biosciences (550539)	1:500	AR6; heat	IHC
Rabbit anti-Iba1	Synaptic Systems (234013)	1:1000		IHC
Goat anti-Chicken IgY (Alexa Fluor® 488)	Invitrogen (Thermo Fisher Scientific; A11039)	1:1000		IHC
Goat anti-Mouse IgG (Cy3)	Dianova (115-165-003)	1:1000		IHC
Goat anti-Mouse IgG (Alexa Fluor® 647)	Invitrogen (Thermo Fisher Scientific; A21236)	1:1000		IHC
Goat anti-Rabbit IgG (Alexa Fluor® 546)	Invitrogen (Thermo Fisher Scientific; A11010)	1:1000		IHC
Goat anti-Rabbit IgG (Alexa Fluor® 633)	Invitrogen (Thermo Fisher Scientific; A21070)	1:1000		IHC
Goat anti-Rat IgG (Alexa Fluor® 546)	Invitrogen (Thermo Fisher Scientific; A11081)	1:1000		IHC
DAPI (4',6-Diamidino-2- phenyl-indol- dihydrochlorid)	Sigma-Aldrich (D9542)	4 µg/ml		IHC

#### 4.1.5 Software

Description	Source
2100 expert (Version 2.09.0553)	Agilent
Affinity (Publisher, Photo; Version 1.10.1)	Serif Europe
CytoScape (3.9.0)	Open source (LGPL)
Fiji / ImageJ2 (Version: 2.3./1.53f)	Open source (GPL v2)
FV10-ASW (Version 2.0.0.2)	Olympus
GraphPad Prism (Version 9.3.1)	GraphPad Software, LLC
imageStudio (Version 5.2.5)	LI-COR
Microsoft office 365	Microsoft
Python (Version 3.8.8)	Python Software Foundation
Rstudio (Version 1.4.1106)	RStudio, PBC
ZEN 2.3 (black edition)	Zeiss
ZEN 2.3 (blue edition)	Zeiss

## 4.2 Experimental animals

Adult mice (2-5 months old) of both sexes of the following lines were used: Triple transgenic mice were obtained by crossing  $Emx1^{Cre}$  mice (Iwasato et al., 2000) and  $Glast^{CreERT2}$  mice (Mori et al., 2006) with CAG-CAT-EGFP (CAG-GFP) mice (Nakamura et al., 2006) as well as with  $Ahrfx$  mice (Walisser et al., 2005) (referred to as  $Emx1^{Cre}$  x  $Ahrfx$  x CAG-GFP and  $Glast^{CreERT2}$  x  $Ahrfx$  x CAG-GFP). Animals were kept under standard conditions in a 12h:12h light-dark cycle with access to food and water *ad libitum*. All animal experimental procedures were performed in accordance with the German and European Union guidelines and were approved by the Institutional Animal Care and Use Committee (IACUC) and the Government of Upper Bavaria under the license numbers: ROB-55.2-2532.Vet\_02-19-168, ROB-55.2-2532.Vet\_02-16-210 and ROB-55.2-2532.Vet\_02-15-219

## 4.3 Genotyping

Before each experiment every animal was genotyped by use of standard polymerase chain reaction (PCR) of DNA samples from ear clips.

### 4.3.1 DNA extraction from ear clips

At first, ear clips were lysed in 300  $\mu$ l DNA lysis buffer supplemented with 3  $\mu$ l Proteinase K (100  $\mu$ g/ml) at 55 °C and 700 rpm on a ThermoMixer C. Samples were then centrifuged at 15,000 g and 4 °C for 20 min. Subsequent to transferring the supernatant, 300  $\mu$ l of ice-cold isopropanol was added and mixed well. After an incubation time of 10 min on-ice the samples were centrifuged (15,000 g, 4 °C) for 5 min. Supernatant was removed and pellet dried at room temperature (RT) for approximately 5 min with an open tube. Dry pellet was then dissolved in 30  $\mu$ l TE buffer.

### 4.3.2 Polymerase chain reaction

Standard PCR was performed specifically for each mouse line. The used primers (from metabion), PCR solution mix and thermocycler conditions are listed below:

**Table 1: Primers used for genotyping**

Mouse line	Gene	Primer ID	Sequence
Emx1 <sup>Cre</sup> x Ahrfx x CAG-GFP	Emx1 <sup>Cre/wt</sup>	Cre F	GTG AGT GCA TGT GCC AGG CTT
		Cre R	TGG GGT GAG GAT AGT TGA GCG
		Test Cre	GCG GCA TAA CCA GTG AAA CAG
Emx1 <sup>Cre</sup> x Ahrfx x CAG-GFP Glast <sup>CreERT2</sup> x Ahrfx x CAG-GFP	CAG <sup>GFP</sup>	AG-2	CTG CTA ACC ATG TTC ATG CC
		CAT-2	GGT ACA TTG AGC AAC TGA CTG
	Ahrfx	oIMR6075 (F1)	CAG TGG GAA TAA GGC AAG AGT GA
		oIMR6076 (R)	GGT ACA AGT GCA CAT GCC TGC
	Ahrfx excised	OL4062 (F2)	GTC ACT CAG CAT TAC ACT TTC TA
	Glast <sup>CreERT2</sup> x Ahrfx x CAG-GFP	Glast <sup>CreERT2/wt</sup>	Primer F8
Primer R3			GAG GAG ATC CTG ACC GAT CAG TTG G
Primer CER1			GGT GTA CGG TCA GTA AAT TGG ACA T

**Table 2: PCR solution mix used for genotyping**

	Emx1 <sup>Cre</sup>	Emx1 <sup>wt</sup>	Glast <sup>CreERT2/wt</sup>	CAG-GFP	Ahrfx	Ahrfx excised
H <sub>2</sub> O	13.8 µl	13.8 µl	10.5 µl	16 µl	16 µl	16 µl
Buffer (10X)	2.5 µl	2.5 µl	2.5 µl	2.5 µl	2.5 µl	2.5 µl
MgCl (25 mM)	2.5 µl	2.5 µl	2.5 µl	2.5 µl	2.5 µl	2.5 µl
Primer 1	Cre F: 1 µl	Cre F: 1 µl	F8: 0.5 µl	AG-2: 0.5 µl	F1: 0.5 µl	F2: 0.5 µl
Primer 2	Cre R: 1 µl	Test Cre: 1 µl	R3: 0.5 µl	CAT-2: 0.5 µl	R: 0.5 µl	R: 0.5 µl
Primer 3			CER1: 0.5 µl			
Q-Solution	5 µl	5 µl	5 µl			
dNTPs (10 mM)	0.5 µl	0.5 µl	0.5 µl	0.5 µl	0.5 µl	0.5 µl
Taq Polymerase	0.2 µl	0.2 µl	0.5 µl	0.5 µl	0.5 µl	0.5 µl
DNA	1 µl	1 µl	2 µl	2 µl	2 µl	2 µl
End volume	25 µl	25 µl	25 µl	25 µl	25 µl	25 µl

The PCR was performed with a positive and negative (wildtype DNA sample) control and a water control (DNA-free) to rule out contaminations and verify the results.

**Table 3: Thermocycler conditions for each PCR reaction**

	Emx1 <sup>Cre</sup>	Emx1 <sup>wt</sup>	Glast <sup>CreERT2/wt</sup>	CAG-GFP	Ahrfx	Ahrfx excised
Initialization	94 °C, 5'	94 °C, 5'	94 °C, 3'	94 °C, 3'	94 °C, 3'	94 °C, 3'
X cycles	36 X	36 X	35 X	35 X	35 X	35 X
i) Denaturation	94 °C, 30"	94 °C, 30"	94 °C, 30"	94 °C, 30"	94 °C, 30"	94 °C, 30"
ii) Annealing	64 °C, 60"	64 °C, 60"	60 °C, 40"	60 °C, 40"	60 °C, 40"	65 °C, 40"
iii) Elongation	72 °C, 30"	72 °C, 30"	72 °C, 40"	72 °C, 40"	72 °C, 40"	72 °C, 40"
Final elongation	72 °C, 5'	72 °C, 5'	72 °C, 3'	72 °C, 3'	72 °C, 3'	72 °C, 3'
Final hold	4 °C, ∞	4 °C, ∞	4 °C, ∞	4 °C, ∞	4 °C, ∞	4 °C, ∞

### 4.3.3 Gel electrophoresis

For PCR products from Emx1<sup>Cre</sup>, Emx1<sup>wt</sup>, Glast<sup>CreERT2/wt</sup> and CAG-GFP 1 % agarose gels were used. For the PCR products of Ahrfx and its excised version 3 % agarose gels were used for the electrophoresis. Agarose gels were made with a 1X TAE buffer containing ethidium bromide (1:10,000) to visualize the DNA. In all cases 10 µl of each PCR product was loaded on the respective gel and ran at 120 V for 45 min. DNA bands were detected using UV-light in an E-BOX.

## 4.4 Application of tamoxifen

Glast<sup>CreERT2</sup> x Ahrfx x CAG-GFP mice received in three consecutive days daily one intraperitoneal (i.p.) injection of 40 µg tamoxifen solution (20 mg/ml) per g of body weight. For the single cell RNA sequencing (scRNAseq) experiment (10x Genomics) mice received i.p. injections of tamoxifen (40 µg/g of body weight) for 2 cycles for 5 consecutive days in the period of three weeks. Fourteen days after the last injection animals were used for surgical procedures.

## 4.5 Surgical procedure

Before performing surgery, animals were anesthetized with an i.p. injection of sleep solution containing midazolam (5 µg/g of body weight), medetomidine (0.5 µg/g) and fentanyl (0.05 µg/g). When animals were fully anesthetized – no toe and eye reflex left – the fur on top of the head was removed and Bepanthen was administered to the eyes to prevent them from drying out. Mice were then fixed in a stereotactic apparatus and underwent an incision on the head to expose the skull beneath the skin. For local anesthesia lidocaine gel (2 %) was applied

on the skull surface. Subsequent, the bregma was defined and a small cranial window with a diameter of approximately 3 mm was drilled. The cranial window was collected in a drop of NaCl solution (0.9 %). The stab wound microlesion was performed by inserting the V-lance knife in the grey matter parenchyma of the somatosensory cortex and moving it once caudal and then back rostral at the following coordinates:

Medio-lateral (x):  $\pm 1.0$  mm from bregma

Rostro-caudal (y): -1.2 to -2.2 mm from bregma

Dorso-ventral (z): -0.6 mm from meninges

The craniotomy was covered with the cranial window and the skin was sutured with at least three stitches. For the antagonization of the anesthesia the awake solution containing atipamezole (2.5  $\mu\text{g/g}$  of body weight), flumazenil (0.5  $\mu\text{g/g}$ ) and buprenorphine (0.1  $\mu\text{g/g}$ ) was applied subcutaneous. Animals recovered on a pre-warmed heating pad until being fully awake and were given the same day and the day after postoperative analgesia by subcutaneous or oral application of meloxicam (1  $\mu\text{g/g}$ ). For all experiments but the scRNAseq experiment the microlesion was performed unilateral on the right hemisphere. For the scRNAseq experiment the microlesions were performed bilateral to reduce the number of animals used to 6 animals per condition (intact and injured).

#### 4.6 BrdU and EdU labeling

To label proliferating cells the thymidine analogues 5-bromo-2'-deoxyuridine (BrdU) and 5-ethynyl-2'-deoxyuridine (EdU) were applied to mice by water administration for 5 days after injury and i.p. injection 50 min before sacrificing the animal, respectively. The BrdU water contained 1 % sucrose and 1 mg/ml BrdU in tap water. EdU was dissolved in a concentration of 5 mg/ml and injected 50  $\mu\text{g/g}$  of body weight.

#### 4.7 Perfusion and brain sectioning

Prior to perfusion, animals were deeply anesthetized by i.p. injection of high dose Ketamine-Xylazine solution (10  $\mu\text{l/g}$  of body weight). After loss of reflexes mice were fixed and the heart exposed. Subsequently, they were perfused by inserting the canula into the left ventricle and perforation of the right atrium to ensure drainage of the blood and perfusion solution. First, they were perfused with 1X PBS for about 10 minutes and then followed by freshly prepared PFA solution (4 %) for about 20 minutes to ensure proper fixation of the tissue. The brain was then dissected out of the skull and post-fixated in the same fixative at 4 °C overnight. Next, the brain was washed in 1X PBS, the cerebellum and olfactory bulbs were

removed, and the remaining tissue was dried and embed in 3 % agarose solution in an embedding mold. After polymerization at RT the brain tissue was cut into 50-70  $\mu\text{m}$  thick coronal sections, which were collected in 1X PBS. Sections that were not immediately stained were kept in storing solution at  $-20\text{ }^{\circ}\text{C}$ .

## 4.8 Immunohistochemistry and EdU detection

For EdU detection on sections the Click-iT Edu Alexa Fluor 647 Imaging Kit was used and performed as instructed from step 3.2 on. After EdU detection, sections were pre-treated with HCl (4 N) for 20 min at RT to expose intercalated BrdU. Sections were then washed with borate buffer (0.1 M) and then 1X PBS. Subsequently, sections were incubated with primary antibodies against BrdU and GFP in primary antibody staining solution at  $4\text{ }^{\circ}\text{C}$  overnight. For all other immunohistochemical (IHC) stainings the EdU detection and HCl pre-treatment was not performed. Here, sections were directly incubated in primary antibody staining solution at  $4\text{ }^{\circ}\text{C}$  overnight, except for staining against CD45, which did need a heat mediated pre-treatment in 1X AR6 buffer for 20 min in a steamer (about  $95\text{ }^{\circ}\text{C}$ ). After cooldown of these sections at RT for about 5 min pre-treated sections were washed in 1X PBS and proceeded with primary antibody staining (section 4.1.4). Next, sections were washed with 1X PBS and incubated with secondary antibody staining solution containing fluorophore conjugated secondary antibodies against the appropriate species (section 4.1.4) at RT in the dark. Afterwards, nuclei were visualized using DAPI solution on the sections for about 10 min in the dark. Following extensive washing with 1X PBS, sections were mounted on microscope slides using Aqua-Poly/Mount.

## 4.9 Confocal microscopy

Images of IHC stained sections were taken using laser-scanning confocal microscopes LSM 710 (Zeiss) using the ZEN software (black edition) and FLUOVIEW FV1000 (Olympus) using the FV10-ASW software with 20x to 63x objectives. Analysis was done with Fiji / ImageJ2 and for quantification the plug-in Cell Counter was used while carefully inspecting every optical section of the confocal Z-stack.

## 4.10 Protein extraction and Western Blot

Brains were dissected and put in HBSS-Hepes. Brain punches from the somatosensory cortex of both hemispheres were collected using a biopunch with a diameter of 2.5 mm. Meninges and white matter of the punches were removed and samples were then immediately frozen in liquid nitrogen. Next, proteins were extracted by adding 150  $\mu\text{l}$  RIPA buffer supplemented with 1X protease inhibitor to the sample. The tissue was ruptured by pipetting

up and down, first with a pipette and then with a syringe and cannula (26 G). The mixture was then incubated for 30 min on ice. Subsequently, the samples were centrifuged at 15,000 g at 4 °C and supernatant was transferred into a new tube and frozen at -80 °C.

Western Blot was performed with the Trans-Blot System from BioRad. Extracted proteins were mixed with 4X SDS in a ratio of 1:1, denatured at 95 °C for 5 min and 12 µl were loaded next to a Chameleon® protein ladder (10 µl) for the electrophoresis of proteins, which was done on a 10 % running gel in combination with a 4 % stacking gel at 10-30 mA/gel in 1X electrophoresis buffer. After proper separation the proteins were transferred onto a nitrocellulose membrane using a wet transfer with 1X transfer buffer for 90 min at 100 V. The blots were then blocked in 5 % milk in 1X TBST for at least 30 min at RT or overnight at 4 °C. Next, the blots were washed with 1X TBST, followed by an incubation with primary antibodies (section 4.1.4) diluted in 5 % milk in 1X TBST at 4 °C overnight. Afterwards, blots were washed again (1X TBST) and then incubated with appropriate secondary antibodies (section 4.1.4) diluted in 5 % milk in 1X TBST for 1h at RT protected from light. Following extensive washing with 1X TBST the stained proteins on the blots were detected using the ODYSSEY CLx (LI-COR) with the imageStudio software, which was also used to analyze the blots.

#### 4.11 Neurosphere assay

For the neurosphere assay brains were dissected and immediately put in ice-cold HBSS-Hepes. A brain punch (2.5 mm diameter) was taken from the injured somatosensory cortex of the right hemisphere and meninges and white matter of the punches were removed. In addition, the subependymal zone (SEZ) of the same hemisphere was dissected. Both tissues were put separately into 5 ml HBSS-Hepes on ice and let settle down. HBSS-Hepes was exchanged with 1 ml dissociation medium, and samples were incubated for 15 min at 37 °C. Following trituration of the tissue (10 times) to break up the pellet without introducing air bubbles, the samples were incubated again for 15 min at 37 °C. Next, 1 Volume of ice-cold Solution III was added to inactivate the trypsin. After trituration, cells were passed through a cell strainer (70 µm) into a fresh tube and centrifuged for 5 min at 272 g at 4 °C. Supernatant was then removed and the pellet of cells was resuspended in 5 ml of ice-cold Solution II. Following a 10 min centrifugation at 644 g at 4 °C the supernatant was removed, and cells were resuspended in 1 ml of ice-cold neurosphere medium. Next, the cells in neurosphere medium were carefully added to a 15 ml tube containing 8 ml of Solution III. Cells were then centrifuged for 7 min at 362 g at 4 °C, supernatant was removed, and cells were resuspended in 200 µl neurosphere medium. Cells were counted with trypan blue using a hemocytometer and subsequently plated on 24-well plates in a density of 1 cell/µl to enable clonal analysis of the neurospheres.

SEZ derived neurospheres were counted after 7 days in vitro (div) using an inverted microscope (Axio Observer.Z1) and the ZEN software (blue edition). Neurospheres derived from the injured cortex were counted and analyzed at 14 div. The left hemisphere of the brain was immersed into a fresh PFA solution (4 %) and incubated for 36 h at 4 °C for further procedure at the vibratome to control for the recombination rate per animal.

## 4.12 Single cell RNA sequencing

For this experiment three male and three female mice were used per condition, intact and injured (5 dpi, bilateral), to obtain in total 12 punches from the somatosensory cortex. Furthermore, all animals went through the extended protocol of tamoxifen induction (s. section 4.4).

### 4.12.1 Sample preparation

Five days after injury animals were sacrificed and brains were dissected. The brain punch (2.5 µm diameter) was taken, and white matter and meninges were removed. Next, the samples were collected in buffer Z in C-tubes from the “Adult Brain Dissociation Kit, mouse and rat”. The dissociation of the brain punches was performed according to manual with used volumes for up to 1 g neural tissue and the gentleMACS program 37C\_ABDK\_02. The debris removal was performed twice, and red blood cell removal was skipped. Subsequently, astrocytes were labeled with the “Anit-ACSA-2 MicroBead Kit, mouse” to achieve an enrichment of these cells. Following the assumption of obtaining  $< 10^7$  total cells after dissociation of the brain tissue, the labeling of astrocytes was performed as instructed by the manual using the MS column. After the elution step of ACSA-2<sup>+</sup> cells, the cells were counted, centrifuged (300 g, 5 min, 4 °C) and resuspended in 1X PBS to a concentration of 800 cells/µl.

### 4.12.2 Library preparation and sequencing

For the library preparation of the single cell RNA sequencing (scRNAseq), the protocol of the 10x Genomics kit “Chromium Next GEM Single Cell 3' GEM, Library & Gel Bead Kit v3.1” was used and the manual instructions were followed in detail. The samples of the ACSA-2<sup>+</sup> sorted fractions from intact and injured brain were loaded each twice on the Chromium Next GEM Chip G, resulting in 4 samples used for library preparation in order to increase the number of recovered cells to be analyzed. For each reaction 20.6 µl of the ACSA-2<sup>+</sup> sorted cells were loaded to aim for a targeted cell recovery of 10,000 cells per sample. In step 2.4, using the Agilent Bioanalyzer, the calculated cDNA yield was between 89.3 and 138.5 ng for the being carried forward in the protocol resulting in 13 cycles in the sample index PCR (step 3.5). The uniquely barcoded libraries were then multiplexed onto one lane of a NovaSeq™ Flow cell Type S2 and

the 100 bp paired-end sequencing was carried out at the Next Generation Sequencing facility at the Helmholtz Zentrum München on the NovaSeq™ 6000 Sequencing System aiming for 25,000 reads per cell.

#### 4.12.3 Analysis of sequenced data

Raw sequencing data was demultiplexed, aligned to the GRCm38 mouse genome library extended by the EGFP sequence and pre-processed with the 10x Genomics Cell Ranger 5.0.0 pipeline. The pre-processing was performed on a high-performance computational cluster provided by the Bioinformatic Core Facility at the Biomedical Center in Munich. The resulting matrices were then loaded into the Python package Scanpy (version 1.7.1), which was used for the analysis (Wolf et al., 2018). Cells were filtered during the first quality control steps and kept for analysis, if the following parameters were fulfilled: gene counts  $\geq 300$ ; reads per cell  $\leq 40,000$ ; mitochondrial fraction  $\leq 0.3$ . In addition, only genes found in at least 20 cells were used for analysis. The doublet score, an event when more than one cell is present in a single GEM (Gel Beads-in-emulsion), was calculated using Scrublet and all cells with a doublet score  $\geq 0.05$  were excluded (Wolock et al., 2019). Each cell was then normalized by total counts over all genes and the data matrix was logarithmized using Scanpy. Furthermore, expression values have been normalized by dividing the measured counts by the size factor, an estimation of cell-specific RNA molecules that were initially in the cells, for each cell. The size factor was calculated using scran by calling R from Python. For visualization, dimensionality reduction by principal component analysis (PCA) based on 2,000 highly variable genes (HVG) was applied. The used number of principle components (PC, 7 to 9 dimensions) was based on an Elbow plot followed by a k-nearest neighbor (KNN) based neighborhood calculation with 30 local neighbors, which was then projected onto a uniform manifold approximation and projection (UMAP) (McInnes et al., 2018). Clustering of cells into subgroups was performed with the Leiden algorithm (Traag et al., 2019).

The ranking of genes per cluster was calculated with the 't-test\_overestim\_var' method, which performs a t-test with overestimating the variance of each group. Differential gene expression analysis comparing the two conditions of AhR-KO and NR cells within the cluster 5\_5dpi was executed with diffxpy using the Wald test (<https://github.com/theislab/diffxpy>).

The transcription factor (TF) ranking analysis was performed by Pawel Smialowski using the method described in Angerilli et al. with a threshold of the adjusted p-value  $< 0.05$  or q-value  $< 0.5$  from the differentially expressed genes (Angerilli et al., 2018; Rackham et al., 2016). The top 15 regulated TFs with highest scores were used to plot the interaction network with CytoScape (Shannon et al., 2003) and STRING database (Szklarczyk et al., 2021).

Velocity analysis computing the ratio of unspliced pre-mRNA and spliced mRNA was performed with the scVelo pipeline (Bergen et al., 2020). The data from the injured (5 dpi) astrocytes was split into non-recombined and AhR-KO cells and then velocity was calculated based on the top 2,000 high variable genes after a filtering step of including only genes that are expressed by at least 20 cells. The moments for velocity estimation were computed with default settings including 30 neighbors and 30 PCs. The velocity was then plotted on the UMAP embedding of the 5 dpi astrocyte data set.

#### 4.12.4 Gene Ontology analysis

Gene Ontology (GO) analysis was used to detect enriched biological processes of significantly regulated genes ( $p$ -value  $< 0.05$ , fold change  $> 2$ ) using the Database for Annotation, Visualization and Integrated Discovery (DAVID) 2021 (Huang et al., 2009a, 2009b). To reduce redundant GO terms a threshold of fold enrichment  $> 2$  was applied and only the most significant GO terms containing at least 3 genes were highlighted in the dot plots. GO terms were visualized using RStudio with the ggplot2 and pathview package (W. Luo & Brouwer, 2013; Wickham, 2016).

#### 4.13 Statistical analysis

Numbers of biological replicates are indicated on the dot plots and in the figure legend. Dot plots in Figure 2 to 5 are presented as median  $\pm$  interquartile range (IQR), if not otherwise indicated. IQR was calculated in GraphPad Prism. For the neurosphere experiments, the statistical analysis was executed in GraphPad Prism using the non-parametric Mann-Whitney test. When comparing the GFP<sup>+</sup> and GFP<sup>-</sup> neurospheres the data was presented in a contingency graph and the Fisher's exact test was performed to account for zero-inflated data. Statistical tests were only performed with at least 4 biological replicates and significance is indicated in each figure legend.



## 5 Abbreviations

ACSA-2	astrocyte cell surface antigen-2
AD	Alzheimer's Disease
AhR	aryl hydrocarbon receptor
AhRR	AhR repressor
AIP	AhR-interacting protein
ALDH1L1	aldehyde dehydrogenase 1 family, member L1
aNSC	adult neural stem cell
Arnt2	AhR nuclear translocator 2
Ascl1	achaete-scute homolog 1
A $\beta$ 42	Amyloid-beta 42
BBB	blood-brain barrier
bHLH	basic helix-loop-helix
BMP	bone morphogenic protein
BNF	$\beta$ -naphthoflavone
BP	biological processes
c-Myc	MYC proto-oncogene
Ccl4	C-C motif chemokine ligand 4
CCR2	C-C motif chemokine receptor 2
CD24	cluster of differentiation 24
Cdk1	cyclin dependent kinase 1
CNS	central nervous system
CreERT2	Cre fused to a mutant estrogen ligand-binding domain
CSC	cancer stem cell
CSF	cerebrospinal fluid
Cyp1a1	Cytochrome P450 family 1 subfamily a member 1
DAMP	damage-associated molecular patterns
DAVID	Database for Annotation, Visualization and Integrated Discovery
DEG	differentially expressed genes
DER	dioxin responsive element
DG	dentate gyrus
div	days <i>in vitro</i>
dpi	days post injury
ECM	extracellular matrix
EGF	epidermal growth factor
Emx1	empty spiracle homeobox 1
ERK	extracellular signal-regulated protein kinase
ESC	embryonic stem cell
FGF2	basic fibroblast growth factor
FICZ	6-formylindolo[3,2-b]carbazole
Fos	FBJ osteosarcoma oncogene
GABA	$\gamma$ -aminobutyric acid
GFAP	glial acidic fibrillary protein
GFP	green fluorescent protein

GLAST	L-glutamate/L-aspartate transporter
GLT1	excitatory amino acid transporter 2
GO	gene ontology
HSC	hematopoietic stem cell
HSP90	heat shock protein 90
HVG	high variable genes
i.p.	intraperitoneal
Iba1	ionized calcium-binding adapter molecule
IDO	indoleamine 2,3-dioxygenase
IFN- $\beta$	type-I interferon $\beta$
IHC	immunohistochemistry
Il1r2	interleukin 1 receptor, type II
iPSC	induced pluripotent stem cell
IQR	interquartile range
JNK	Jun N-terminal kinase
Jun	jun proto-oncogene
KEGG	Kyoto Encyclopedia of Genes and Genomes
Ki67	marker of proliferation Ki-67
Klf4	kruppel like factor 4
KNN	k-nearest neighbor
KO	knock-out
Lyar	Ly1 antibody reactive
MACS	magnetic-activated cell sorting
MAPK	mitogen-activated protein kinase
MS	multiple sclerosis
mTOR	mammalian target of rapamycin
Neurog2	Neurogenin 2
NR	non-recombined
NSC	neural stem cell
Nurr1	nuclear receptor related 1 protein
Oct-3/4	octamer-binding transcription factor 3/4
OPC	oligodendrocyte precursor cell
PAS	PER-ARNT-SIM domain
Pax6	paired box 6
PBS	phosphate-buffered saline
PCA	principal component analysis
PCR	polymerase chain reaction
PER	period circadian protein
PFA	paraformaldehyde
PTEN	phosphatase and tensin homolog
RGC	radial glia cell
RNA	ribonucleic acid
RT	room temperature
Runx1	runt related transcription factor 1
scRNAseq	single-cell RNA sequencing

SDS	sodium dodecyl sulfate
SEZ	subependymal zone
SGZ	subgranular zone
Shh	sonic hedgehog
shRNA	short hairpin RNA
SIM	single minded protein
Sox2	SRY-Box transcription factor 2
STAT3	signal transducer and activator of transcription 3
TAM	tamoxifen
TBI	traumatic brain injury
TBST	tris-buffered saline with Tween®
TCDD	2,3,7,8-tetrachlorodibenzo-p-dioxin
TCF1	transcription factor 1
TDO	tryptophan 2,3-dioxygenase
TF	transcription factor
TGFβ	transforming growth factor β
Trf	transferrin
UMAP	uniform manifold approximation and projection
Vim	vimentin
WB	western blot
Wnt	wingless-type
wt	wildtype



## 6 References

- Adachi, K., Mirzadeh, Z., Sakaguchi, M., Yamashita, T., Nikolcheva, T., Gotoh, Y., Peltz, G., Gong, L., Kawase, T., Alvarez-Buylla, A., Okano, H., & Sawamoto, K. (2007).  $\beta$ -Catenin Signaling Promotes Proliferation of Progenitor Cells in the Adult Mouse Subventricular Zone. *Stem Cells*, 25(11), 2827–2836. <https://doi.org/10.1634/stemcells.2007-0177>
- Alam, A., Thelin, E. P., Tajsic, T., Khan, D. Z., Khellaf, A., Patani, R., & Helmy, A. (2020). Cellular infiltration in traumatic brain injury. *Journal of Neuroinflammation*, 17(1), 328. <https://doi.org/10.1186/s12974-020-02005-x>
- Anderson, M. A., Burda, J. E., Ren, Y., Ao, Y., O'Shea, T. M., Kawaguchi, R., Coppola, G., Khakh, B. S., Deming, T. J., & Sofroniew, M. V. (2016). Astrocyte scar formation aids central nervous system axon regeneration. *Nature*, 532(7598), 195–200. <https://doi.org/10.1038/nature17623>
- Angerilli, A., Smialowski, P., & Rupp, R. A. (2018). The *Xenopus* animal cap transcriptome: building a mucociliary epithelium. *Nucleic Acids Research*, 46(17), 8772–8787. <https://doi.org/10.1093/nar/gky771>
- Anthony, T. E., & Heintz, N. (2007). The folate metabolic enzyme ALDH1L1 is restricted to the midline of the early CNS, suggesting a role in human neural tube defects. *The Journal of Comparative Neurology*, 500(2), 368–383. <https://doi.org/10.1002/cne.21179>
- Antonsson, C., Whitelaw, M. L., McGuire, J., Gustafsson, J. A., & Poellinger, L. (1995). Distinct roles of the molecular chaperone hsp90 in modulating dioxin receptor function via the basic helix-loop-helix and PAS domains. *Molecular and Cellular Biology*, 15(2), 756–765. <https://doi.org/10.1128/MCB.15.2.756>
- Asrican, B., Wooten, J., Li, Y.-D., Quintanilla, L., Zhang, F., Wander, C., Bao, H., Yeh, C.-Y., Luo, Y.-J., Olsen, R., Lim, S.-A., Hu, J., Jin, P., & Song, J. (2020). Neuropeptides Modulate Local Astrocytes to Regulate Adult Hippocampal Neural Stem Cells. *Neuron*, 108(2), 349–366.e6. <https://doi.org/10.1016/j.neuron.2020.07.039>
- Bachoo, R. M., Maher, E. A., Ligon, K. L., Sharpless, N. E., Chan, S. S., You, M. J., Tang, Y., DeFrances, J., Stover, E., Weissleder, R., Rowitch, D. H., Louis, D. N., & DePinho, R. A. (2002). Epidermal growth factor receptor and Ink4a/Arf. *Cancer Cell*, 1(3), 269–277. [https://doi.org/10.1016/S1535-6108\(02\)00046-6](https://doi.org/10.1016/S1535-6108(02)00046-6)
- Barbosa, J. S., Sanchez-Gonzalez, R., Di Giaimo, R., Baumgart, E. V., Theis, F. J., Götz, M., & Ninkovic, J. (2015). Live imaging of adult neural stem cell behavior in the intact and injured zebrafish brain. *Science*, 348(6236), 789–793. <https://doi.org/10.1126/science.aaa2729>
- Bardehle, S., Krüger, M., Buggenthin, F., Schwausch, J., Ninkovic, J., Clevers, H., Snippert, H. J., Theis, F. J., Meyer-Luehmann, M., Bechmann, I., Dimou, L., & Götz, M. (2013). Live imaging of astrocyte responses to acute injury reveals selective juxtavascular proliferation. *Nature Neuroscience*, 16(5), 580–586. <https://doi.org/10.1038/nn.3371>
- Basak, O., Krieger, T. G., Muraro, M. J., Wiebrands, K., Stange, D. E., Frias-Aldeguer, J., Rivron, N. C., van de Wetering, M., van Es, J. H., van Oudenaarden, A., Simons, B. D., & Clevers, H. (2018). Troy+ brain stem cells cycle through quiescence and regulate their number by sensing niche occupancy. *Proceedings of the National Academy of Sciences*, 115(4), E610–E619. <https://doi.org/10.1073/pnas.1715911114>
- Baser, A., Skabkin, M., Kleber, S., Dang, Y., Gülcüler Balta, G. S., Kalamakis, G., Göpferich, M., Ibañez, D. C., Schefzik, R., Lopez, A. S., Bobadilla, E. L., Schultz, C., Fischer, B., & Martin-Villalba, A. (2019). Onset of differentiation is post-transcriptionally controlled in adult neural stem cells. *Nature*, 566(7742), 100–104. <https://doi.org/10.1038/s41586-019-0888-x>

- Batiuk, M. Y., de Vin, F., Duqué, S. I., Li, C., Saito, T., Saido, T., Fiers, M., Belgard, T. G., & Holt, M. G. (2017). An immunoaffinity-based method for isolating ultrapure adult astrocytes based on ATP1B2 targeting by the ACSA-2 antibody. *Journal of Biological Chemistry*, *292*(21), 8874–8891. <https://doi.org/10.1074/jbc.M116.765313>
- Batiuk, M. Y., Martirosyan, A., Wahis, J., de Vin, F., Marneffe, C., Kusserow, C., Koeppen, J., Viana, J. F., Oliveira, J. F., Voet, T., Ponting, C. P., Belgard, T. G., & Holt, M. G. (2020). Identification of region-specific astrocyte subtypes at single cell resolution. *Nature Communications*, *11*(1), 1220. <https://doi.org/10.1038/s41467-019-14198-8>
- Baumgart, E. V., Barbosa, J. S., Bally-cuif, L., Götz, M., & Ninkovic, J. (2012). Stab wound injury of the zebrafish telencephalon: A model for comparative analysis of reactive gliosis. *Glia*, *60*(3), 343–357. <https://doi.org/10.1002/glia.22269>
- Bayraktar, O. A., Bartels, T., Holmqvist, S., Kleshchevnikov, V., Martirosyan, A., Polioudakis, D., Ben Haim, L., Young, A. M. H., Batiuk, M. Y., Prakash, K., Brown, A., Roberts, K., Paredes, M. F., Kawaguchi, R., Stockley, J. H., Sabeur, K., Chang, S. M., Huang, E., Hutchinson, P., ... Rowitch, D. H. (2020). Astrocyte layers in the mammalian cerebral cortex revealed by a single-cell in situ transcriptomic map. *Nature Neuroscience*, *23*(4), 500–509. <https://doi.org/10.1038/s41593-020-0602-1>
- Bélanger, M., Allaman, I., & Magistretti, P. J. (2011). Brain Energy Metabolism: Focus on Astrocyte-Neuron Metabolic Cooperation. *Cell Metabolism*, *14*(6), 724–738. <https://doi.org/10.1016/j.cmet.2011.08.016>
- Belenguer, G., Duart-Abadia, P., Jordán-Pla, A., Domingo-Muelas, A., Blasco-Chamarro, L., Ferrón, S. R., Morante-Redolat, J. M., & Fariñas, I. (2021). Adult Neural Stem Cells Are Alerted by Systemic Inflammation through TNF- $\alpha$  Receptor Signaling. *Cell Stem Cell*, *28*(2), 285–299.e9. <https://doi.org/10.1016/j.stem.2020.10.016>
- Belvindrah, R., Rougon, G., & Chazal, G. (2002). Increased Neurogenesis in Adult mCD24-Deficient Mice. *The Journal of Neuroscience*, *22*(9), 3594–3607. <https://doi.org/10.1523/JNEUROSCI.22-09-03594.2002>
- Bergander, L., Wincent, E., Rannug, A., Foroozesh, M., Alworth, W., & Rannug, U. (2004). Metabolic fate of the Ah receptor ligand 6-formylindolo[3,2-b]carbazole. *Chemico-Biological Interactions*, *149*(2–3), 151–164. <https://doi.org/10.1016/j.cbi.2004.08.005>
- Bergen, V., Lange, M., Peidli, S., Wolf, F. A., & Theis, F. J. (2020). Generalizing RNA velocity to transient cell states through dynamical modeling. *Nature Biotechnology*, *38*(12), 1408–1414. <https://doi.org/10.1038/s41587-020-0591-3>
- Boitano, A. E., Wang, J., Romeo, R., Bouchez, L. C., Parker, A. E., Sutton, S. E., Walker, J. R., Flaveny, C. A., Perdew, G. H., Denison, M. S., Schultz, P. G., & Cooke, M. P. (2010). Aryl Hydrocarbon Receptor Antagonists Promote the Expansion of Human Hematopoietic Stem Cells. *Science*, *329*(5997), 1345–1348. <https://doi.org/10.1126/science.1191536>
- Bonaguidi, M. A., Wheeler, M. A., Shapiro, J. S., Stadel, R. P., Sun, G. J., Ming, G., & Song, H. (2011). In Vivo Clonal Analysis Reveals Self-Renewing and Multipotent Adult Neural Stem Cell Characteristics. *Cell*, *145*(7), 1142–1155. <https://doi.org/10.1016/j.cell.2011.05.024>
- Bonvento, G., & Bolaños, J. P. (2021). Astrocyte-neuron metabolic cooperation shapes brain activity. *Cell Metabolism*, *33*(8), 1546–1564. <https://doi.org/10.1016/j.cmet.2021.07.006>
- Brannan, K. W., Chaim, I. A., Marina, R. J., Yee, B. A., Kofman, E. R., Lorenz, D. A., Jagannatha, P., Dong, K. D., Madrigal, A. A., Underwood, J. G., & Yeo, G. W. (2021). Robust single-cell discovery of RNA targets of RNA-binding proteins and ribosomes. *Nature Methods*, *18*(5), 507–519. <https://doi.org/10.1038/s41592-021-01128-0>
- Bruno, S., & Darzynkiewicz, Z. (1992). Cell cycle dependent expression and stability of the nuclear protein detected by Ki-67 antibody in HL-60 cells. *Cell Proliferation*, *25*(1), 31–40.

<https://doi.org/10.1111/j.1365-2184.1992.tb01435.x>

- Buffo, A., Rite, I., Tripathi, P., Lepier, A., Colak, D., Horn, A.-P., Mori, T., & Götz, M. (2008). Origin and progeny of reactive gliosis: A source of multipotent cells in the injured brain. *Proceedings of the National Academy of Sciences*, *105*(9), 3581–3586. <https://doi.org/10.1073/pnas.0709002105>
- Burda, J. E., & Sofroniew, M. V. (2014). Reactive Gliosis and the Multicellular Response to CNS Damage and Disease. *Neuron*, *81*(2), 229–248. <https://doi.org/10.1016/j.neuron.2013.12.034>
- Bush, T. G., Puvanachandra, N., Horner, C. H., Polito, A., Ostenfeld, T., Svendsen, C. N., Mucke, L., Johnson, M. H., & Sofroniew, M. V. (1999). Leukocyte Infiltration, Neuronal Degeneration, and Neurite Outgrowth after Ablation of Scar-Forming, Reactive Astrocytes in Adult Transgenic Mice. *Neuron*, *23*(2), 297–308. [https://doi.org/10.1016/S0896-6273\(00\)80781-3](https://doi.org/10.1016/S0896-6273(00)80781-3)
- Calzolari, F., Michel, J., Baumgart, E. V., Theis, F., Götz, M., & Ninkovic, J. (2015). Fast clonal expansion and limited neural stem cell self-renewal in the adult subependymal zone. *Nature Neuroscience*, *18*(4), 490–492. <https://doi.org/10.1038/nn.3963>
- Casado, F. L. (2016). The Aryl Hydrocarbon Receptor Relays Metabolic Signals to Promote Cellular Regeneration. *Stem Cells International*, *2016*, 1–8. <https://doi.org/10.1155/2016/4389802>
- Casella, G. T. B., Marcillo, A., Bunge, M. B., & Wood, P. M. (2002). New Vascular Tissue Rapidly Replaces Neural Parenchyma and Vessels Destroyed by a Contusion Injury to the Rat Spinal Cord. *Experimental Neurology*, *173*(1), 63–76. <https://doi.org/10.1006/exnr.2001.7827>
- Chan, S. J., Niu, W., Hayakawa, K., Hamanaka, G., Wang, X., Cheah, P. S., Guo, S., Yu, Z., Arai, K., Selim, M. H., Kurisawa, M., Spector, M., & Lo, E. H. (2019). Promoting Neuro-Supportive Properties of Astrocytes with Epidermal Growth Factor Hydrogels. *Stem Cells Translational Medicine*, *8*(12), 1242–1248. <https://doi.org/10.1002/sctm.19-0159>
- Chen, W.-C., Chang, L.-H., Huang, S.-S., Huang, Y.-J., Chih, C.-L., Kuo, H.-C., Lee, Y.-H., & Lee, I.-H. (2019). Aryl hydrocarbon receptor modulates stroke-induced astrogliosis and neurogenesis in the adult mouse brain. *Journal of Neuroinflammation*, *16*(1), 187. <https://doi.org/10.1186/s12974-019-1572-7>
- Codeluppi, S., Svensson, C. I., Hefferan, M. P., Valencia, F., Silldorff, M. D., Oshiro, M., Marsala, M., & Pasquale, E. B. (2009). The Rheb-mTOR Pathway Is Upregulated in Reactive Astrocytes of the Injured Spinal Cord. *Journal of Neuroscience*, *29*(4), 1093–1104. <https://doi.org/10.1523/JNEUROSCI.4103-08.2009>
- Colak, D., Mori, T., Brill, M. S., Pfeifer, A., Falk, S., Deng, C., Monteiro, R., Mummery, C., Sommer, L., & Götz, M. (2008). Adult neurogenesis requires Smad4-mediated bone morphogenic protein signaling in stem cells. *The Journal of Neuroscience: The Official Journal of the Society for Neuroscience*, *28*(2), 434–446. <https://doi.org/10.1523/JNEUROSCI.4374-07.2008>
- Colotta, F., Re, F., Muzio, M., Bertini, R., Polentarutti, N., Sironi, M., Giri, J. G., Dower, S. K., Sims, J. E., & Mantovani, A. (1993). Interleukin-1 Type II Receptor: A Decoy Target for IL-1 That Is Regulated by IL-4. *Science*, *261*(5120), 472–475. <https://doi.org/10.1126/science.8332913>
- Daneman, R., & Prat, A. (2015). The Blood–Brain Barrier. *Cold Spring Harbor Perspectives in Biology*, *7*(1), a020412. <https://doi.org/10.1101/cshperspect.a020412>
- Davarinos, N. A., & Pollenz, R. S. (1999). Aryl Hydrocarbon Receptor Imported into the Nucleus following Ligand Binding Is Rapidly Degraded via the Cytosolic Proteasome following Nuclear Export. *Journal of Biological Chemistry*, *274*(40), 28708–28715.

<https://doi.org/10.1074/jbc.274.40.28708>

- Denis, M., Cuthill, S., Wikström, A.-C., Poellinger, L., & Gustafsson, J.-Å. (1988). Association of the dioxin receptor with the Mr 90,000 heat shock protein: A structural kinship with the glucocorticoid receptor. *Biochemical and Biophysical Research Communications*, *155*(2), 801–807. [https://doi.org/10.1016/S0006-291X\(88\)80566-7](https://doi.org/10.1016/S0006-291X(88)80566-7)
- Denison, M. S., Fisher, J. M., & Whitlock, J. P. (1988a). Inducible, receptor-dependent protein-DNA interactions at a dioxin-responsive transcriptional enhancer. *Proceedings of the National Academy of Sciences of the United States of America*, *85*(8), 2528–2532. <https://doi.org/10.1073/pnas.85.8.2528>
- Denison, M. S., Fisher, J. M., & Whitlock, J. P. (1988b). The DNA recognition site for the dioxin-Ah receptor complex. Nucleotide sequence and functional analysis. *The Journal of Biological Chemistry*, *263*(33), 17221–17224. [https://doi.org/10.1016/S0021-9258\(19\)77819-3](https://doi.org/10.1016/S0021-9258(19)77819-3)
- Dever, D. P., Adham, Z. O., Thompson, B., Genestine, M., Cherry, J., Olschowka, J. A., DiCiccio-Bloom, E., & Opanashuk, L. A. (2016). Aryl hydrocarbon receptor deletion in cerebellar granule neuron precursors impairs neurogenesis. *Developmental Neurobiology*, *76*(5), 533–550. <https://doi.org/10.1002/dneu.22330>
- Dewan, M. C., Rattani, A., Gupta, S., Baticulon, R. E., Hung, Y.-C., Punchak, M., Agrawal, A., Adeleye, A. O., Shrimel, M. G., Rubiano, A. M., Rosenfeld, J. V., & Park, K. B. (2019). Estimating the global incidence of traumatic brain injury. *Journal of Neurosurgery*, *130*(4), 1080–1097. <https://doi.org/10.3171/2017.10.JNS17352>
- Di Giaimo, R., Durovic, T., Barquin, P., Kociaj, A., Lepko, T., Aschenbroich, S., Breunig, C. T., Irmeler, M., Cernilogar, F. M., Schotta, G., Barbosa, J. S., Trümbach, D., Baumgart, E. V., Neuner, A. M., Beckers, J., Wurst, W., Stricker, S. H., & Ninkovic, J. (2018). The Aryl Hydrocarbon Receptor Pathway Defines the Time Frame for Restorative Neurogenesis. *Cell Reports*, *25*(12), 3241–3251.e5. <https://doi.org/10.1016/j.celrep.2018.11.055>
- Dimou, L., & Götz, M. (2014). Glial Cells as Progenitors and Stem Cells: New Roles in the Healthy and Diseased Brain. *Physiological Reviews*, *94*(3), 709–737. <https://doi.org/10.1152/physrev.00036.2013>
- Do, J. T., & Schöler, H. R. (2009). Regulatory circuits underlying pluripotency and reprogramming. *Trends in Pharmacological Sciences*, *30*(6), 296–302. <https://doi.org/10.1016/j.tips.2009.03.003>
- Doetsch, F., Petreanu, L., Caille, I., Garcia-Verdugo, J.-M., & Alvarez-Buylla, A. (2002). EGF Converts Transit-Amplifying Neurogenic Precursors in the Adult Brain into Multipotent Stem Cells. *Neuron*, *36*(6), 1021–1034. [https://doi.org/10.1016/S0896-6273\(02\)01133-9](https://doi.org/10.1016/S0896-6273(02)01133-9)
- Donat, C. K., Scott, G., Gentleman, S. M., & Sastre, M. (2017). Microglial Activation in Traumatic Brain Injury. *Frontiers in Aging Neuroscience*, *9*(JUN). <https://doi.org/10.3389/fnagi.2017.00208>
- Dorrier, C. E., Aran, D., Haenelt, E. A., Sheehy, R. N., Hoi, K. K., Pintarić, L., Chen, Y., Lizama, C. O., Cautivo, K. M., Weiner, G. A., Popko, B., Fancy, S. P. J., Arnold, T. D., & Daneman, R. (2021). CNS fibroblasts form a fibrotic scar in response to immune cell infiltration. *Nature Neuroscience*, *24*(2), 234–244. <https://doi.org/10.1038/s41593-020-00770-9>
- Falk, S., & Götz, M. (2017). Glial control of neurogenesis. *Current Opinion in Neurobiology*, *47*, 188–195. <https://doi.org/10.1016/j.conb.2017.10.025>
- Faulkner, J. R., Herrmann, J. E., Woo, M. J., Tansey, K. E., Doan, N. B., & Sofroniew, M. V. (2004). Reactive astrocytes protect tissue and preserve function after spinal cord injury. *Journal of Neuroscience*, *24*(9), 2143–2155. <https://doi.org/10.1523/JNEUROSCI.3547-03.2004>
- Feil, R. (2007). Conditional somatic mutagenesis in the mouse using site-specific recombinases.

- Handbook of Experimental Pharmacology*, 178(178), 3–28. [https://doi.org/10.1007/978-3-540-35109-2\\_1](https://doi.org/10.1007/978-3-540-35109-2_1)
- Feil, S., Valtcheva, N., & Feil, R. (2009). Inducible Cre Mice. In *Methods in Molecular Biology* (Vol. 530, Issue Chapter 18, pp. 343–363). Humana Press. [https://doi.org/10.1007/978-1-59745-471-1\\_18](https://doi.org/10.1007/978-1-59745-471-1_18)
- Fraser, M. M., Zhu, X., Kwon, C.-H., Uhlmann, E. J., Gutmann, D. H., & Baker, S. J. (2004). Pten Loss Causes Hypertrophy and Increased Proliferation of Astrocytes In vivo. *Cancer Research*, 64(21), 7773–7779. <https://doi.org/10.1158/0008-5472.CAN-04-2487>
- Friedmann-Morvinski, D., Bushong, E. A., Ke, E., Soda, Y., Marumoto, T., Singer, O., Ellisman, M. H., & Verma, I. M. (2012). Dedifferentiation of Neurons and Astrocytes by Oncogenes Can Induce Gliomas in Mice. *Science*, 338(6110), 1080–1084. <https://doi.org/10.1126/science.1226929>
- Friedmann-Morvinski, D., & Verma, I. M. (2014). Dedifferentiation and reprogramming: origins of cancer stem cells. *EMBO Reports*, 15(3), 244–253. <https://doi.org/10.1002/embr.201338254>
- Frik, J., Merl-Pham, J., Plesnila, N., Mattugini, N., Kjell, J., Kraska, J., Gómez, R. M., Hauck, S. M., Sirko, S., & Götz, M. (2018). Cross-talk between monocyte invasion and astrocyte proliferation regulates scarring in brain injury. *EMBO Reports*, 19(5). <https://doi.org/10.15252/embr.201745294>
- Frinchi, M., Bonomo, A., Trovato-Salinaro, A., Condorelli, D. F., Fuxe, K., Spampinato, M. G., & Mudò, G. (2008). Fibroblast growth factor-2 and its receptor expression in proliferating precursor cells of the subventricular zone in the adult rat brain. *Neuroscience Letters*, 447(1), 20–25. <https://doi.org/10.1016/j.neulet.2008.09.059>
- Fukunaga, B. N., Probst, M. R., Reisz-Porszasz, S., & Hankinson, O. (1995). Identification of Functional Domains of the Aryl Hydrocarbon Receptor. *Journal of Biological Chemistry*, 270(49), 29270–29278. <https://doi.org/10.1074/jbc.270.49.29270>
- Gadea, A., Schinelli, S., & Gallo, V. (2008). Endothelin-1 Regulates Astrocyte Proliferation and Reactive Gliosis via a JNK/c-Jun Signaling Pathway. *Journal of Neuroscience*, 28(10), 2394–2408. <https://doi.org/10.1523/JNEUROSCI.5652-07.2008>
- Gascón, S., Murenu, E., Masserdotti, G., Ortega, F., Russo, G. L., Petrik, D., Deshpande, A., Heinrich, C., Karow, M., Robertson, S. P., Schroeder, T., Beckers, J., Irmeler, M., Berndt, C., Angeli, J. P. F., Conrad, M., Berninger, B., & Götz, M. (2016). Identification and Successful Negotiation of a Metabolic Checkpoint in Direct Neuronal Reprogramming. *Cell Stem Cell*, 18(3), 396–409. <https://doi.org/10.1016/j.stem.2015.12.003>
- Gasiewicz, T. A., Singh, K. P., & Bennett, J. A. (2014). The Ah receptor in stem cell cycling, regulation, and quiescence. *Annals of the New York Academy of Sciences*, 1310(1), 44–50. <https://doi.org/10.1111/nyas.12361>
- George, N., & Geller, H. M. (2018). Extracellular matrix and traumatic brain injury. *Journal of Neuroscience Research*, 96(4), 573–588. <https://doi.org/10.1002/jnr.24151>
- Gomez-Pinilla, F., Vu, L., & Cotman, C. (1995). Regulation of astrocyte proliferation by FGF-2 and heparan sulfate in vivo. *The Journal of Neuroscience*, 15(3), 2021–2029. <https://doi.org/10.1523/JNEUROSCI.15-03-02021.1995>
- Göritz, C., Dias, D. O., Tomilin, N., Barbacid, M., Shupliakov, O., & Frisén, J. (2011). A Pericyte Origin of Spinal Cord Scar Tissue. *Science*, 333(6039), 238–242. <https://doi.org/10.1126/science.1203165>
- Gorski, J. A., Talley, T., Qiu, M., Puelles, L., Rubenstein, J. L. R., & Jones, K. R. (2002). Cortical Excitatory Neurons and Glia, But Not GABAergic Neurons, Are Produced in the Emx1-Expressing Lineage. *The Journal of Neuroscience*, 22(15), 6309–6314.

<https://doi.org/10.1523/JNEUROSCI.22-15-06309.2002>

- Götz, S., Bribian, A., López-Mascaraque, L., Götz, M., Grothe, B., & Kunz, L. (2021). Heterogeneity of astrocytes: Electrophysiological properties of juxtavascular astrocytes before and after brain injury. *Glia*, *69*(2), 346–361. <https://doi.org/10.1002/glia.23900>
- Grade, S., & Götz, M. (2017). Neuronal replacement therapy: previous achievements and challenges ahead. *Npj Regenerative Medicine*, *2*(1), 29. <https://doi.org/10.1038/s41536-017-0033-0>
- Groves, A., Kihara, Y., Jonnalagadda, D., Rivera, R., Kennedy, G., Mayford, M., & Chun, J. (2018). A Functionally Defined In Vivo Astrocyte Population Identified by c-Fos Activation in a Mouse Model of Multiple Sclerosis Modulated by S1P Signaling: Immediate-Early Astrocytes (ieAstrocytes). *Eneuro*, *5*(5), ENEURO.0239-18.2018. <https://doi.org/10.1523/ENEURO.0239-18.2018>
- Haarbauer-Krupa, J., Pugh, M. J., Prager, E. M., Harmon, N., Wolfe, J., & Yaffe, K. (2021). Epidemiology of Chronic Effects of Traumatic Brain Injury. *Journal of Neurotrauma*, *38*(23), 3235–3247. <https://doi.org/10.1089/neu.2021.0062>
- Hanahan, D. (2022). Hallmarks of Cancer: New Dimensions. *Cancer Discovery*, *12*(1), 31–46. <https://doi.org/10.1158/2159-8290.CD-21-1059>
- Hanieh, H. (2014). Toward Understanding the Role of Aryl Hydrocarbon Receptor in the Immune System: Current Progress and Future Trends. *BioMed Research International*, *2014*, 1–14. <https://doi.org/10.1155/2014/520763>
- Heimann, G., Canhos, L. L., Frik, J., Jäger, G., Lepko, T., Ninkovic, J., Götz, M., & Sirko, S. (2017). Changes in the Proliferative Program Limit Astrocyte Homeostasis in the Aged Post-Traumatic Murine Cerebral Cortex. *Cerebral Cortex*, *27*(8), 4213–4228. <https://doi.org/10.1093/cercor/bhx112>
- Heinrich, C., Blum, R., Gascón, S., Masserdotti, G., Tripathi, P., Sánchez, R., Tiedt, S., Schroeder, T., Götz, M., & Berninger, B. (2010). Directing Astroglia from the Cerebral Cortex into Subtype Specific Functional Neurons. *PLoS Biology*, *8*(5), e1000373. <https://doi.org/10.1371/journal.pbio.1000373>
- Henderson, C. J., McLaughlin, L. A., Osuna-Cabello, M., Taylor, M., Gilbert, I., McLaren, A. W., & Wolf, C. R. (2015). Application of a novel regulatable Cre recombinase system to define the role of liver and gut metabolism in drug oral bioavailability. *Biochemical Journal*, *465*(3), 479–488. <https://doi.org/10.1042/BJ20140582>
- Huang, D. W., Sherman, B. T., & Lempicki, R. A. (2009a). Bioinformatics enrichment tools: paths toward the comprehensive functional analysis of large gene lists. *Nucleic Acids Research*, *37*(1), 1–13. <https://doi.org/10.1093/nar/gkn923>
- Huang, D. W., Sherman, B. T., & Lempicki, R. A. (2009b). Systematic and integrative analysis of large gene lists using DAVID bioinformatics resources. *Nature Protocols*, *4*(1), 44–57. <https://doi.org/10.1038/nprot.2008.211>
- Hughes, E. G., Kang, S. H., Fukaya, M., & Bergles, D. E. (2013). Oligodendrocyte progenitors balance growth with self-repulsion to achieve homeostasis in the adult brain. *Nature Neuroscience*, *16*(6), 668–676. <https://doi.org/10.1038/nn.3390>
- Iwasato, T., Datwani, A., Wolf, A. M., Nishiyama, H., Taguchi, Y., Tonegawa, S., Knöpfel, T., Erzurumlu, R. S., & Itohara, S. (2000). Cortex-restricted disruption of NMDAR1 impairs neuronal patterns in the barrel cortex. *Nature*, *406*(6797), 726–731. <https://doi.org/10.1038/35021059>
- Jassam, Y. N., Izzy, S., Whalen, M., McGavern, D. B., & El Khoury, J. (2017). Neuroimmunology of Traumatic Brain Injury: Time for a Paradigm Shift. *Neuron*, *95*(6), 1246–1265. <https://doi.org/10.1016/j.neuron.2017.07.010>

- Jeannet, G., Boudousquié, C., Gardiol, N., Kang, J., Huelsken, J., & Held, W. (2010). Essential role of the Wnt pathway effector Tcf-1 for the establishment of functional CD8 T cell memory. *Proceedings of the National Academy of Sciences*, *107*(21), 9777–9782. <https://doi.org/10.1073/pnas.0914127107>
- Juricek, L., & Coumoul, X. (2018). The Aryl Hydrocarbon Receptor and the Nervous System. *International Journal of Molecular Sciences*, *19*(9), 2504. <https://doi.org/10.3390/ijms19092504>
- Kang, K., Lee, S.-W., Han, J. E., Choi, J. W., & Song, M.-R. (2014). The complex morphology of reactive astrocytes controlled by fibroblast growth factor signaling. *Glia*, *62*(8), 1328–1344. <https://doi.org/10.1002/glia.22684>
- Kantzer, C. G., Boutin, C., Herzig, I. D., Wittwer, C., Reiß, S., Tiveron, M. C., Drewes, J., Rockel, T. D., Ohlig, S., Ninkovic, J., Cremer, H., Pennartz, S., Jungblut, M., & Bosio, A. (2017). Anti-ACSA-2 defines a novel monoclonal antibody for prospective isolation of living neonatal and adult astrocytes. *Glia*, *65*(6), 990–1004. <https://doi.org/10.1002/glia.23140>
- Kazlauskas, A., Poellinger, L., & Pongratz, I. (1999). Evidence That the Co-chaperone p23 Regulates Ligand Responsiveness of the Dioxin (Aryl Hydrocarbon) Receptor. *Journal of Biological Chemistry*, *274*(19), 13519–13524. <https://doi.org/10.1074/jbc.274.19.13519>
- Kazlauskas, A., Poellinger, L., & Pongratz, I. (2000). The Immunophilin-like Protein XAP2 Regulates Ubiquitination and Subcellular Localization of the Dioxin Receptor. *Journal of Biological Chemistry*, *275*(52), 41317–41324. <https://doi.org/10.1074/jbc.M007765200>
- Kazlauskas, A., Sundström, S., Poellinger, L., & Pongratz, I. (2001). The hsp90 Chaperone Complex Regulates Intracellular Localization of the Dioxin Receptor. *Molecular and Cellular Biology*, *21*(7), 2594–2607. <https://doi.org/10.1128/MCB.21.7.2594-2607.2001>
- Kempf, J., Knelles, K., Hersbach, B. A., Petrik, D., Riedemann, T., Bednarova, V., Janjic, A., Simon-Ebert, T., Enard, W., Smialowski, P., Götz, M., & Masserdotti, G. (2021). Heterogeneity of neurons reprogrammed from spinal cord astrocytes by the proneural factors *Ascl1* and *Neurogenin2*. *Cell Reports*, *36*(3), 109409. <https://doi.org/10.1016/j.celrep.2021.109409>
- Keshavarzi, M., Khoshnoud, M. J., Ghaffarian Bahraman, A., & Mohammadi-Bardbori, A. (2020). An Endogenous Ligand of Aryl Hydrocarbon Receptor 6-Formylindolo[3,2-b]Carbazole (FICZ) Is a Signaling Molecule in Neurogenesis of Adult Hippocampal Neurons. *Journal of Molecular Neuroscience*, *70*(5), 806–817. <https://doi.org/10.1007/s12031-020-01506-x>
- Kim, S., Kim, H., & Um, J. W. (2018). Synapse development organized by neuronal activity-regulated immediate-early genes. *Experimental & Molecular Medicine*, *50*(4), 1–7. <https://doi.org/10.1038/s12276-018-0025-1>
- Kishimoto, N., Shimizu, K., & Sawamoto, K. (2012). Neuronal regeneration in a zebrafish model of adult brain injury. *Disease Models & Mechanisms*, *5*(2), 200–209. <https://doi.org/10.1242/dmm.007336>
- Knotek, T., Janeckova, L., Kriska, J., Korinek, V., & Anderova, M. (2020). Glia and Neural Stem and Progenitor Cells of the Healthy and Ischemic Brain: The Workplace for the Wnt Signaling Pathway. *Genes*, *11*(7), 804. <https://doi.org/10.3390/genes11070804>
- Konishi, H., Okamoto, T., Hara, Y., Komine, O., Tamada, H., Maeda, M., Osako, F., Kobayashi, M., Nishiyama, A., Kataoka, Y., Takai, T., Udagawa, N., Jung, S., Ozato, K., Tamura, T., Tsuda, M., Yamanaka, K., Ogi, T., Sato, K., & Kiyama, H. (2020). Astrocytic phagocytosis is a compensatory mechanism for microglial dysfunction. *The EMBO Journal*, *39*(22). <https://doi.org/10.15252/embj.2020104464>
- Kroehne, V., Freudenreich, D., Hans, S., Kaslin, J., & Brand, M. (2011). Regeneration of the adult zebrafish brain from neurogenic radial glia-type progenitors. *Development*, *138*(22), 4831–4841. <https://doi.org/10.1242/dev.072587>

- Kuhn, H. G., Winkler, J., Kempermann, G., Thal, L. J., & Gage, F. H. (1997). Epidermal Growth Factor and Fibroblast Growth Factor-2 Have Different Effects on Neural Progenitors in the Adult Rat Brain. *The Journal of Neuroscience*, *17*(15), 5820–5829. <https://doi.org/10.1523/JNEUROSCI.17-15-05820.1997>
- Kyritsis, N., Kizil, C., & Brand, M. (2014). Neuroinflammation and central nervous system regeneration in vertebrates. *Trends in Cell Biology*, *24*(2), 128–135. <https://doi.org/10.1016/j.tcb.2013.08.004>
- Kyritsis, N., Kizil, C., Zocher, S., Kroehne, V., Kaslin, J., Freudenreich, D., Iltzsche, A., & Brand, M. (2012). Acute Inflammation Initiates the Regenerative Response in the Adult Zebrafish Brain. *Science*, *338*(6112), 1353–1356. <https://doi.org/10.1126/science.1228773>
- Lafita-Navarro, M. C., Kim, M., Borenstein-Auerbach, N., Venkateswaran, N., Hao, Y.-H., Ray, R., Brabletz, T., Scaglioni, P. P., Shay, J. W., & Conacci-Sorrell, M. (2018). The aryl hydrocarbon receptor regulates nucleolar activity and protein synthesis in MYC-expressing cells. *Genes & Development*, *32*(19–20), 1303–1308. <https://doi.org/10.1101/gad.313007.118>
- Lai, K., Kaspar, B. K., Gage, F. H., & Schaffer, D. V. (2003). Sonic hedgehog regulates adult neural progenitor proliferation in vitro and in vivo. *Nature Neuroscience*, *6*(1), 21–27. <https://doi.org/10.1038/nn983>
- Lang, B., Liu, H. L., Liu, R., Feng, G. D., Jiao, X. Y., & Ju, G. (2004). Astrocytes in injured adult rat spinal cord may acquire the potential of neural stem cells. *Neuroscience*, *128*(4), 775–783. <https://doi.org/10.1016/j.neuroscience.2004.06.033>
- Lange Canhos, L., Chen, M., Falk, S., Popper, B., Straub, T., Götz, M., & Sirko, S. (2021). Repetitive injury and absence of monocytes promote astrocyte self-renewal and neurological recovery. *Glia*, *69*(1), 165–181. <https://doi.org/10.1002/glia.23893>
- Lanjakornsiripan, D., Pior, B.-J., Kawaguchi, D., Furutachi, S., Tahara, T., Katsuyama, Y., Suzuki, Y., Fukazawa, Y., & Gotoh, Y. (2018). Layer-specific morphological and molecular differences in neocortical astrocytes and their dependence on neuronal layers. *Nature Communications*, *9*(1), 1623. <https://doi.org/10.1038/s41467-018-03940-3>
- Latchney, S. E., Hein, A. M., O'Banion, M. K., DiCicco-Bloom, E., & Opanashuk, L. A. (2013). Deletion or activation of the aryl hydrocarbon receptor alters adult hippocampal neurogenesis and contextual fear memory. *Journal of Neurochemistry*, *125*(3), 430–445. <https://doi.org/10.1111/jnc.12130>
- LeComte, M. D., Shimada, I. S., Sherwin, C., & Spees, J. L. (2015). Notch1–STAT3–ETB R signaling axis controls reactive astrocyte proliferation after brain injury. *Proceedings of the National Academy of Sciences*, *112*(28), 8726–8731. <https://doi.org/10.1073/pnas.1501029112>
- Lee, T. K. W., Castilho, A., Cheung, V. C. H., Tang, K. H., Ma, S., & Ng, I. O. L. (2011). CD24+ Liver Tumor-Initiating Cells Drive Self-Renewal and Tumor Initiation through STAT3-Mediated NANOG Regulation. *Cell Stem Cell*, *9*(1), 50–63. <https://doi.org/10.1016/j.stem.2011.06.005>
- Lees, M. J., Peet, D. J., & Whitelaw, M. L. (2003). Defining the Role for XAP2 in Stabilization of the Dioxin Receptor. *Journal of Biological Chemistry*, *278*(38), 35878–35888. <https://doi.org/10.1074/jbc.M302430200>
- Li, H., Wang, B., Yang, A., Lu, R., Wang, W., Zhou, Y., Shi, G., Kwon, S. W., Zhao, Y., & Jin, Y. (2009). Ly-1 Antibody Reactive Clone Is an Important Nucleolar Protein for Control of Self-Renewal and Differentiation in Embryonic Stem Cells. *Stem Cells*, *27*(6), 1244–1254. <https://doi.org/10.1002/stem.55>
- Li, Q., Lai, Q., He, C., Fang, Y., Yan, Q., Zhang, Y., Wang, X., Gu, C., Wang, Y., Ye, L., Han, L., Lin, X., Chen, J., Cai, J., Li, A., & Liu, S. (2019). RUNX1 promotes tumour metastasis by activating the Wnt/ $\beta$ -catenin signalling pathway and EMT in colorectal cancer. *Journal of*

- Experimental & Clinical Cancer Research*, 38(1), 334. <https://doi.org/10.1186/s13046-019-1330-9>
- Li, X., & Wang, C.-Y. (2021). From bulk, single-cell to spatial RNA sequencing. *International Journal of Oral Science*, 13(1), 36. <https://doi.org/10.1038/s41368-021-00146-0>
- Liddel, S. A., Guttenplan, K. A., Clarke, L. E., Bennett, F. C., Bohlen, C. J., Schirmer, L., Bennett, M. L., Münch, A. E., Chung, W.-S., Peterson, T. C., Wilton, D. K., Frouin, A., Napier, B. A., Panicker, N., Kumar, M., Buckwalter, M. S., Rowitch, D. H., Dawson, V. L., Dawson, T. M., ... Barres, B. A. (2017). Neurotoxic reactive astrocytes are induced by activated microglia. *Nature*, 541(7638), 481–487. <https://doi.org/10.1038/nature21029>
- Lie, D.-C., Colamarino, S. A., Song, H.-J., Désiré, L., Mira, H., Consiglio, A., Lein, E. S., Jessberger, S., Lansford, H., Dearie, A. R., & Gage, F. H. (2005). Wnt signalling regulates adult hippocampal neurogenesis. *Nature*, 437(7063), 1370–1375. <https://doi.org/10.1038/nature04108>
- Logan, T. T., Rusnak, M., & Symes, A. J. (2015). Runx1 promotes proliferation and neuronal differentiation in adult mouse neurosphere cultures. *Stem Cell Research*, 15(3), 554–564. <https://doi.org/10.1016/j.scr.2015.09.014>
- Luo, P., Li, X., Wu, X., Dai, S., Yang, Y., Xu, H., Jing, D., Rao, W., Xu, H., Gao, X., Fei, Z., & Lu, H. (2019). Preso regulates NMDA receptor-mediated excitotoxicity via modulating nitric oxide and calcium responses after traumatic brain injury. *Cell Death & Disease*, 10(7), 496. <https://doi.org/10.1038/s41419-019-1731-x>
- Luo, W., & Brouwer, C. (2013). Pathview: an R/Bioconductor package for pathway-based data integration and visualization. *Bioinformatics*, 29(14), 1830–1831. <https://doi.org/10.1093/bioinformatics/btt285>
- Machold, R., Hayashi, S., Rutlin, M., Muzumdar, M. D., Nery, S., Corbin, J. G., Gritli-Linde, A., Dellovade, T., Porter, J. A., Rubin, L. L., Dudek, H., McMahon, A. P., & Fishell, G. (2003). Sonic Hedgehog Is Required for Progenitor Cell Maintenance in Telencephalic Stem Cell Niches. *Neuron*, 39(6), 937–950. [https://doi.org/10.1016/S0896-6273\(03\)00561-0](https://doi.org/10.1016/S0896-6273(03)00561-0)
- MacVicar, B. A., & Newman, E. A. (2015). Astrocyte Regulation of Blood Flow in the Brain. *Cold Spring Harbor Perspectives in Biology*, 7(5), a020388. <https://doi.org/10.1101/cshperspect.a020388>
- Masserdotti, G., Gillotin, S., Sutor, B., Drechsel, D., Irmeler, M., Jørgensen, H. F., Sass, S., Theis, F. J., Beckers, J., Berninger, B., Guillemot, F., & Götz, M. (2015). Transcriptional Mechanisms of Proneural Factors and REST in Regulating Neuronal Reprogramming of Astrocytes. *Cell Stem Cell*, 17(1), 74–88. <https://doi.org/10.1016/j.stem.2015.05.014>
- Mathew, L. K., Simonich, M. T., & Tanguay, R. L. (2009). AHR-dependent misregulation of Wnt signaling disrupts tissue regeneration. *Biochemical Pharmacology*, 77(4), 498–507. <https://doi.org/10.1016/j.bcp.2008.09.025>
- Mattugini, N., Bocchi, R., Scheuss, V., Russo, G. L., Torper, O., Lao, C. L., & Götz, M. (2019). Inducing Different Neuronal Subtypes from Astrocytes in the Injured Mouse Cerebral Cortex. *Neuron*, 103(6), 1086-1095.e5. <https://doi.org/10.1016/j.neuron.2019.08.009>
- McGarry, T., Biniiecka, M., Veale, D. J., & Fearon, U. (2018). Hypoxia, oxidative stress and inflammation. *Free Radical Biology and Medicine*, 125, 15–24. <https://doi.org/10.1016/j.freeradbiomed.2018.03.042>
- McGuire, J., Whitelaw, M. L., Pongratz, I., Gustafsson, J. A., & Poellinger, L. (1994). A cellular factor stimulates ligand-dependent release of hsp90 from the basic helix-loop-helix dioxin receptor. *Molecular and Cellular Biology*, 14(4), 2438–2446. <https://doi.org/10.1128/mcb.14.4.2438-2446.1994>
- McInnes, L., Healy, J., Saul, N., & Großberger, L. (2018). UMAP: Uniform Manifold Approximation

- and Projection. *Journal of Open Source Software*, 3(29), 861. <https://doi.org/10.21105/joss.00861>
- Medina, M. A., Ugarte, G. D., Vargas, M. F., Avila, M. E., Necuñir, D., Elorza, A. A., Gutiérrez, S. E., & De Ferrari, G. V. (2016). Alternative RUNX1 Promoter Regulation by Wnt/ $\beta$ -Catenin Signaling in Leukemia Cells and Human Hematopoietic Progenitors. *Journal of Cellular Physiology*, 231(7), 1460–1467. <https://doi.org/10.1002/jcp.25258>
- Meyer, B. K., & Perdew, G. H. (1999). Characterization of the AhR–hsp90–XAP2 Core Complex and the Role of the Immunophilin-Related Protein XAP2 in AhR Stabilization. *Biochemistry*, 38(28), 8907–8917. <https://doi.org/10.1021/bi982223w>
- Middeldorp, J., & Hol, E. M. (2011). GFAP in health and disease. *Progress in Neurobiology*, 93(3), 421–443. <https://doi.org/10.1016/j.pneurobio.2011.01.005>
- Middleton, J., Patterson, A. M., Gardner, L., Schmutz, C., & Ashton, B. A. (2002). Leukocyte extravasation: chemokine transport and presentation by the endothelium. *Blood*, 100(12), 3853–3860. <https://doi.org/10.1182/blood.V100.12.3853>
- Mimura, J., Ema, M., Sogawa, K., & Fujii-Kuriyama, Y. (1999). Identification of a novel mechanism of regulation of Ah (dioxin) receptor function. *Genes & Development*, 13(1), 20–25. <https://doi.org/10.1101/gad.13.1.20>
- Min, R., & van der Knaap, M. S. (2018). Genetic defects disrupting glial ion and water homeostasis in the brain. *Brain Pathology*, 28(3), 372–387. <https://doi.org/10.1111/bpa.12602>
- Miniero, R., De Felip, E., Ferri, F., & di Domenico, A. (2001). An overview of TCDD half-life in mammals and its correlation to body weight. *Chemosphere*, 43(4–7), 839–844. [https://doi.org/10.1016/S0045-6535\(00\)00442-2](https://doi.org/10.1016/S0045-6535(00)00442-2)
- Moore, E. E., Moore, H. B., Kornblith, L. Z., Neal, M. D., Hoffman, M., Mutch, N. J., Schöch, H., Hunt, B. J., & Sauaia, A. (2021). Trauma-induced coagulopathy. *Nature Reviews Disease Primers*, 7(1), 30. <https://doi.org/10.1038/s41572-021-00264-3>
- Morales, J. L., & Perdew, G. H. (2007). Carboxyl Terminus of hsc70-Interacting Protein (CHIP) Can Remodel Mature Aryl Hydrocarbon Receptor (AhR) Complexes and Mediate Ubiquitination of Both the AhR and the 90 kDa Heat-Shock Protein (hsp90) in Vitro. *Biochemistry*, 46(2), 610–621. <https://doi.org/10.1021/bi062165b>
- Mori, T., Tanaka, K., Buffo, A., Wurst, W., Kühn, R., & Götz, M. (2006). Inducible gene deletion in astroglia and radial glia—A valuable tool for functional and lineage analysis. *Glia*, 54(1), 21–34. <https://doi.org/10.1002/glia.20350>
- Morizawa, Y. M., Hirayama, Y., Ohno, N., Shibata, S., Shigetomi, E., Sui, Y., Nabekura, J., Sato, K., Okajima, F., Takebayashi, H., Okano, H., & Koizumi, S. (2017). Reactive astrocytes function as phagocytes after brain ischemia via ABCA1-mediated pathway. *Nature Communications*, 8(1), 28. <https://doi.org/10.1038/s41467-017-00037-1>
- Mulero-Navarro, S., & Fernandez-Salguero, P. M. (2016). New Trends in Aryl Hydrocarbon Receptor Biology. *Frontiers in Cell and Developmental Biology*, 4(MAY). <https://doi.org/10.3389/fcell.2016.00045>
- Muñoz, M. F., Puebla, M., & Figueroa, X. F. (2015). Control of the neurovascular coupling by nitric oxide-dependent regulation of astrocytic Ca<sup>2+</sup> signaling. *Frontiers in Cellular Neuroscience*, 9. <https://doi.org/10.3389/fncel.2015.00059>
- Nacarino-Palma, A., González-Rico, F. J., Rejano-Gordillo, C. M., Ordiales-Talavera, A., Merino, J. M., & Fernández-Salguero, P. M. (2021). The aryl hydrocarbon receptor promotes differentiation during mouse preimplantational embryo development. *Stem Cell Reports*, 16(9), 2351–2363. <https://doi.org/10.1016/j.stemcr.2021.08.002>

- Nakamura, T., Colbert, M. C., & Robbins, J. (2006). Neural Crest Cells Retain Multipotential Characteristics in the Developing Valves and Label the Cardiac Conduction System. *Circulation Research*, 98(12), 1547–1554. <https://doi.org/10.1161/01.RES.0000227505.19472.69>
- Nimmerjahn, A., Kirchhoff, F., & Helmchen, F. (2005). Resting Microglial Cells Are Highly Dynamic Surveillants of Brain Parenchyma in Vivo. *Science*, 308(5726), 1314–1318. <https://doi.org/10.1126/science.1110647>
- Ninkovic, J., & Götz, M. (2013). Fate specification in the adult brain - lessons for eliciting neurogenesis from glial cells. *BioEssays*, 35(3), 242–252. <https://doi.org/10.1002/bies.201200108>
- Ohlig, S., Clavreul, S., Thorwirth, M., Simon-Ebert, T., Bocchi, R., Ulbricht, S., Kannayian, N., Rossner, M., Sirko, S., Smialowski, P., Fischer-Sternjak, J., & Götz, M. (2021). Molecular diversity of diencephalic astrocytes reveals adult astrogenesis regulated by Smad4. *The EMBO Journal*, 40(21). <https://doi.org/10.15252/embj.2020107532>
- Okada, S., Nakamura, M., Katoh, H., Miyao, T., Shimazaki, T., Ishii, K., Yamane, J., Yoshimura, A., Iwamoto, Y., Toyama, Y., & Okano, H. (2006). Conditional ablation of Stat3 or Socs3 discloses a dual role for reactive astrocytes after spinal cord injury. *Nature Medicine*, 12(7), 829–834. <https://doi.org/10.1038/nm1425>
- Okey, A. B. (2007). An Aryl Hydrocarbon Receptor Odyssey to the Shores of Toxicology: The Deichmann Lecture, International Congress of Toxicology-XI. *Toxicological Sciences*, 98(1), 5–38. <https://doi.org/10.1093/toxsci/kfm096>
- Operaña, T. N., Nguyen, N., Chen, S., Beaton, D., & Tukey, R. H. (2007). Human CYP1A1GFP Expression in Transgenic Mice Serves as a Biomarker for Environmental Toxicant Exposure. *Toxicological Sciences*, 95(1), 98–107. <https://doi.org/10.1093/toxsci/kfl144>
- Ostapiuk, A., & Urbanska, E. M. (2022). Kynurenic acid in neurodegenerative disorders—unique neuroprotection or double-edged sword? *CNS Neuroscience & Therapeutics*, 28(1), 19–35. <https://doi.org/10.1111/cns.13768>
- Pekny, M., & Pekna, M. (2014). Astrocyte Reactivity and Reactive Astrogliosis: Costs and Benefits. *Physiological Reviews*, 94(4), 1077–1098. <https://doi.org/10.1152/physrev.00041.2013>
- Perdew, G. H. (1988). Association of the Ah receptor with the 90-kDa heat shock protein. *Journal of Biological Chemistry*, 263(27), 13802–13805. [https://doi.org/10.1016/S0021-9258\(18\)68314-0](https://doi.org/10.1016/S0021-9258(18)68314-0)
- Perdew, G. H., & Bradfield, C. (1996). Mapping the 90 kDa heat shock protein binding region of the Ah receptor. *IUBMB Life*, 39(3), 589–593. <https://doi.org/10.1080/15216549600201651>
- Pietras, E. M., Mirantes-Barbeito, C., Fong, S., Loeffler, D., Kovtonyuk, L. V., Zhang, S., Lakshminarasimhan, R., Chin, C. P., Techner, J.-M., Will, B., Nerlov, C., Steidl, U., Manz, M. G., Schroeder, T., & Passequé, E. (2016). Chronic interleukin-1 exposure drives haematopoietic stem cells towards precocious myeloid differentiation at the expense of self-renewal. *Nature Cell Biology*, 18(6), 607–618. <https://doi.org/10.1038/ncb3346>
- Pilz, G.-A., Bottes, S., Betizeau, M., Jörg, D. J., Carta, S., Simons, B. D., Helmchen, F., & Jessberger, S. (2018). Live imaging of neurogenesis in the adult mouse hippocampus. *Science*, 359(6376), 658–662. <https://doi.org/10.1126/science.aao5056>
- Pongratz, I., Mason, G. G., & Poellinger, L. (1992). Dual roles of the 90-kDa heat shock protein hsp90 in modulating functional activities of the dioxin receptor. Evidence that the dioxin receptor functionally belongs to a subclass of nuclear receptors which require hsp90 both for ligand binding activity and for transcriptional activity. *Journal of Biological Chemistry*, 267(19), 13728–13734.

[https://doi.org/10.1016/S0021-9258\(18\)42274-0](https://doi.org/10.1016/S0021-9258(18)42274-0)

- Pruszek, J., Ludwig, W., Blak, A., Alavian, K., & Isacson, O. (2009). CD15, CD24, and CD29 Define a Surface Biomarker Code for Neural Lineage Differentiation of Stem Cells. *Stem Cells*, 27(12), 2928–2940. <https://doi.org/10.1002/stem.211>
- Qu, Q., Sun, G., Li, W., Yang, S., Ye, P., Zhao, C., Yu, R. T., Gage, F. H., Evans, R. M., & Shi, Y. (2010). Orphan nuclear receptor TLX activates Wnt/ $\beta$ -catenin signalling to stimulate neural stem cell proliferation and self-renewal. *Nature Cell Biology*, 12(1), 31–40. <https://doi.org/10.1038/ncb2001>
- Quintana, F. J., & Sherr, D. H. (2013). Aryl Hydrocarbon Receptor Control of Adaptive Immunity. *Pharmacological Reviews*, 65(4), 1148–1161. <https://doi.org/10.1124/pr.113.007823>
- Rackham, O. J. L., Firas, J., Fang, H., Oates, M. E., Holmes, M. L., Knaupp, A. S., Suzuki, H., Nefzger, C. M., Daub, C. O., Shin, J. W., Petretto, E., Forrest, A. R. R., Hayashizaki, Y., Polo, J. M., & Gough, J. (2016). A predictive computational framework for direct reprogramming between human cell types. *Nature Genetics*, 48(3), 331–335. <https://doi.org/10.1038/ng.3487>
- Raison, C. L., Dantzer, R., Kelley, K. W., Lawson, M. A., Woolwine, B. J., Vogt, G., Spivey, J. R., Saito, K., & Miller, A. H. (2010). CSF concentrations of brain tryptophan and kynurenines during immune stimulation with IFN- $\alpha$ : relationship to CNS immune responses and depression. *Molecular Psychiatry*, 15(4), 393–403. <https://doi.org/10.1038/mp.2009.116>
- Rannug, A., Rannug, U., Rosenkranz, H. S., Winqvist, L., Westerholm, R., Agurell, E., & Grafström, A. K. (1987). Certain photooxidized derivatives of tryptophan bind with very high affinity to the Ah receptor and are likely to be endogenous signal substances. *Journal of Biological Chemistry*, 262(32), 15422–15427. [https://doi.org/10.1016/S0021-9258\(18\)47743-5](https://doi.org/10.1016/S0021-9258(18)47743-5)
- Reynolds, B. A., & Weiss, S. (1992). Generation of Neurons and Astrocytes from Isolated Cells of the Adult Mammalian Central Nervous System. *Science*, 255(5052), 1707–1710. <https://doi.org/10.1126/science.1553558>
- Rim, E. Y., Clevers, H., & Nusse, R. (2022). The Wnt Pathway: From Signaling Mechanisms to Synthetic Modulators. *Annual Review of Biochemistry*, 91(1), 571–598. <https://doi.org/10.1146/annurev-biochem-040320-103615>
- Robel, S., Berninger, B., & Götz, M. (2011). The stem cell potential of glia: lessons from reactive gliosis. *Nature Reviews Neuroscience*, 12(2), 88–104. <https://doi.org/10.1038/nrn2978>
- Rolfs, A., Kvietikova, I., Gassmann, M., & Wenger, R. H. (1997). Oxygen-regulated Transferrin Expression Is Mediated by Hypoxia-inducible Factor-1. *Journal of Biological Chemistry*, 272(32), 20055–20062. <https://doi.org/10.1074/jbc.272.32.20055>
- Rothhammer, V., Mascanfroni, I. D., Bunse, L., Takenaka, M. C., Kenison, J. E., Mayo, L., Chao, C.-C., Patel, B., Yan, R., Blain, M., Alvarez, J. I., Kébir, H., Anandasabapathy, N., Izquierdo, G., Jung, S., Obholzer, N., Pochet, N., Clish, C. B., Prinz, M., ... Quintana, F. J. (2016). Type I interferons and microbial metabolites of tryptophan modulate astrocyte activity and central nervous system inflammation via the aryl hydrocarbon receptor. *Nature Medicine*, 22(6), 586–597. <https://doi.org/10.1038/nm.4106>
- Rothhammer, V., & Quintana, F. J. (2019). The aryl hydrocarbon receptor: an environmental sensor integrating immune responses in health and disease. *Nature Reviews Immunology*, 19(3), 184–197. <https://doi.org/10.1038/s41577-019-0125-8>
- Safe, S., Han, H., Goldsby, J., Mohankumar, K., & Chapkin, R. S. (2018). Aryl hydrocarbon receptor (AhR) ligands as selective AhR modulators: Genomic studies. *Current Opinion in Toxicology*, 11–12, 10–20. <https://doi.org/10.1016/j.cotox.2018.11.005>
- Sanchez-Gonzalez, R., Koupourtidou, C., Lepko, T., Zambusi, A., Novoselc, K. T., Durovic, T., Aschenbroich, S., Schwarz, V., Breunig, C. T., Straka, H., Huttner, H. B., Irmeler, M., Beckers,

- J., Wurst, W., Zwergal, A., Schauer, T., Straub, T., Czopka, T., Trümbach, D., ... Ninkovic, J. (2022). Innate Immune Pathways Promote Oligodendrocyte Progenitor Cell Recruitment to the Injury Site in Adult Zebrafish Brain. *Cells*, *11*(3), 520. <https://doi.org/10.3390/cells11030520>
- Schiering, C., Wincent, E., Metidji, A., Iseppon, A., Li, Y., Potocnik, A. J., Omenetti, S., Henderson, C. J., Wolf, C. R., Nebert, D. W., & Stockinger, B. (2017). Feedback control of AHR signalling regulates intestinal immunity. *Nature*, *542*(7640), 242–245. <https://doi.org/10.1038/nature21080>
- Schimmel, S., Acosta, S., & Lozano, D. (2017). Neuroinflammation in traumatic brain injury: A chronic response to an acute injury. *Brain Circulation*, *3*(3), 135. [https://doi.org/10.4103/bc.bc\\_18\\_17](https://doi.org/10.4103/bc.bc_18_17)
- Shan, Q., Hu, S., Chen, X., Danahy, D. B., Badovinac, V. P., Zang, C., & Xue, H.-H. (2021). Ectopic Tcf1 expression instills a stem-like program in exhausted CD8+ T cells to enhance viral and tumor immunity. *Cellular & Molecular Immunology*, *18*(5), 1262–1277. <https://doi.org/10.1038/s41423-020-0436-5>
- Shannon, P., Markiel, A., Ozier, O., Baliga, N. S., Wang, J. T., Ramage, D., Amin, N., Schwikowski, B., & Ideker, T. (2003). Cytoscape: A Software Environment for Integrated Models of Biomolecular Interaction Networks. *Genome Research*, *13*(11), 2498–2504. <https://doi.org/10.1101/gr.1239303>
- Siddiqui, T., Bhattarai, P., Popova, S., Cosacak, M. I., Sariya, S., Zhang, Y., Mayeux, R., Tosto, G., & Kizil, C. (2021). KYNA/Ahr Signaling Suppresses Neural Stem Cell Plasticity and Neurogenesis in Adult Zebrafish Model of Alzheimer’s Disease. *Cells*, *10*(10), 2748. <https://doi.org/10.3390/cells10102748>
- Sirko, S., Behrendt, G., Johansson, P. A., Tripathi, P., Costa, M. R., Bek, S., Heinrich, C., Tiedt, S., Colak, D., Dichgans, M., Fischer, I. R., Plesnila, N., Staufienbiel, M., Haass, C., Snapyan, M., Saghatelyan, A., Tsai, L.-H., Fischer, A., Grobe, K., ... Götz, M. (2013). Reactive Glia in the Injured Brain Acquire Stem Cell Properties in Response to Sonic Hedgehog. *Cell Stem Cell*, *12*(4), 426–439. <https://doi.org/10.1016/j.stem.2013.01.019>
- Sirko, S., Irmeler, M., Gascón, S., Bek, S., Schneider, S., Dimou, L., Obermann, J., De Souza Paiva, D., Poirier, F., Beckers, J., Hauck, S. M., Barde, Y., & Götz, M. (2015). Astrocyte reactivity after brain injury—: The role of galectins 1 and 3. *Glia*, *63*(12), 2340–2361. <https://doi.org/10.1002/glia.22898>
- Sirko, S., Neitz, A., Mittmann, T., Horvat-Bröcker, A., Holst, A. von, Eysel, U. T., & Faissner, A. (2009). Focal laser-lesions activate an endogenous population of neural stem/progenitor cells in the adult visual cortex. *Brain*, *132*(8), 2252–2264. <https://doi.org/10.1093/brain/awp043>
- Soderblom, C., Luo, X., Blumenthal, E., Bray, E., Lyapichev, K., Ramos, J., Krishnan, V., Lai-Hsu, C., Park, K. K., Tsoulfas, P., & Lee, J. K. (2013). Perivascular Fibroblasts Form the Fibrotic Scar after Contusive Spinal Cord Injury. *Journal of Neuroscience*, *33*(34), 13882–13887. <https://doi.org/10.1523/JNEUROSCI.2524-13.2013>
- Sofroniew, M. V. (2015). Astrocyte barriers to neurotoxic inflammation. *Nature Reviews Neuroscience*, *16*(5), 249–263. <https://doi.org/10.1038/nrn3898>
- Sofroniew, M. V. (2020). Astrocyte Reactivity: Subtypes, States, and Functions in CNS Innate Immunity. *Trends in Immunology*, *41*(9), 758–770. <https://doi.org/10.1016/j.it.2020.07.004>
- Sofroniew, M. V., & Vinters, H. V. (2010). Astrocytes: biology and pathology. *Acta Neuropathologica*, *119*(1), 7–35. <https://doi.org/10.1007/s00401-009-0619-8>
- Sofroniew, M. V. (2009). Molecular dissection of reactive astrogliosis and glial scar formation.

- Trends in Neurosciences*, 32(12), 638–647. <https://doi.org/10.1016/j.tins.2009.08.002>
- Stocchetti, N., & Zanier, E. R. (2016). Chronic impact of traumatic brain injury on outcome and quality of life: a narrative review. *Critical Care*, 20(1), 148. <https://doi.org/10.1186/s13054-016-1318-1>
- Stockinger, B., Meglio, P. Di, Gialitakis, M., & Duarte, J. H. (2014). The Aryl Hydrocarbon Receptor: Multitasking in the Immune System. *Annual Review of Immunology*, 32(1), 403–432. <https://doi.org/10.1146/annurev-immunol-032713-120245>
- Stoddard-Bennett, T., & Reijo Pera, R. (2019). Treatment of Parkinson’s Disease through Personalized Medicine and Induced Pluripotent Stem Cells. *Cells*, 8(1), 26. <https://doi.org/10.3390/cells8010026>
- Swanson, H. I., & Perdew, G. H. (1993). Half-Life of Aryl Hydrocarbon Receptor in Hepam 1 Cells: Evidence for Ligand-Dependent Alterations in Cytosolic Receptor Levels. *Archives of Biochemistry and Biophysics*, 302(1), 167–174. <https://doi.org/10.1006/abbi.1993.1195>
- Szklarczyk, D., Gable, A. L., Nastou, K. C., Lyon, D., Kirsch, R., Pyysalo, S., Doncheva, N. T., Legeay, M., Fang, T., Bork, P., Jensen, L. J., & von Mering, C. (2021). The STRING database in 2021: customizable protein–protein networks, and functional characterization of user-uploaded gene/measurement sets. *Nucleic Acids Research*, 49(D1), D605–D612. <https://doi.org/10.1093/nar/gkaa1074>
- Takahashi, K., & Yamanaka, S. (2006). Induction of Pluripotent Stem Cells from Mouse Embryonic and Adult Fibroblast Cultures by Defined Factors. *Cell*, 126(4), 663–676. <https://doi.org/10.1016/j.cell.2006.07.024>
- Takanaga, H., Yoshitake, T., Yatabe, E., Hara, S., & Kunimoto, M. (2004). beta-Naphthoflavone disturbs astrocytic differentiation of C6 glioma cells by inhibiting autocrine interleukin-6. *Journal of Neurochemistry*, 90(3), 750–757. <https://doi.org/10.1111/j.1471-4159.2004.02681.x>
- Tao, Y., Black, I. B., & DiCicco-Bloom, E. (1997). In vivo neurogenesis is inhibited by neutralizing antibodies to basic fibroblast growth factor. *Journal of Neurobiology*, 33(3), 289–296. [https://doi.org/10.1002/\(SICI\)1097-4695\(199709\)33:3<289::AID-NEU7>3.0.CO;2-Y](https://doi.org/10.1002/(SICI)1097-4695(199709)33:3<289::AID-NEU7>3.0.CO;2-Y)
- Tirosh, I., Izar, B., Prakadan, S. M., Wadsworth, M. H., Treacy, D., Trombetta, J. J., Rotem, A., Rodman, C., Lian, C., Murphy, G., Fallahi-Sichani, M., Dutton-Regester, K., Lin, J.-R., Cohen, O., Shah, P., Lu, D., Genshaft, A. S., Hughes, T. K., Ziegler, C. G. K., ... Garraway, L. A. (2016). Dissecting the multicellular ecosystem of metastatic melanoma by single-cell RNA-seq. *Science*, 352(6282), 189–196. <https://doi.org/10.1126/science.aad0501>
- Traag, V. A., Waltman, L., & van Eck, N. J. (2019). From Louvain to Leiden: guaranteeing well-connected communities. *Scientific Reports*, 9(1), 5233. <https://doi.org/10.1038/s41598-019-41695-z>
- Tsai, H.-H., Li, H., Fuentealba, L. C., Molofsky, A. V., Taveira-Marques, R., Zhuang, H., Tenney, A., Murnen, A. T., Fancy, S. P. J., Merkle, F., Kessaris, N., Alvarez-Buylla, A., Richardson, W. D., & Rowitch, D. H. (2012). Regional Astrocyte Allocation Regulates CNS Synaptogenesis and Repair. *Science*, 337(6092), 358–362. <https://doi.org/10.1126/science.1222381>
- VanInsberghe, M., van den Berg, J., Andersson-Rolf, A., Clevers, H., & van Oudenaarden, A. (2021). Single-cell Ribo-seq reveals cell cycle-dependent translational pausing. *Nature*, 597(7877), 561–565. <https://doi.org/10.1038/s41586-021-03887-4>
- Vaughan, K. L., Franchini, A. M., Kern, H. G., & Lawrence, B. P. (2021). The Aryl Hydrocarbon Receptor Modulates Murine Hematopoietic Stem Cell Homeostasis and Influences Lineage-Biased Stem and Progenitor Cells. *Stem Cells and Development*, 30(19), 970–980. <https://doi.org/10.1089/scd.2021.0096>
- Verkhatsky, A., Matteoli, M., Parpura, V., Mothet, J., & Zorec, R. (2016). Astrocytes as secretory

- cells of the central nervous system: idiosyncrasies of vesicular secretion. *The EMBO Journal*, 35(3), 239–257. <https://doi.org/10.15252/embj.201592705>
- Verkhatsky, A., & Nedergaard, M. (2018). Physiology of Astroglia. *Physiological Reviews*, 98(1), 239–389. <https://doi.org/10.1152/physrev.00042.2016>
- Vollmer, T. L., Sorensen, P. S., Selmaj, K., Zipp, F., Havrdova, E., Cohen, J. A., Sasson, N., Gilgun-Sherki, Y., & Arnold, D. L. (2014). A randomized placebo-controlled phase III trial of oral laquinimod for multiple sclerosis. *Journal of Neurology*, 261(4), 773–783. <https://doi.org/10.1007/s00415-014-7264-4>
- von Streitberg, A., Jäkel, S., Eugenin von Bernhardt, J., Straube, C., Buggenthin, F., Marr, C., & Dimou, L. (2021). NG2-Glia Transiently Overcome Their Homeostatic Network and Contribute to Wound Closure After Brain Injury. *Frontiers in Cell and Developmental Biology*, 9, 662056. <https://doi.org/10.3389/fcell.2021.662056>
- Walisser, J. A., Glover, E., Pande, K., Liss, A. L., & Bradfield, C. A. (2005). Aryl hydrocarbon receptor-dependent liver development and hepatotoxicity are mediated by different cell types. *Proceedings of the National Academy of Sciences*, 102(49), 17858–17863. <https://doi.org/10.1073/pnas.0504757102>
- Wanner, I. B., Anderson, M. A., Song, B., Levine, J., Fernandez, A., Gray-Thompson, Z., Ao, Y., & Sofroniew, M. V. (2013). Glial Scar Borders Are Formed by Newly Proliferated, Elongated Astrocytes That Interact to Corral Inflammatory and Fibrotic Cells via STAT3-Dependent Mechanisms after Spinal Cord Injury. *Journal of Neuroscience*, 33(31), 12870–12886. <https://doi.org/10.1523/JNEUROSCI.2121-13.2013>
- Wei, G. Z., Martin, K. A., Xing, P. Y., Agrawal, R., Whiley, L., Wood, T. K., Hejndorf, S., Ng, Y. Z., Low, J. Z. Y., Rossant, J., Nechanitzky, R., Holmes, E., Nicholson, J. K., Tan, E.-K., Matthews, P. M., & Pettersson, S. (2021). Tryptophan-metabolizing gut microbes regulate adult neurogenesis via the aryl hydrocarbon receptor. *Proceedings of the National Academy of Sciences*, 118(27). <https://doi.org/10.1073/pnas.2021091118>
- White, B. D., Nathe, R. J., Maris, D. O., Nguyen, N. K., Goodson, J. M., Moon, R. T., & Horner, P. J. (2010).  $\beta$ -Catenin Signaling Increases in Proliferating NG2+ Progenitors and Astrocytes during Post-Traumatic Gliogenesis in the Adult Brain. *Stem Cells*, 28(2), 297–307. <https://doi.org/10.1002/stem.268>
- Wickham, H. (2016). *ggplot2: Elegant Graphics for Data Analysis*. Springer-Verlag New York. <https://doi.org/10.1007/978-0-387-98141-3>
- Wincent, E., Amini, N., Luecke, S., Glatt, H., Bergman, J., Crescenzi, C., Rannug, A., & Rannug, U. (2009). The Suggested Physiologic Aryl Hydrocarbon Receptor Activator and Cytochrome P4501 Substrate 6-Formylindolo[3,2-b]carbazole Is Present in Humans. *Journal of Biological Chemistry*, 284(5), 2690–2696. <https://doi.org/10.1074/jbc.M808321200>
- Wolf, F. A., Angerer, P., & Theis, F. J. (2018). SCANPY: large-scale single-cell gene expression data analysis. *Genome Biology*, 19(1), 15. <https://doi.org/10.1186/s13059-017-1382-0>
- Wolock, S. L., Lopez, R., & Klein, A. M. (2019). Scrublet: Computational Identification of Cell Doublets in Single-Cell Transcriptomic Data. *Cell Systems*, 8(4), 281–291.e9. <https://doi.org/10.1016/j.cels.2018.11.005>
- Wu, C., Yu, S., Tan, Q., Guo, P., & Liu, H. (2018). Role of AhR in regulating cancer stem cell-like characteristics in choriocarcinoma. *Cell Cycle*, 17(18), 2309–2320. <https://doi.org/10.1080/15384101.2018.1535219>
- Wu, J. Q., Seay, M., Schulz, V. P., Hariharan, M., Tuck, D., Lian, J., Du, J., Shi, M., Ye, Z., Gerstein, M., Snyder, M. P., & Weissman, S. (2012). Tcf7 Is an Important Regulator of the Switch of Self-Renewal and Differentiation in a Multipotential Hematopoietic Cell Line. *PLoS Genetics*, 8(3), e1002565. <https://doi.org/10.1371/journal.pgen.1002565>

- Xiong, Y., Mahmood, A., & Chopp, M. (2018). Current understanding of neuroinflammation after traumatic brain injury and cell-based therapeutic opportunities. *Chinese Journal of Traumatology*, 21(3), 137–151. <https://doi.org/10.1016/j.cjtee.2018.02.003>
- Yang, C., Liu, X., Cheng, T., Xiao, R., Gao, Q., Ming, F., Jin, M., Chen, H., & Zhou, H. (2019). LYAR Suppresses Beta Interferon Induction by Targeting Phosphorylated Interferon Regulatory Factor 3. *Journal of Virology*, 93(21). <https://doi.org/10.1128/JVI.00769-19>
- Zamanian, J. L., Xu, L., Foo, L. C., Nouri, N., Zhou, L., Giffard, R. G., & Barres, B. A. (2012). Genomic Analysis of Reactive Astrogliosis. *Journal of Neuroscience*, 32(18), 6391–6410. <https://doi.org/10.1523/JNEUROSCI.6221-11.2012>
- Zamboni, M., Llorens-Bobadilla, E., Magnusson, J. P., & Frisén, J. (2020). A Widespread Neurogenic Potential of Neocortical Astrocytes Is Induced by Injury. *Cell Stem Cell*, 27(4), 605-617.e5. <https://doi.org/10.1016/j.stem.2020.07.006>
- Zeisel, A., Hochgerner, H., Lönnerberg, P., Johnsson, A., Memic, F., van der Zwan, J., Häring, M., Braun, E., Borm, L. E., La Manno, G., Codeluppi, S., Furlan, A., Lee, K., Skene, N., Harris, K. D., Hjerling-Leffler, J., Arenas, E., Ernfors, P., Marklund, U., & Linnarsson, S. (2018). Molecular Architecture of the Mouse Nervous System. *Cell*, 174(4), 999-1014.e22. <https://doi.org/10.1016/j.cell.2018.06.021>
- Zhou, X., Yu, S., Zhao, D.-M., Harty, J. T., Badovinac, V. P., & Xue, H.-H. (2010). Differentiation and Persistence of Memory CD8+ T Cells Depend on T Cell Factor 1. *Immunity*, 33(2), 229–240. <https://doi.org/10.1016/j.immuni.2010.08.002>
- Zhu, C., Chen, Y.-L., Wang, X.-J., Hu, X.-S., Yu, Z.-B., & Han, S.-P. (2012). ShRNA-mediated gene silencing of AHR promotes the differentiation of P19 mouse embryonic carcinoma cells into cardiomyocytes. *Molecular Medicine Reports*, 6(3), 513–518. <https://doi.org/10.3892/mmr.2012.941>

## 7 Acknowledgments

My first and sincere thanks goes to Jovica. Thank you for your continuous scientific guidance, enthusiasm, and motivation to carry through these challenging times during my PhD. I am grateful that you always found time to support me and gave me the freedom to pursue my ideas. This helped me to grow not only as a scientist but also as a person.

I also want to acknowledge Magdalena. Your knowledge, suggestions, and critical questions helped to guide the project in the right direction. Your enthusiasm for science is very inspiring and I always felt privileged to work in your lab. Thank you for your support throughout all these years.

Next, I would like to thank Prof. Dr. Martin Kerschensteiner and Prof. Dr. Mikael Simons who were part of my thesis advisory committee. I very much appreciated you taking your time for the annual meetings and your valuable input on the scientific part. Thanks to the GSN for all the support provided and for fun activities during my time as a PhD student.

Many thanks go to Andrea and Tatiana, who taught me everything regarding cell culture, sorting, and staining. You were a big help for my neurosphere assay and whenever I was struggling with experiments in the lab. In addition, I want to thank Tatiana and Judith for guiding me through the single-cell RNA library preparation. I also want to thank Judith for her support in planning this experiment.

Next to Andrea and Tatiana, I would like to express my deep gratitude to all the technicians I have worked with during this time. You did a fantastic job and without you, this PhD thesis would not be possible. Thank you.

A big thank you goes to Pawel. It was a pleasure working with you together on this project and I am indebted to your quick responses when the time was pressuring me. Also, I want to acknowledge Tobias and Tamas for their statistical guidance and the possibility to use the high-performance computational cluster provided by the Bioinformatic Core Facility at the Biomedical Center. Many thanks go to Christina and Nacho, who always took their time when I needed help and support regarding my single-cell analysis.

Warm thanks go to my colleagues Veronika and Christina who helped me to dissect the brains at light speed for the single-cell analysis, as well as to Klara, Alessandro, Tamara, Priya, Finja, Tjasa, Anita, Sofia, Viviane, and Julia from the AG Ninkovic that accompanied me during my time as a master's and PhD student. I spent most of my time here in Munich with you and it was a pleasure. I am very grateful for the delightful environment that we worked in together.

Also, I want to thank you for all your help and ideas that pushed forward this project. A special thank you goes to my PhD sister Klara who also brought back the fun of climbing.

A big thanks also goes to the colleagues from AG Götz and AG Kiebler who were always helpful and made it fun to collaborate. I am deeply grateful to Rico for the excellent collaborations we had and for proofreading my thesis. Thank you for filling my free time with joy and for being around when I needed you, Rico and Lars. It was always a pleasure meeting with you guys!

Ein großes Dankeschön auch an meine engsten Freunde aus der Zeit von Stuttgart und Tübingen: Baumann, Phil, David, Marco und Lisa. Es ist einfach großartig Freunde wie euch zu haben mit denen man immer eine gute Zeit verbringt, und wenn es mal brenzlig wird dda, immer zur Stelle sind und einen unterstützen.

Ich möchte mich auch bei meinen Eltern bedanken. Ohne euch wäre all das nicht möglich gewesen. Auch möchte ich meinen Dank meinem Opa aussprechen. Vielen Dank für all die gute Zeit und die Witze und guten Sprüche die Du auf Lager hast. Ich hoffe wir können noch einige Jahre miteinander verbringen. Danke natürlich auch an meinen Bruder Jens. Es war schön die letzten knapp 3 Jahre mit Dir hier in München zu verbringen. Vielen Dank für deine Unterstützung.

Finally, I want to express my deepest gratitude to Elvira, who is standing by my side for more than 8 years. Thank you for your patience and constant support during the good and bad times. It is impossible to find the right words to express how glad I am that you share your love and trust with me, and encourage me to be a better person day by day. Thank you for all the wonderful time we experienced together and hopefully will experience in the future. Without you, I would not be able to achieve all this. ¡Muchas gracias!

## 8 List of publications

- Di Giaimo, R., **S. Aschenbroich**, and J. Ninkovic. 2019. "Fluorescence-Activated Cell Sorting-Based Isolation and Characterization of Neural Stem Cells from the Adult Zebrafish Telencephalon." *Methods Mol Biol* 1938:49–66.
- Di Giaimo, R.\* , T. Durovic\*, P. Barquin, A. Kocaj, T. Lepko, **S. Aschenbroich**, C. T. Breunig, M. Irmeler, F. M. Cernilogar, G. Schotta, J. S. Barbosa, D. Trumbach, E. V. Baumgart, A. M. Neuner, J. Beckers, W. Wurst, S. H. Stricker, and J. Ninkovic. 2018. "The Aryl Hydrocarbon Receptor Pathway Defines the Time Frame for Restorative Neurogenesis." *Cell Rep* 25(12):3241-3251 e5.
- Sanchez-Gonzalez, R., C. Koupourtidou, T. Lepko, A. Zambusi, K. T. Novoselc, T. Durovic, **S. Aschenbroich**, V. Schwarz, C. T. Breunig, H. Straka, H. B. Huttner, M. Irmeler, J. Beckers, W. Wurst, A. Zwergal, T. Schauer, T. Straub, T. Czopka, D. Trümbach, M. Götz, S. H. Stricker, and J. Ninkovic. 2022. "Innate Immune Pathways Promote Oligodendrocyte Progenitor Cell Recruitment to the Injury Site in Adult Zebrafish Brain." *Cells* 11(3):520.



## 9 List of contributions

The author of this dissertation planned and executed the experiments, collected and analyzed the data, created the figures and interpreted the results, and wrote the manuscript.

Dr. Pawel Smialowski performed the transcription factor ranking analysis. The data from this analysis was then presented in Figures 17A and 18I with his consent.

Sven Aschenbroich

Prof. Dr. Jovica Ninkovic